Department of Physics and Technology

Master's thesis

A study of the Coriolis flowmeter as a reference instrument in multiphase flow

by:
Sigve Naustdal

University of Bergen - Department of Physics and Technology

September 10, 2015

Acknowledgements

I would like to express my gratitude to Christian Michelsen Research (CMR) for the use of their facilities, and for offering me the equipment I needed for executing this work. This could not have been done without the contribution from many people. In full gratitude I would like to acknowledge and thank these individuals:

My supervisor Dr. Bjørn Tore Hjertaker for guiding me through the learning process of this master thesis. For helpfull comments, valuable discussions and friendly advice.

I would like to thank Anders Hallanger at CMR for proposing the topic of this thesis, and for training, organizing the execution of, and support in using the CMR multi-phase flow-rig.

My co-supervisor Dr. Camilla Sætre, for valuable input during the process and when writing this thesis.

Stian Husevik Stavland at CMR for many good discussions and guidance during the entire process. Commenting on progress and results during the experimental work.

For valuable discussions on thesis related topics, I would like to thank Dr. Ivar Øyvind Sand at CMR. I would also like to thank Dr. Hao Zhu from Endress+Hauser and Dr. Joel D. Weinstein from Micro Motion for responses to my emails.

My fellow students and office mates Mang Li and Truls Andersen for two great years and much needed support. I must thank all my other friends as well, for support and comforting words.

Last, but not least, I would like to thank my family for support, love and attempts to keep me cheerful during this period. Special thanks goes to Linn Anja, my love, for keeping up with me.

Abstract

The objective of this thesis was to investigate how a two-liquid mixture, and injected gas, affects the measurements of a Coriolis flowmeter. Furthermore it was of interest to investigate whether entrained gas could be detected, and to estimate the effect this has on the reference measurements in the CMR flow rig.

A mathematical model of particle motion in an oscillating environment was used to simulate particle movement; The results were used to estimate the damping of the motion in the Coriolis flowmeter. Flow measurements, with and without injected gas, were carried out. Measurements of diesel/water mixtures were compared to the mathematical model, and uncertainty contributions were estimated. Based on measurements of high liquid flow rates, an estimate of the entrained gas quantity was made.

The CMR flow rig behave as foreseen when changing the particle size and viscosity. The injected gas have significant impact on the damping. The uncertainty calculations show that measurements of diesel/water mixtures can be done without major uncertainty contributions. In the cases studied in this work, the uncertainty contribution is limited maximum -0.5%. The amount of entrained gas is probably less than $\approx 0.02\%$ GVF and uncertainty contribution will in the studied cases be limited to a maximum of $\approx -0.01\%$.

The contribution from a diesel/water mixture is small and CMR's uncertainty estimates are sufficient. The contribution from decoupling is so small that it is only of academic interest. The underlying conditions should however be studied more in detail. The measurements of entrained gas and its uncertainty contribution suggests that entrained gas does not affect the reference measurements in the flow rig.

Sammendrag

Målet med denne oppgaven var å undersøke om en blanding av to væsker påvirker måleresultatet i et Coriolis-meter, samt å undersøke hvordan injisert gass påvirker de samme målingene. Med dette var det ønskelig å se om medrevet gass kunne påvises og eventuelt hvor mye dette påvirker referansemålingene i CMRs strømningsrigg.

En matematisk modell av partikkelbevegelse i oscillerende omgivelser ble brukt for å simulere partikkelbevegelse i instrumentet. Resultater fra simuleringen ble brukt til å estimere demping av den oscillatoriske bevegelsen i Coriolis-meteret. Målinger av diesel/vann-blandinger, med og uten injisert gass er foretatt i CMRs strømningsrigg. Målingene uten gass ble vurdert mot den matematiske modellen, og usikkerhetsbidrag ble estimert. Basert på målinger av høy væskerate, ble det gjort et anslag av mulig medrevet gassmengde i strømningsriggen.

Demping i CMRs strømningsrigg oppfører seg som forutsett ved endring av partikkelstørrelse og viskositet. Injisert gass gir store utslag i demping. Usikkerhetsberegningene viser at måling av diesel/vann-blanding kan gjøres uten store usikkerhetsbidrag. I undersøkte tilfeller begrenser usikkerhetsbidraget seg til maksimalt -0,5%. Mengden medrevet gass er trolig under $\approx 0.02\%$ GVF, og usikkerhetsbidraget fra medrevet gass vil i undersøkte tilfelle begrense seg til maksimalt $\approx -0.01\%$.

Usikkerhetsbidraget i en diesel/vann-blanding er lite, og CMRs usikkerhetsanslag for referansemålinger er tilstrekkelig. Bidraget fra dekobling er bare av akademisk interesse. Forholdene som ligger til grunn bør studeres grundigere. Målinger av medrevet gass, og usikkerhetsbidraget fra denne tilsier at medrevet gass ikke påvirker referansemålingene.

List of Figures

2.1 A simplified Coriolis tube. A mass element, with length Δx moves through the oscillating tube, with velocity v. The Coriolis tube will experience a torque, T about the centerline (CF). Made with inspiration from Bentley [4]. 13

2.2 Cross section of a liquid (grey) filled Coriolis tube, containing a bubble (white), undergoing oscillations. The bubble will oscillate with a different amplitude than the Coriolis tube. 17

2.3 Cross section of a Coriolis tube, showing movement of the center of gravity (+) and direction of liquid flow around a bubble (white). The Coriolis tube undergoes oscillations. The expected location of the center of gravity, in the case of no relative motion between bubble and liquid, is marked with an "x". Made with inspiration from [10] 18

2.4 A generic two-phase vertical flow map, note that superficial velocities are used along the axis [5]. 20

2.5 A generic two-phase horizontal flow map, note that superficial velocities are used along the axis [5]. 20

3.1 Estimated effective viscosity for different WLR of a diesel/water mixture, at 20°C . Viscosity of diesel, $\eta_{diesel} = 4\ mPa\ s$ and for water, $\eta_{water} = 1\ mPa\ s$. Change of continuous phase at WLR = 45% 32

3.2 Results for particle displacement, using the invicid model. Showing displacement as a function of time, where frequency = 400 Hz, water density, $\rho_{water} = 1000\ kg/m^3$, diesel density, $\rho_{diesel} = 830\ kg/m^3$, and nitrogen density, $\rho_{gas} = 1\ kg/m^3$ 33

3.3 Results when solving the viscous model for velocity. Diesel droplet (red) in water (blue). Reference conditions, Table 3.1 are used, and WLR = 60%. 34

3.4 Results when solving the viscous model for velocity. Nitrogen bubble (red) in water (blue). Reference conditions, Table 3.1 are used, and WLR = 100%, no concentration effects are considered. 35

3.5 Phase difference and amplitude ratio between particle and continuous phase, when solving for reference conditions, Table 3.1. Results shown for all WLR, with continuous phase change at WLR = 45%. 36

3.6 Power dissipation per cycle and power dissipation per volume, for each particle, when solving for reference conditions, Table 3.1. Results shown for all WLR, with continuous phase change at WLR = 45%. 37

3.7 An expression for total power dissipation per cycle when solving for reference conditions, Table 3.1. Results shown for all WLR, with continuous phase change at WLR = 45%. Values for power dissipation are not valid for numerical comparison. 38

4.1 Simplified PI&D of the CMR multiphase flow loop. [22] 40
4.2 Typical sweep through WLR range over time, using the WLR sweep method. 45

5.1 Experiment 1, part 1, day 1. Excitation current vs. WLR at pump power rates 50% (blue) and 90% (red), and $Q_l = 50\frac{m^3}{h}$. 51
5.2 Experiment 1, part 1, day 2: Excitation current vs. WLR at pump power rates: 40 (blue), 60 (red), 70 (green) and 80% (black), and $Q_l = 50\frac{m^3}{h}$. . . 52
5.3 Experiment 1, part 1: Hysteresis plot of excitation current vs. WLR at pump power rate 50% and $Q_l = 50\frac{m^3}{h}$. Increasing WLR is marked with green, and decreasing WLR with blue. 53
5.4 Experiment 1, part 2: Excitation current vs. WLR at pump power rates: 70 (black), 80 (red) and 90% (blue), and $Q_l = 70\frac{m^3}{h}$. 54
5.5 Experiment 1, part 2: Hysteresis plot of excitation current vs. WLR at pump power rate 90%, and $Q_l = 70\frac{m^3}{h}$. Increasing WLR is marked with green, and decreasing WLR with blue. 54
5.6 Experiment 1, part 3: Excitation current vs. WLR at pump power rates: 70 (blue), 80 (red) and 90% (black), and $Q_l = 30\frac{m^3}{h}$. 55
5.7 Experiment 1, part 3: Hysteresis plot of excitation current vs. WLR at pump power rate 70%, and and $Q_l = 30\frac{m^3}{h}$. Increasing WLR is marked with green, and decreasing WLR with blue. 56
5.8 Experiment 2, part 1: Hysteresis plot. Excitation current vs. WLR at pump power rate 90%. $Q_l = 50\ \frac{m^3}{h}$. Increasing WLR is marked with green, and decreasing WLR with blue. 58
5.9 Experiment 2, part 2: Excitation current vs. WLR. PP = 90. GVF injected in 0.1% steps, and $Q_l = 50\ \frac{m^3}{h}$. 0.0% is green, 0.1% - red, 0.2% - turquoise, 0.3% - magenta, 0.4% - yellow and 0.5% - black 59
5.10 Experiment 2, part 3: Excitation current vs. WLR. GVF = 0.5%. PP = 70 (red), 80 (green) and 90% (blue), and $Q_l = 50\ \frac{m^3}{h}$ 60
5.11 Experiment 3, part 1: Excitation current against GVF, at high liquid flow rates. One standard deviation is shown as error bars. Blue: $Q_l = 120\frac{m^3}{h}$ and $PP = 80\%$. Red: $Q_l = 120\frac{m^3}{h}$ and $PP = 90\%$. Lime: $Q_l = 140\frac{m^3}{h}$ and $PP = 90\%$. Magenta: $Q_l = 160\frac{m^3}{h}$ and $PP = 90\%$. Black: $Q_l = 180\frac{m^3}{h}$ and $PP = 90\%$. 63
5.12 Experiment 3, part 2: Excitation current against high liquid flow rates, no injected gas. One standard deviation is shown as error bars. 64
5.13 Experiment 3, part 3: Excitation current against WLR, at liquid flow rate $Q_V = 250\ \frac{h^3}{h}$ and PP = 90%. 65
5.14 Experiment 3, part 4: Excitation current against GVF, at liquid flow rate $Q_V = 250\ \frac{h^3}{h}$ and PP = 90%. One standard deviation is shown as error bars. 66

6.1 Estimated density error for different WLR, using reference conditions. Continuous-phase change at WLR = 45%. 70
6.2 Estimated density error for different GVF, nitrogen bubble in water . . . 71

D.1 Phase difference and amplitude ratio between particle and continuous phase, when solving for reference conditions, Table 3.1. Results shown for all WLR, with continuous phase change at WLR = 45%. 93
D.2 Power dissipation per cycle and power dissipation per volume, for each particle, when solving for reference conditions, Table 3.1. Results shown for all WLR, with continuous phase change at WLR = 45%. 94
D.3 An expression for total power dissipation per cycle when solving for reference conditions, Table 3.1. Results shown for all WLR, with continuous phase change at WLR = 45%. Values for power dissipation are not valid for numerical comparison. 94
D.4 Phase difference and amplitude ratio between particle and continuous phase, when solving for high pump speed conditions, Table 3.2. Results shown for all WLR, with continuous phase change at WLR = 45%. . . . 95
D.5 Power dissipation per cycle and power dissipation per volume, for each particle, when solving for high pump speed conditions, Table 3.2. Results shown for all WLR, with continuous phase change at WLR = 45%. . . . 95
D.6 An expression for total power dissipation per cycle when solving for high pump speed conditions, Table 3.2. Results shown for all WLR, with continuous phase change at WLR = 45%. Values for power dissipation are not valid for numerical comparison. 96
D.7 Phase difference and amplitude ratio between particle and continuous phase, when solving for low pump speed conditions, Table 3.2. Results shown for all WLR, with continuous phase change at WLR = 45%. . . . 96
D.8 Power dissipation per cycle and power dissipation per volume, for each particle, when solving for low pump speed conditions, Table 3.2. Results shown for all WLR, with continuous phase change at WLR = 45%. . . . 97
D.9 An expression for total power dissipation per cycle when solving for low pump speed conditions, Table 3.2. Results shown for all WLR, with continuous phase change at WLR = 45%. Values for power dissipation are not valid for numerical comparison. 97
D.10 Phase difference and amplitude ratio between particle and continuous phase, when solving for high temperature conditions, Table 3.2. Results shown for all WLR, with continuous phase change at WLR = 45%. . . . 98
D.11 Power dissipation per cycle and power dissipation per volume, for each particle, when solving for high temperature conditions, Table 3.2. Results shown for all WLR, with continuous phase change at WLR = 45%. . . . 98
D.12 An expression for total power dissipation per cycle when solving for high temperature conditions, Table 3.2. Results shown for all WLR, with continuous phase change at WLR = 45%. Values for power dissipation are not valid for numerical comparison. 99

E.1 Estimated density error for different WLR, using reference conditions. Continuous-phase change at WLR = 45%. 101
E.2 Estimated density error for different WLR, using high pump speed conditions. Continuous-phase change at WLR = 45%. 102
E.3 Estimated density error for different WLR, using low pump speed conditions. Continuous-phase change at WLR = 45%. 102
E.4 Estimated density error for different WLR, using high temperature conditions. Continuous-phase change at WLR = 45%. 103

List of Tables

3.1 Reference conditions used when solving the viscous equations 34
3.2 Conditions used to investigate change in power dissipation when conditions changes 37

4.1 Reference instruments used in the CMR Multiphase flow loop, with ranges and uncertainties. Each instruments PI&D label, and flow line is also presented. [22] 41
4.2 Uncertainties (95% conf. interval) in flow parameters in the CMR Multiphase flow loop [22]. 42
4.3 Technical specifications for Bronkhorst F-201CV [23]. 42

5.1 Experiment 1, part 1: Settings for measurements taken at $Q_l = 50\frac{m^3}{h}$, Day 1 49
5.2 Experiment 1, part 1: Settings for measurements taken at $Q_l = 50\frac{m^3}{h}$, Day 2 49
5.3 Experiment 1, part 2: Settings for measurements taken at $Q_l = 70\frac{m^3}{h}$ . . 50
5.4 Experiment 1, part 3: Settings for measurements taken at $Q_l = 30\frac{m^3}{h}$ . . 50
5.5 Experiment 2, part 2: Steps of GVF used for measurements 57
5.6 Experiment 2, part 3: Steps of pump power rates used for measurements 58
5.7 Experiment 3, part 1: Measurement steps, pump power rates and liquid flow rates. 61
5.8 Experiment 3, part 2: Measurement steps, different liquid flow rates . . . 62
5.9 Experiment 3, part 4: Measurement steps, different GVF 62

List of abbreviations

CG Center of Gravity.

CMR Christian Michelsen Research.

EC Excitation Current.

GVF Gas Volume Fraction.

PP Pump Power rate.

VP Valve Power rate.

WLR Water Liquid Ratio.

List of symbols

A Area [m^2].

B Bulk modulus, $\frac{N}{m^2}$.

$\dot{M}$ Mass flow rate [$\frac{kg}{t}$].

M Molar mass [$\frac{kg}{mol}$].

P Absolute pressure [Pa].

Q Volume flow rate [$\frac{m^3}{t}$].

R Specific gas constant, $\frac{\bar{R}}{M}$ [$\frac{J}{kgK}$].

$\bar{R}$ Ideal gas constant [$\frac{J}{molK}$].

Re Reynolds number, dimensionless.

T Absolute temperature [K].

V Volume [m^3].

η Dynamic viscosity [Pa s].

γ Specific heat ratio, $\frac{C_p}{C_v}$.

ν Kinematic viscosity [$\frac{m^2}{s}$].

ω Angular velocity, $\frac{rad}{s}$.

ρ Density [kg m^{-3}].

a Radius [m].

c Elastic stiffness, $\frac{N}{m}$.

f Frequency, s^{-1}.

g Gravity of Earth, $\approx 9.81\frac{m}{s^2}$.

l Length [m].

m Mass [kg].

n Amount of substance [mol].

r Radius $[m]$.

u Velocity [m/s].

$\bar{v}$ Mean velocity $[\frac{m}{s}]$.

v Velocity $[\frac{m}{s}]$.

z Heigh, $[m]$.

Contents

Acknowledgements ii
Abstract iii
Sammendrag v

List of figures **vii**

List of tables **xi**

List of abbreviations **xiii**

List of symbols **xv**

1 Introduction **1**
1.1 Motivation and objectives 2
1.2 Outline 3

2 Background and Theory **5**
2.1 Fluids - Liquids and gases 5
2.2 Flow profiles, laminar and turbulent flow 6
2.3 Single point velocity measurements 7
2.4 Volume flow measurements 7
2.5 Mass flow measurements 9
2.5.1 Inferential methods 10
2.5.2 Direct methods 10
2.6 The Coriolis effect 11
2.7 Coriolis flowmeter 11
2.8 Multiphase flow, and effects in Coriolis flow meters 15
2.8.1 Decoupling 16
2.8.2 Compressibility 18
2.8.3 Flow conditions 19
2.8.4 Effective viscosity 21

3 Mathematical model **23**
3.1 Equations of motion - Inviscid model 23
3.2 Equations of motion - Viscous model 24
3.3 Assumptions and methodology 27
3.4 Calculating WLR 29
3.5 Calculating GVF 30

3.6 Estimating effective viscosity . . . 31
3.7 Estimating decoupling ratio - Invicid model . . . 32
3.8 Estimating decoupling ratio - Viscous model . . . 34

4 Experimental set-up and methods 39
4.1 CMR multiphase flow loop . . . 40
4.2 Bronkhorst F-201CV . . . 42
4.3 Experimental set-up . . . 43
4.4 Methods . . . 44
4.4.1 Point measurement . . . 44
4.4.2 WLR sweep . . . 45

5 Experiments 47
5.1 Experiment 1: The no-gas experiment . . . 48
5.1.1 Measurement set up . . . 48
5.1.2 Procedure . . . 48
5.1.3 Results and discussion . . . 50
5.2 Experiment 2: The gas-injection experiment . . . 57
5.2.1 Measurement set up . . . 57
5.2.2 Procedure . . . 57
5.2.3 Results and discussion . . . 58
5.3 Experiment 3: The CMR flow-rig stress test . . . 61
5.3.1 Measurement set up . . . 61
5.3.2 Procedure . . . 61
5.3.3 Results and discussion . . . 62

6 Measurement uncertainty and error sources 67
6.1 Model uncertainties . . . 67
6.2 Measurement uncertainties . . . 68
6.3 Density error . . . 68
6.4 Density error calculations . . . 70
6.5 Discussion . . . 71

7 Summary and conclusion 73
7.1 Outlook . . . 75

Bibliography 77

Appendix A CMR Multiphase Flow Loop 79

Appendix B Bronkhorst F-201CV Datasheet 85

Appendix C Diesel Quality Certificate 91

Appendix D Viscous motion, results 93

Appendix E Density error estimations 101

Chapter 1

Introduction

Measurement of flow has been important throughout time [1]. Knowledge about air flow speed and direction was important to ancient navigators, ancient communities relied on the ability to measure water flow though the aqueducts to ensure fair distribution of water. The first scientific breakthrough in flow measurements came with Daniel Bernoulli's *Hydrodynamica* in 1738. The concept of *Conservation of energy* for fluid flows was introduced [1]. Bernoulli and Leonhard Euler wanted to study fluid flow, particularly the relationship between pressure and speed of flowing blood [2]. By puncturing an artery with a glass tube, they found that the pressure in the blood flow made the blood rise in the glass tube. The pressure in the flow was dependent on its speed [2]. The discoveries made by Euler and Bernoulli led to Henri Pitot inventing the predecessor to the Pitot-static tube, which is still in use for measuring the airspeed of aircrafts [3].

Flow measurements are used in a variety of applications and industries where measurements of flow rate though pipes are important. This can be industries including food, steel, chemical, oil and gas [4]. Methods and conditions may vary, but the purpose remains the same; to measure the amount of substance flowing through a pipe, as it flows by. Different physical principles are used to measure fluid flow, e.g. [1];

Differential pressure based on Bernoulli's discoveries
Electromagnetic methods based on Michael Faraday's work
Ultrasound measurements, e.g. based on Christian Doppler's Doppler effect
Vortices in an obstructed fluid flow, based on Theodore von Karman's observations
The Coriolis effect based on Gaspard-Gustave Coriolis' discoveries.

These principles all have different limitations, but in general it is a problem when the measured fluid is contaminated by other components. In various applications it is known that the fluid consists of more than one component, and for several decades there has been a need for measuring this kind of flow, also known as multiphase flow [5]. This has

been specially important in the oil and gas industry, where multiphase flow measurements are now considered a separate discipline. Other industries also take advantage of the development of new measurement methods [5].

1.1 Motivation and objectives

It is known that gas bubbles in liquid flow, or liquid droplets in gas flow affects measurements in Coriolis flowmeters. A major cause of this is the large density differences between gas and liquid. The effects of small gas concentrations in liquid flow are investigated in this project. Coriolis flowmeters are commonly used for measurement of two-component liquid mixtures, i.e. diesel-water. The effect of inhomogeneities in these mixtures is also investigated in this project, to see if the small density differences between water and diesel affect measurements. The physical cause of these effects is studied, to better understand the mechanisms behind and how to prevent or utilize these effects.

Christian Michelsen Research (CMR) made their multiphase flowloop available for the experimental work in this thesis. The reference instrument is a Coriolis flowmeter, an Endress+Hauser ProMass 80F. The presence of entrained gas from the separator tank has not been proven, it is therefore of interest to see if entrained gas is present and how it contributes to the uncertainty in the reference measurements.

The objectives of the work are as follows:

1. **To detect a liquid/liquid mix, and find how the measurement quality is affected by the liquid/liquid mixture.** Are we able to detect and quantify a mix of two liquids? Does the flow conditions affect uncertainty if there is a liquid/liquid mix flowing though the Coriolis flow meter?

2. **To detect gas in a liquid/liquid flow, and find how this affects measurements** Are we able to detect if gas is present in a liquid/liquid flow? Can the amount of gas in the flow be quantified? How does gas in the mixture affect measurement quality?

3. **How small amounts of gas is it possible to detect using the Coriolis flowmeter?** Are we able to detect small enough quantities to discover entrained gas in the mixture?

4. **What flow rates can be achieved in CMR's flow rig, without gas entrainment in the liquid.** Can the flow rate limits for when entrained gas occurs be found?

5. **How can the effects of entrained gas or liquid mix be minimized?** If the rig has to be used outside the limits where entrainment occurs, how can the effects of entrained gas be minimized or corrected for? How can effects of liquid mix be minimized or corrected for?

1.2 Outline

The outline of this thesis is as follows:

- **Chapter 1 - Introduction** starts with a short introduction to flow measurements. The motive behind this work and the objectives of the thesis.
- **Chapter 2 - Background and Theory** provides background information about flow measurements, and the physical principles of the Coriolis meter. It also explains the behavior and effects of bubbles in oscillating fluid flow, inside a Coriolis meter.
- **Chapter 3 - Mathematical model** presents a mathematical model of a particle inside the Coriolis flow meter. This is compared to the results of the experimental work. Assumptions made during the modelling are explained and justified, and the results of the modelling are presented.
- **Chapter 4 - Experimental set-up and methods** explains the experimental set-up used in the experiments and CMR's multiphase flowloop, which is used for all the experiments in this thesis. This chapter also includes measurement methods used in multiple experiments.
- **Chapter 5 - Experiments** contains the experimental procedure, results, discussion and any deviations from the general experiment set-up. The chapter starts with a short introduction to the different experiments, and how they relate to the objectives of this thesis.
- **Chapter 6 - Measurement uncertainty and error sources** discusses the different error contributions and uncertainties, both general theory and specific contributions from physical effects.
- **Chapter 7 - Summary and conclusion** contains the summary and conclusion of the thesis. An outlook with future potential of this work is also presented here.

Chapter 2

Background and Theory

This chapter includes background information on fluid flow. It will explain important concepts such as; *fluids*, *flow profiles* and *multiphase flow*. Examples on different measurement principles will be given, as well as thorough description of the *Coriolis flowmeter* and its working principles. Some effects caused by multiphase flow will be explained. In Chapter 3 the impact of these effects are shown.

Flow measurements can be divided into three main groups; *single point velocity measurements*, *volume flow* measurements and *mass flow* measurements. This thesis will focus on mass flow measurements, as the Coriolis flowmeter measures mass flow, but some examples of the others will also be included.

2.1 Fluids - Liquids and gases

Both liquids and gases are fluids, and share fluid properties [4]. In everyday language the term *fluid* is commonly misused as a synonym for liquid, even though this is scientifically wrong. A fluid will flow under the presence of deforming shear forces. The fluid can therefore flow to fit its surrounding container [6]. A fluids resistance against flowing is known as dynamic viscosity, η. A solid will not flow, but remain its shape or deform [4].

Liquids and gases have distinct differences. Gases are in general easy to compress, and density depends on temperature and pressure [4]. The ideal gas law describes this relationship:

$$PV = n\bar{R}T \tag{2.1}$$

where P, V, n and T are absolute pressure, volume, amount of substance and absolute temperature, respectively. $\bar{R}$ is the ideal gas constant. The amount of substance, n is equal to mass, m divided by molar mass, M. The specific gas constant, R is defined as

$\bar{R}$ divided by M giving:

$$PV = \frac{m}{M}\bar{R}T = m\frac{\bar{R}}{M}T = mRT \tag{2.2}$$

Mass per volume is density, ρ. Inserting for ρ shows how density is dependent on pressure and temperature, as R is constant for the specific gas.

$$P = \rho RT \tag{2.3}$$

Equations (2.1), (2.2) and (2.3) are only valid for ideal gases, which are theoretical. For real gases a compressibility factor should be included in the equations [4].

Liquids are considered incompressible, which means that they have no change in volume for a given pressure change. Density, ρ is independent of pressure, but dependent on temperature [4].

2.2 Flow profiles, laminar and turbulent flow

Fluid flow is dependent on flow conditions, there are two distinct types of flow [4]. The ratio between inertial forces and viscous forces determines if the flow is *laminar* or *turbulent*. This ratio between inertial and viscous forces is named Reynolds number, Re, which is dimensionless:

$$Re = \frac{vl\rho}{\eta} = \frac{vl}{\nu} \tag{2.4}$$

The inertial forces are proportional to time average velocity, v, length of the situation, l and density, ρ. Length of the situation could be the diameter of a pipe. The viscous forces are proportional to dynamic viscosity, η. Dividing by ρ gives kinematic viscosity, ν. Multiplying by $\frac{vl\rho}{vl\rho}$, shows that the inertial components in the nominator and the viscous component in the denominator are proportional to force.

If Reynolds number is low (Re <2 000), the flow is considered laminar. A transition region is located between 2 000 and 10 000 (2 000 <Re <10 000). Above 10 000 (Re >10 000) the flow is considered turbulent [4]. It is important to note that these limits are approximations, and different text books will provide different limits.

Laminar flow occurs when viscous forces are large [4]. The viscous forces keeps the particles in the fluid in an orderly manner, and their relative position remains the same. Through a circular, axes symmetric pipe the flow profile can be considered as several annular layers. Their velocity increase from zero close to the pipe wall, to maximum in the center of the pipe. Between each layer there are significant viscous shear stresses. Seen as a cross-section from the side of the pipe, the velocity vectors will create a

parabolic shape, with faster flowing layers in the middle [4].

Turbulent flow occurs when inertial forces dominate viscous forces. The viscous forces are not longer able to keep the particles in an orderly manner, and the movement will have random components in all three dimensions. This leads to random fluctuations of pressure and velocity for a given point in the pipe. The flow profile of a turbulent flow is found by taking the time average velocity, v for each given point in the pipe. Even if the particles are moving randomly, the average velocity will move in one direction. The profile of a turbulent flow resemble laminar profile, but with a flat and wide center.

2.3 Single point velocity measurements

Single point velocity measurements are important in the study of velocity profiles in a tube or velocity distributions around an object placed in a wind tunnel [4]. There are different methods of measuring velocity at a single point. A commonly used meter is the Pitot-static tube, which measures pressure differences. Based on these pressure measurements, flow velocity for a single point can be calculated. This can be applied for both compressible and incompressible fluids. Other methods exist, e.g. hot-wire and hot-film anemometers. These are based on the principles that flow will cool a hot surface, and that the electrical resistance in metal and semi-conductors are temperature dependent. The element is heated by passing a current through it. Heat transfer is dependent on velocity of surrounding fluid flow. Measuring the resistance of the element will provide information for flow velocity calculations. The wire or film is sufficiently small for the measurement to be considered a single point measurement [4].

Consider a circular pipe, we divide this pipe into several annular layers with thickness, Δr, located at a radius, r from the center of the pipe. Each layer will have the cross-sectional area, $A = 2\pi r\Delta r$. The velocity profile for a given point in the pipe is given as $v(r)$. The flow rate for the given point in the pipe, ΔQ is the area of element times velocity [4]:

$$\Delta Q = 2\pi r \Delta r v(r) \tag{2.5}$$

2.4 Volume flow measurements

The total volume flow rate, Q through a circular pipe is the sum of flow rates for all points in the pipe. Evaluating Equation (2.5) for all r in a pipe with radius R, we get:

$$Q = 2\pi \int_0^R v(r) r \, \mathrm{d}r \tag{2.6}$$

It would be impractical and in many cases impossible to consider the velocity variations in the pipe. In many cases it is a sufficient assumption that the cross-sectional flow velocity is constant, and equal to the mean velocity, $\bar{v}$. Mean velocity is defined as total volume flow rate divided by cross-sectional area of the flow [4]:

$$\bar{v} = \frac{Q}{A} \tag{2.7}$$

Another important concept in volume flow rate measurements is the conservation of volume flow. It assumes an incompressible fluid, and is given as:

$$A_1\bar{v}_1 = A_2\bar{v}_2 = Q \tag{2.8}$$

Meaning that if the cross-sectional area of a pipe increases (diameter increases) the mean velocity will decrease [4]. In this case, index 1 is given for the location immediately before any change in flow, and index 2for the location immediately after. Total energy is also conserved. With the assumption that mass is conserved and incompressible fluid, total energy is:

$$E_{tot} = E_1 = \frac{P_1}{\rho_1} + \frac{1}{2}\bar{v}_1^2 + gz_1 = E_2 = \frac{P_2}{\rho_2} + \frac{1}{2}\bar{v}_2^2 + gz_2 \tag{2.9}$$

Where P is pressure, ρ is density, $\bar{v}$ is mean velocity, g is the acceleration constant of gravity on Earth and z is height [4]. Indexes 1 and 2 indicates the locations immediately before and after any change in the fluid flow. For compressible fluids, Equation (2.9) must be modified by adding a term for specific heat ratio, γ to take into account the adiabatic expansion and contraction of the fluid [4]:

$$\left(\frac{\gamma}{\gamma-1}\right)\frac{P_1}{\rho_1} + \frac{1}{2}\bar{v}_1^2 + gz_1 = \left(\frac{\gamma}{\gamma-1}\right)\frac{P_2}{\rho_2} + \frac{1}{2}\bar{v}_2^2 + gz_2 \tag{2.10}$$

Several methods for measuring volume flow rate exist, and the most common for measuring clean fluids are the differential pressure flowmeters [4]. Obstructing the flow will generate a pressure difference. This difference is measured, and based on laws of conservation, volumetric flow rate can be calculated. Examples of differential pressure flowmeters are the orifice plate meter and the Venturi meter. The theoretical equation for volume flow calculations, using differential pressure, in an incompressible fluid is given [4]:

$$Q_{Th} = \frac{A_2}{\sqrt{1 - \left(\frac{A_2}{A_1}\right)^2}}\sqrt{\frac{2(P_1 - P_2)}{\rho}} \tag{2.11}$$

Both area and density are constant, so we can see from Equation (2.11) that by knowing

pressure difference, we can calculate Q. Practical equations for compressible flow can be developed.

Mechanical flowmeters such as the turbine meter also exist. This consists of a turbine placed in the path of the flow. The flow will turn the turbine in a rate proportional to the flow rate. As the volume in the turbine meter is known, the volume flowrate can be calculated by measuring the angular velocity, ω of the turbine. Mechanical flowmeters are often used to count the total amount of fluid passing by over a given time interval [4].

Vortex flowmeters follows the physical principle discovered by von Karman. If a flow is obstructed by an object, a trail of alternating vortices will be generated downstream of the object [4]. As long as the flow is turbulent, the frequency of the vortices are proportional to the velocity of the flow. This assumes an incompressible flow and conservation of volume flow rate. As the volume of the pipe is known, Q can be calculated [4].

Other principles of measuring volume flow rate are also used [4]: Electromagnetic flowmeters measure the velocity, v of a conducting fluid. Based on velocity and known volume, Q can be found. Ultrasound flowmeters measure sound speed in the fluid. There will be a slight time difference if the sound travels with or against the flow direction. Based on the difference in speed of the travelling signal, flow rate can be found. Volume of the pipe is constant, and thus Q can be calculated [4].

All the methods mentioned above utilize different physical principles, but all measure volume flow rate.

2.5 Mass flow measurements

Crude oil, natural gases and hydrocarbon products are bought and sold in units of mass, and often transferred through pipelines from one company to another [4]. Flow measurements are important in custody transfers [7], and accurate measurement are crucial. It is therefore essential to know the exact mass, m, of the fluid that has been transferred through the pipe in a given time.

Equation (2.8) is derived from the concept of conserved mass, assuming no change in density. As mass equals density times volume, mass flow rate, $\dot{M}$ equals density times volume flow rate [4]:

$$m = \rho V \tag{2.12}$$

$$\dot{M} = \rho Q = \rho A \bar{v} \tag{2.13}$$

And conservation of mass flow rate:

$$\rho_1 A_1 \bar{v}_1 = \rho_2 A_2 \bar{v}_2 = \dot{M} \tag{2.14}$$

As we can see, if density is constant, this reduces to conservation of volume flow rate, Equation (2.8). The two main methods of measuring mass are *inferential* and *direct* [4].

2.5.1 Inferential methods

The principles of inferential methods are computing mass flow rate from volume flow rate and density, using the relationship between mass, density and volume, see Equation (2.13).

For pure liquids, the density is dependent on temperature only. Density is assumed to be constant if temperature fluctuations are small. Measurements of volume flow can be obtained from e.g. a mechanical flow meter, and thereafter used to calculate $\dot{M}$, according to equation (2.13). Measurements of density are necessary if variations in temperature are significant. Both temperature and composition affect density in liquid mixtures, thus ρ must be measured. This also applies to gases. For pure gases density is dependent on both pressure and temperature, and for gas mixtures density is dependent on pressure and temperature, in addition to composition [4].

An example of a mass flow measurement, using the inferential method, could be a turbine meter measuring volume flow. To calculate mass flow, a density measurement is required. This is usually taken using vibrating element density transducer. The transducer gives a frequency which is dependent on fluid density. These values combined can be used to calculate mass flow rate [4].

2.5.2 Direct methods

Direct measurements of mass flow rate, $\dot{M}$, can also be referred to as true measurements of mass flow rate [4]. In these methods the measurement of $\dot{M}$ is directly dependent on the mass flow through the pipe. The direct methods can be more accurate than the inferential methods, due to independence from other measurements and calculations. Coriolis flowmeters, which is based on the Coriolis effect, are currently the most used direct mass flow meters [4].

Even though there can be difficulties related to entrained gas, direct mass flow meters have an advantage over volume flow meters when measuring liquids with entrained gas. Because the density of gas is so small compared to that of the liquid, the mass flow measurement is close to that of a pure liquid. In the opposite case, when measuring wet

gas, the direct mass flow meter would encounter problems because the density of the droplets is high compared to that of the gas [7].

2.6 The Coriolis effect

The Coriolis effect is a fictitious force, in the sense that it is necessary for Newton's laws to apply for a rotating system (constantly accelerating) [8]. It can be seen as a correction factor in a rotational system. If an object move across a rotating surface, the movement can be described from an inertial viewpoint, and the object will move in a straight line. If however, the viewpoint is fixed to the rotational surface, the objects movement will deflect and move in a curved path [8].

This was first described mathematically by the French scientist Gaspard-Gustave Coriolis. Coriolis described the effect when working with water wheels. Later it has seen other applications, such as in metorology and the Coriolis flowmeter [8].

The effect is easy to observe on weather forecast maps. The Coriolis effect cause moving objects in the nothern hemisphere to deflect clockwise (and opposite in the southern hemisphere) [8]. This is why we in Bergen, Norway would like the low pressure systems to arrive the coastline south of us. That would make the winds come from a south-east direction, which is good. If the low pressure system arrive north of Bergen, the winds will come in from a cold north-west direction. Note that since winds blow towards low pressure systems, the system seems to rotate in counter-clockwise direction.

2.7 Coriolis flowmeter

During the last decades the Coriolis flowmeter have become common for measurements of mass flow and density in various industries. Especially in offshore production installations, it is becoming a widely acknowledged technology [9]. Coriolis flowmeters have gained acceptance, and new fields of applications continuously develop every year. The Coriolis flowmeter has several advantages, examples being: Direct mass flow measurements and density measurements at the same time, high accuracy and repeatability [10]. The fact that both density and mass flow rate are measured at the same time gives the possibility to calculate the Water Liquid Ratio (WLR) directly [9].

The Coriolis flowmeter utilizes the Coriolis effect to measure mass flow. Eriksson *et al.* [11] has a thorough derivation of the Coriolis acceleration, a_c, giving Equation (2.15). This involves studying the transformation from a fixed or inertial reference frame to a

rotating reference frame.

$$a_c = -2\boldsymbol{\omega} \times \boldsymbol{v} = -2\omega v \sin(\theta) \tag{2.15}$$

Where θ is the angle between the vectors. Multiplying by mass, the magnitude of the Coriolis force, F_c becomes [12]:

$$F_c = 2m\omega v \sin(\theta) \tag{2.16}$$

A very simple Coriolis flowmeter could consist of a U-shaped tube, which is oscillated by a driving circuit, and sensors to measure frequency, amplitude and phase of the oscillating tube. The phase sensors are used to find the phase difference between the inlet and the outlet of the tube. For commercial flow meters, the shape of the tube will be different from one vendor to another. The shape will also differ to meet different operational benefits [10]. There is no need for the angular velocity ω to be constant, the Coriolis force is also present if the rotating frame is oscillating [12]. If ω varies sinusoidally with time, at constant frequency, f, and maximum amplitude, $\hat{\omega}$, ω is given as:

$$\omega = \hat{\omega} \sin(2\pi f t) \tag{2.17}$$

The necessary contributions for the Coriolis force to appear are given by oscillation of the tube, ω, fluid velocity, v and mass of the fluid, m. The Coriolis force causes the tube to twist, and the twist angle can be measured by measuring phase difference between inlet and outlet of the tube [10].

Figure 2.1 shows a simplified Coriolis flowmeter, represented as a U-shaped tube, **ABCDE**. The tube will oscillate sinusoidally, with constant frequency, f, and varying angular velocity, ω about the axis **AE**. A theoretical mass element, with the length Δx, travels trough the pipe with velocity v. The mass of the element will be

$$\Delta m = \rho A \Delta x \tag{2.18}$$

Where ρ is density of the mass element and A is the cross-section of the tube. From (2.16) it is given that the mass element experiences a force of magnitude

$$\Delta F = 2\Delta m \omega v \sin(\theta) = 2\rho A \omega v \Delta x \sin(\theta) \tag{2.19}$$

Looking at only one leg (**AB**) of the tube, with the length l, we calculate the total force

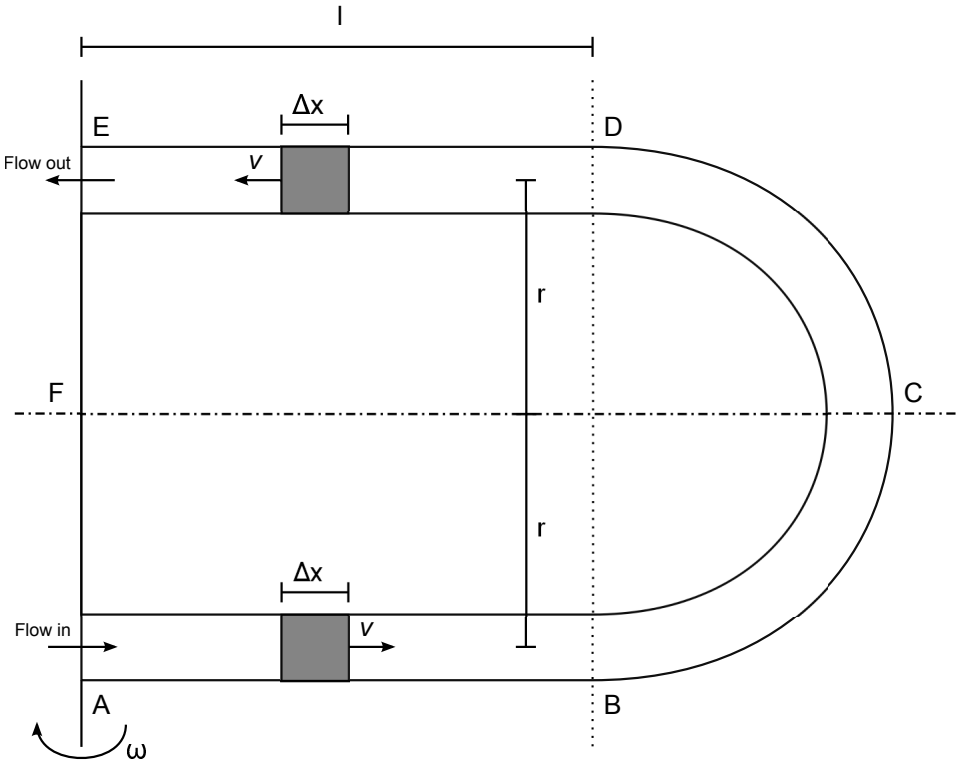

Figure 2.1: A simplified Coriolis tube. A mass element, with length Δx moves through the oscillating tube, with velocity v. The Coriolis tube will experience a torque, T about the centerline (CF). Made with inspiration from Bentley [4].

on that leg. The angle between the v and ω is 90 degrees, giving $\sin(90) = 1$:

$$F = 2\rho A\omega v \int_A^B \mathrm{d}x = 2\rho A\omega v l \tag{2.20}$$

An equal, but opposite directed force will affect the other leg (**DE**). In the bend **BCD**, the velocity vector is considered close to or parallel to ω. If the angle between v and ω is ≈ 0, Equation (2.16) will give $F_c \approx 0$, since $\sin(0) = 0$.

A torque is experienced by the tube about the center line (**CF**):

$$T = F2r = 4lr\omega\rho Av \tag{2.21}$$

Inserting mass flow rate, $\dot{M} = \rho Av$ from Equation (2.13) we get

$$T = 4lr\omega\dot{M} \tag{2.22}$$

saying that the torque is proportional to $\dot{M}$. The twist angle of the tube, θ is given by

$$\theta = \frac{T}{c} = \frac{4lr\omega}{c}\dot{M} \tag{2.23}$$

the elastic stiffness of the tube is denoted c. As ω varies sinusoidally over time, so does the twist angle [4].

The Coriolis flowmeter can also provide accurate density measurements at the same time as the flow measurement. A peak detector circuit, or phase lock loop, will keep the excitation of the tube at the resonance frequency of the measuring tube [10]. The natural frequency is determined by the material properties of the tube, and also by the density of the content within the tube. Therefore, by knowing the natural frequency of the tube, one can calculate the density of its contents, since the other contributors to the natural frequency are constants [12].

Plache [12], writes that the period of oscillation of a mass/spring system is given by

$$\tau = \sqrt{\frac{2\pi m}{k}} \tag{2.24}$$

It is however assumed that this equation should be:

$$\tau = 2\pi\sqrt{\frac{m}{k}} \tag{2.25}$$

Where m is the mass of the system, k is the system spring constant and τ is the period of oscillation. Mass is determined by two factors, the properties of the tube and the content within the tube. Dividing this into two parts, the mass of the tube, m_t and the mass of the content in the tube, m_f:

$$\tau = 2\pi\sqrt{\frac{m_t + m_f}{k}} \tag{2.26}$$

further, m_f can be split up into the volume of the tube, V_t and the density of the fluid, ρ_f

$$\tau = 2\pi\sqrt{\frac{m_t + V_t\rho_f}{k}} \tag{2.27}$$

where m_t, V_t and k are all fixed constants, defined by the geometry and properties of the flow meter. Thus, the density of the fluid, ρ_f is the only variable to affect the oscillation period, τ [12].

Coriolis flowmeters have some disadvantages, especially in two- or multiphase flows. These flow conditions are typical for the oil and gas industry [10]. Aerated liquids can cause significant measurement errors, even with small void fractions of entrained gas, manufacturers are making an effort in sorting out these problems [13]. The decreased performance expected when measuring liquid mixtures can be diminished when the mixture is well dispersed [9].

2.8 Multiphase flow, and effects in Coriolis flow meters

The term *multiphase flow* is used to describe flow that consists of more than one component. This could be gas and liquid or liquid and solids. In the oil and gas industry it is considered multiphase even if the components are the same phase, as in a diesel/water mixture. Two important expression commonly used when describing multiphase mixtures are WLR and Gas Volume Fraction (GVF).

Water Liquid Ratio (WLR) is a ratio that tells how much water it is in a liquid/liquid flow. This can be expressed in terms of void fraction, α and mean velocity of the liquid, $\bar{v}$. This is usually used for oil/water flows, e.g.

$$WLR = \frac{\alpha_{water}\bar{v}_{water}}{\alpha_{water}\bar{v}_{water} + (1-\alpha_{water})\bar{v}_{oil}} \quad \text{and} \quad \alpha_{water} + \alpha_{oil} = 1 \tag{2.28}$$

This could also be expressed in terms of volume flows:

$$WLR = \frac{Q_{water}}{Q_{water} + Q_{oil}} \quad \text{and} \quad Q_{water} + Q_{oil} = Q_{total} \tag{2.29}$$

Gas Volume Fraction (GVF) is a ratio that tells how much gas it is in a mixture, typically a liquid/gas flow. As for WLR, this can also be expressed in terms of void fraction, α and mean velocity of the fluid, $\bar{v}$, where:

$$Q_{gas} = \alpha_{gas}\bar{v}_{gas} \tag{2.30}$$

Q_{liquid} represents the total volume flow of liquids, giving:

$$GVF = \frac{Q_{gas}}{Q_{liquid} + Q_{gas}} \quad \text{and} \quad Q_{liquid} + Q_{gas} = Q_{total} \tag{2.31}$$

Multiphase flow can introduce problems when using a Coriolis meter, despite its inherent advantages in some of these conditions. High viscosity can trap gas within liquid, and bring gas downstream to places one could assume the flow to be single-phase. Pump cavitation could create gas bubbles. You could also intentionally measure fluids of two or several phases [10].

Experiments show that both density and mass flow rate measurements deviate from the true values in the case of two-phase flow [14]. Even single phase flows, with small amounts of another phase, i.e liquid flow with entrained gas, decrease the accuracy of the Coriolis flowmeter's performance [10].

There are several effects which can influence Coriolis mass flow and density measurements: *Decoupling*, also referred to as the particle effect or bubble effect. *Compressibility*, also known as the resonator effect or velocity of sound effect [7], [10], [15]. Asymmetry in bubble distribution [15] and suboptimal installation [9] could also lead to error in Coriolis flowmeters. Error contributions caused by multiphase flow are usually dominated by decoupling effects [15]. This thesis will mainly focus on decoupling, later in this chapter it will be explained how compressibility errors are positive and decoupling errors negative.

Error caused by asymmetry in bubble distribution usually happen at low flow rates. Coriolis flowmeters calculate the mass flow rate based on phase difference between inlet and outlet ends of the measuring tube. Any content differences between the inlet and outlet would cause mass flow measurement errors. Dependent on installation orientation gas can accumulate on either inlet or outlet end of the measuring tube. This can give rise to altered damping caused by decoupling. Higher flow rates preventing gas from accumulating, and giving a more homogeneous mix will prevent this effect [15].

Installation induced errors are also most likely to occur at low flow rates. This effect is caused by uneven distribution between two measuring tubes in a two-tube Coriolis flowmeter. The problem occurs if the meter is installed with the measuring tubes pointing horizontally out from a horizontal flow line. Gravitational forces can cause uneven distribution of components of different densities [9]. The uneven distribution of mass cause unbalanced vibration. This will cause the Coriolis meter to be more sensitive to external vibrations which can result in mass flow and density measurement errors. This effect can be prevented with high flow rates and homogeneous mixing, in addition to well planned installation of the Coriolis flowmeter [9], [15].

2.8.1 Decoupling

A pure liquid is assumed to move in the transverse direction through the flow tube, with centre of gravity of the fluid located in the middle of the cross-section of the tube. If the flow consists of more than one component, and these components are of different density, this assumption is not longer valid.

In the case of an oscillating environment, less dense bubbles will experience higher acceleration in the direction of tube oscillations than denser bubbles of the same size. This leads to relative motion between particles and fluids of different densities, and changes in the mixture's Center of Gravity (CG). *Decoupling* refers to this relative motion, perpendicular to flow direction, between components of different density [15]. Decoupling must not be confused with phase slip, which is difference in velocity between

components in the direction of flow.

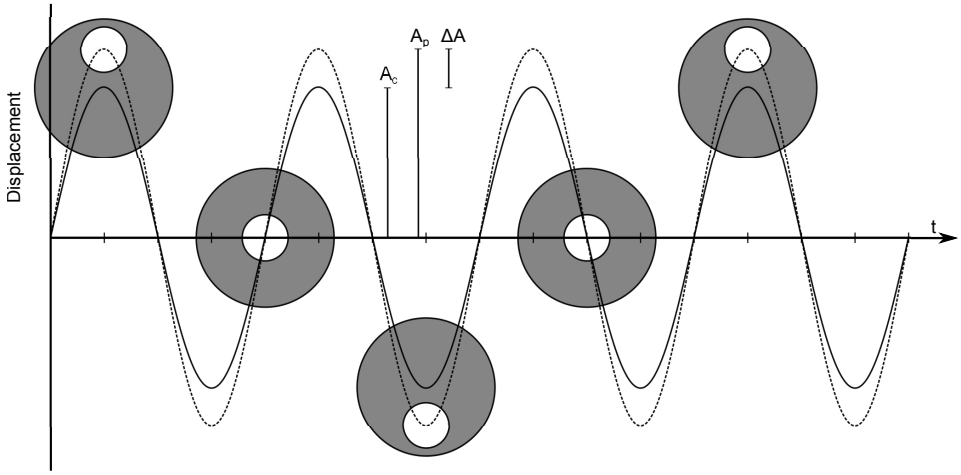

Figure 2.2: Cross section of a liquid (grey) filled Coriolis tube, containing a bubble (white), undergoing oscillations. The bubble will oscillate with a different amplitude than the Coriolis tube.

Figure 2.2 shows the cross section of a tube, containing liquid (grey) and a gas bubble (white). The bubble is less dense than the surrounding liquid. When the tube oscillates, the bubble will oscillate with a different amplitude than the tube. In the figure, tube amplitude, A_c, bubble amplitude A_p and amplitude difference, ΔA, are shown.

The relative motion between the liquid and bubble will generate a flow of liquid around the bubble. In the case of a bubble, with lower density than the surrounding liquid, this liquid flow will move in the opposite direction of the oscillating tube. The inertia of the liquid felt by the tube wall will be reduced, and some of the liquid will be undetected by the meter. This leads to underestimation of mass flow and density measurements [10], [15].

Figure 2.3 shows the tube containing liquid and a gas bubble. When the tube is at the center point of the oscillations (left), the bubble is located in the center of the tube. Center of Gravity (CG), illustrated with "+", is also located in the center. When the tube moves upwards (middle), the bubble's displacement will be greater than the tube's. CG will move inside the tube, and a flow will be generated around the bubble. At the peak point of the oscillation (right), the bubble movement has caused CG to be at a different location than expected. The expected location of CG, in the case of no relative motion, is marked with an "x".

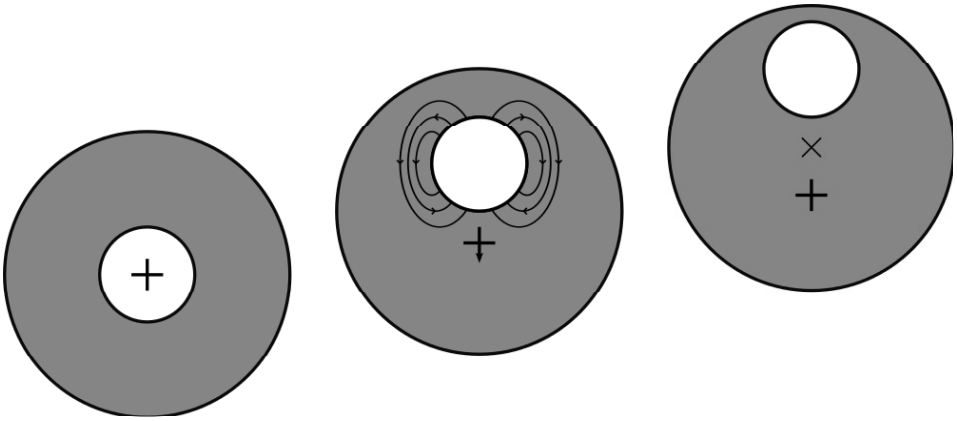

Figure 2.3: Cross section of a Coriolis tube, showing movement of the center of gravity (+) and direction of liquid flow around a bubble (white). The Coriolis tube undergoes oscillations. The expected location of the center of gravity, in the case of no relative motion between bubble and liquid, is marked with an "x". Made with inspiration from [10]

2.8.2 Compressibility

If the sonic velocity of the fluid is low, or the oscillation frequency of the measurement tube is high, compressibility effects can cause measurement errors [15]. This is usually not a problem in pure flows, even for gases with low sonic velocities. A mixture has lower sonic velocity than any of its individual components. The Newton-Laplace equation gives the speed of sound, c

$$c = \sqrt{\frac{B}{\rho}} \tag{2.32}$$

Where ρ is density and B is bulk modulus. If a pure liquid gets just a small fraction of gas mixed in, the density would remain nearly the same as initially, but the compressibility would increase. As bulk modulus is the inverse of compressibility, speed of sound would decrease. An acoustic resonance could be produced within the tube, and if the tube oscillation frequency approaches the resonance frequency, resonant motion of the fluid is expected. [16]. In single-phase fluids, with high sonic velocity, the resonance frequency is much greater than the driving frequency of the measuring tube. If gas is introduced to a liquid flow, speed of sound will decrease and resonance can occur [15]. This will cause the fluid to move faster than the tube, and more inertia will be sensed by the tube wall, which leads to overestimation of both density and mass flow rate [16]. This effect can also be explained by the fluid being compressed against the wall of the tube. This causes the fluid to be denser at one side of the tube, or movement of CG. The inertia felt by the tube wall will be greater, which leads to positive density and mass flow measurement errors.

Both compressibility errors and decoupling error are caused by movement of CG, but

in opposite directions. This causes the error contributions to be in opposite directions as well: decoupling causes negative errors and compressibility causes positive errors.

2.8.3 Flow conditions

Multiphase flow is difficult to predict and model [5]. The distribution of different phases can vary over time and space, and single-phase methods of describing flow are no longer sufficient. How the different phases are distributed, *flow regimes*, are dependent on many factors, such as: Flow rate, orientation of the tube, geometry of the tube, temperature, pressure, density, viscosity, and more. The cause of different flow regimes can be divided into three main mechanisms [5]:

- **Transient effects** are caused by changes in the boundary conditions of the system, such as opening and closing of valves.
- **Geometry and terrain effects** are effects due to changes in geometry and inclination of the pipe.
- **Hydrodynamic effects** are effects caused by fluid properties, pipe properties and flow rate. These are the only contributors to steady state flow regimes in the absence of transient effects and geometry and terrain effects.

The flow regimes caused by said mechanisms can also be divided into three groups:

- **Dispersed flow.** Uniform phase distribution is the characterization of dispersed flow. This distribution has to be uniform both in axial and radial directions. Bubble flow and mist flow are examples of dispersed flow.
- **Separated flow.** If the flow has non-continuous phase distribution in the radial direction, and continuous in the axial direction, it is a separated flow. Annular and stratified flow are examples of separated flow.
- **Intermittent flow.** In the case of continuous phase distribution in the radial direction, and non-continuous in the axial direction, it is a intermittent flow. Examples being slug and churn flow.

Liquid/liquid interactions cause less pronounced flow regimes than liquid/gas interactions. In a multiphase flow, the liquid/liquid part of the flow can be seen as a dispersed flow, with some reservations regarding volumetric ratio of the liquid components [5].

Flow regime maps can be created to illustrate how flow regimes are dependent on superficial flow rates of different phases. In the *Handbook of multiphase flow metering*

[5] two such maps are presented, Figure 2.4 and 2.5. Superficial velocity is the velocity the specific component would have, if it was the only component present in the flow. Note that these maps do not include physical parameters such as: Density, viscosity, surface tension, etc [5].

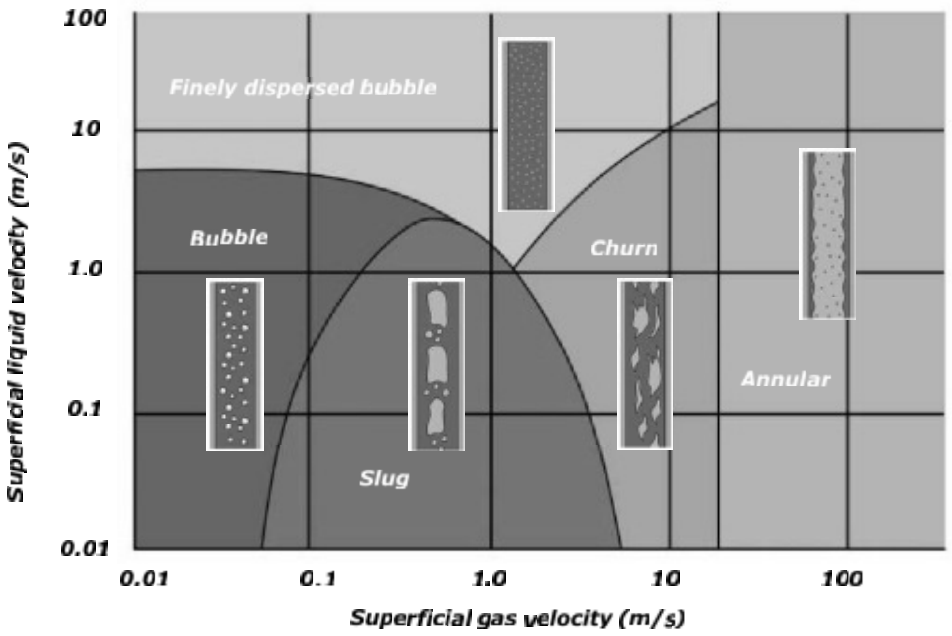

Figure 2.4: A generic two-phase vertical flow map, note that superficial velocities are used along the axis [5].

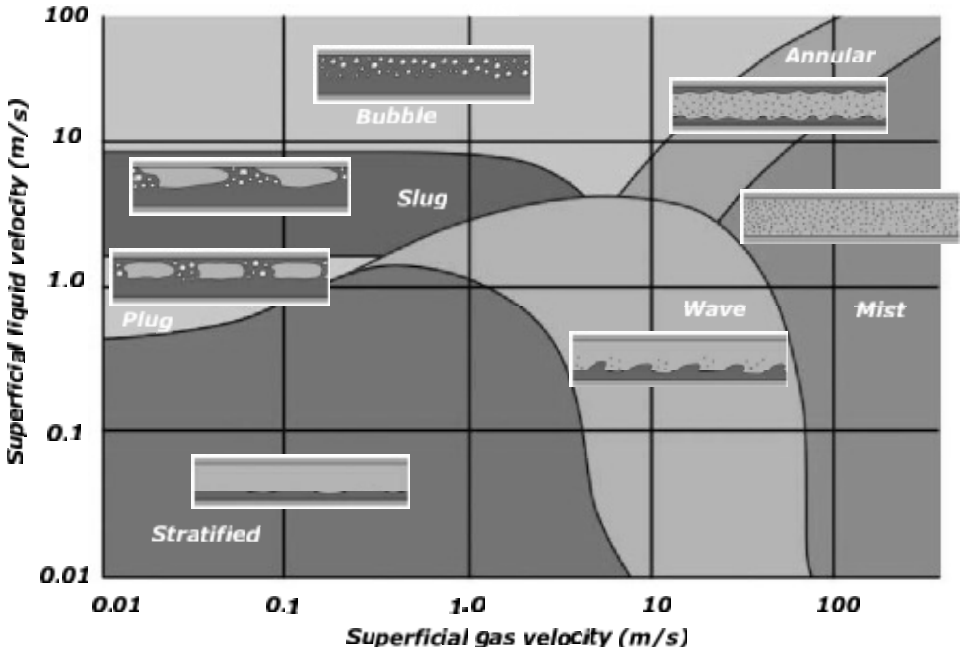

Figure 2.5: A generic two-phase horizontal flow map, note that superficial velocities are used along the axis [5].

2.8.4 Effective viscosity

Viscosity affects the movement of bubbles and particles though a medium [17]. A particle moving through a two-phase medium induce a movement in the continuous phase, which again causes movement of other particles dispersed in the mixture. These particles combined will cause stresses to the surrounding fluid, due to the fact that they are more rigid against deformations than the fluid. These stresses cause the original particle to experience more resistance against its movement than it would if it was the only particle in the fluid. This increased resistance appear as increased viscosity. This makes the experienced viscosity dependent on concentration, fluid viscosity and particle viscosity. To estimate the viscosity of a mixture, Ishii *et al.* [17] developed Equation (2.33).

$$\frac{\mu_m}{\mu_c} = \left(1 - \frac{\alpha_d}{\alpha_{dm}}\right)^{-2.5\alpha_{dm}\frac{\mu_d+0.4\mu_c}{\mu_d+\mu_c}} \tag{2.33}$$

Where a_{dm} is the maximum packing factor of particles, a_d is particle void fraction, μ_m is mixture viscosity, μ_c is viscosity of the continuous phase and μ_d is the viscosity of the particles. Maximum packing factor should be set to 0.62 for solid particle systems. For fluid particle systems, packing can get much higher, and a_{dm} should be set to 1 [17].

Chapter 3

Mathematical model

In this chapter a mathematical model for particle movement will be presented. The model is later used to predict change in power dissipation in the Coriolis flowmeter, due to changing conditions. Several cases are studied, to see how different conditions can affect particle movement. The results are compared with the experimental results, when these are discussed in Chapter 5.

A model that explains viscous forces is needed to explain particle movement in fluid. Before a *viscous model* is presented, a model for the *invisid* forces is described.

3.1 Equations of motion - Inviscid model

To investigate the motion of a bubble or particle in a fluid, we start by looking at the inviscid forces acting on the particle. Following the derivation by Basse [18], and explanations by Weinstein [15], we consider the case of a particle in fluid exhibiting oscillatory motion, induced by an external force. The equation is given:

$$F_{total} = F_{addedmass} + F_{buoyancy} = \frac{1}{2}\rho_f V_p \left(\frac{du}{dt} - \frac{dv}{dt}\right) + \rho_f V_p \frac{du}{dt} \tag{3.1}$$

Where ρ is density, V is volume, u is fluid velocity and v is particle velocity. Subscripts "p" and "f" are particle and fluid, respectively. Two forces act on the particle *added mass* and *buoyancy*.

Added mass is a force caused by acceleration of the surrounding fluid the particle displace as the particle moves along. Weinstein [15] states that it is difficult to determine coefficients for this force, if the particle is of an arbitrary shape. A sphere shaped particle however, simplifies the calculation and it is found to be half the mass of the displaced fluid. No compression is considered, so the volume of the sphere particle equals the

volume of the displaced fluid.

The buoyancy force is caused by fluid acceleration relative to an inertial frame. Consider a bottle of water, containing one solid particle (e.g. a stone), by accelerating the bottle in one direction, you would expect the particle to "lag behind" as it is denser than the surrounding fluid. If the bottle contained a gas bubble, the case would be opposite and the bubble would accelerate faster than the bottle. If your view was fixed to the bottle, the acceleration of the particles would resemble the acceleration of particles in water, with only gravity acting on them. A pressure gradient is caused by the acceleration of the fluid. This is the origin of the buoyancy force.

Rearranging, and substituting $F_{total} = m_p \frac{dv}{dt}$ and $m = V\rho$ in Equation (3.1), we get:

$$\frac{dv}{dt} = \frac{du}{dt}\left(\frac{3\rho_f}{2\rho_p + \rho_f}\right) \tag{3.2}$$

Consider the case of a particle surrounded by fluid, in an oscillating tube. If the density of the fluid is close to infinity, and $\rho_f \gg \rho_p$, the particle will experience 3 times the acceleration of the fluid. If the densities are equal, the acceleration will also be equal. If the particle is denser than the fluid, the fluid will have larger acceleration than the particle. As the fluids acceleration is determined by the oscillating tube, a very dense particle will experience no acceleration. Acceleration can be integrated with respect to time, to find velocity or displacement.

3.2 Equations of motion - Viscous model

An invisid model would not be sufficient to describe a real life environment, so a viscous model is necessary. Modelling of a particle's oscillating movement through a fluid is quite complicated, so modifications to pure translational equations must be made. Basset is usually credited for developing equations for unsteady motion through viscous fluid, with no-slip conditions [15], shown in Equation (3.3):

$$\begin{aligned}\frac{4}{3}\pi a^3 \rho_p \frac{dv}{dt} =& \frac{4}{3}\pi a^3 g(\rho_p - \rho_f) + 6\pi\eta_f a(u - v) + \\ & 6a^2\sqrt{\pi\eta_f\rho_f}\int_{-\infty}^{t}\left(\frac{du}{ds} - \frac{dv}{ds}\right)\frac{1}{\sqrt{t-s}}ds + \\ & \frac{2}{3}\pi\rho_f a^3\left(\frac{du}{dt} - \frac{dv}{dt}\right) + \frac{4}{3}\pi\rho_f a^3\frac{du}{dt}\end{aligned} \tag{3.3}$$

Where a, g, ρ, u, v and η is particle radius, gravitational acceleration, density, fluid velocity, particle velocity and viscosity, respectively. Subscripts "f" and "p" are fluid

and particle.

The first term on the right hand side of Equation (3.3) is force due to gravity. When flow rates are high, particles spend only a short time inside the Coriolis flow meter, and gravity has little time to affect the movement of the particle. We assume that the gravity term can be neglected in practical applications. At low flow rates, asymmetry and installation effects can occur due to gravity, see Section 2.8. The second term is the Stokes drag law. Third term is the Basset force or history force, due to the particle moving in it's own wake. The fourth term is the added-mass effect and the final term is the buoyancy-force. When neglecting the gravity-component, the equation for F_{total} can be written:

$$F_{total} = F_{drag} + F_{history} + F_{addedmass} + F_{buoyancy} \tag{3.4}$$

Weinstein [15] presents two sets of equations with modifications for oscillation motion and different boundary conditions, *no-shear-stress* and *no-slip*. *No-shear-stress* applies for very pure bubbles in fluid. In these conditions the bubble would not experience any velocity gradient at the surface. The no-slip equations assume a solid particle, but are also the equations that best describe droplets or impure conditions. For the conditions we want to investigate, the particle's motion will be between the two limiting cases, but the case of *no-slip* will be the model that best describes this motion. Only the no-slip equations will be presented below, no-shear-stress equations can be found in Weinstein [15].

From Section 3.1 we expect forces from added mass and buoyancy, as well as two new forces, *Drag* and *History*:

Bouyancy

This is the force created by the accelerating reference frame. It is the same terms as in the inviscid expression, assuming a sphere particle.

$$F_{buoyancy} = \rho_f V_p \frac{du}{dt} = \frac{4}{3}\pi\rho_f a^3 \frac{du}{dt} \tag{3.5}$$

Added mass

This term is also from the inviscid expression, and is also assuming a sphere particle. The added mass effect is the force experienced by the particle when pushing the surrounding fluid away.

$$F_{addedmass} = \frac{1}{2}\rho_f V_p \left(\frac{du}{dt} - \frac{dv}{dt}\right) = \frac{2}{3}\pi\rho_f a^3 \left(\frac{du}{dt} - \frac{dv}{dt}\right) \tag{3.6}$$

Drag

The equation for Stokes drag force for no-slip conditions is given as follows [15]:

$$F_{drag} = 6\pi\mu_f a(u - v) \tag{3.7}$$

This expression is limited to low Reynolds numbers, instantaneous time-dependent oscillatory Reynolds number, not the common flow-rate related Reynolds number [15]. The Reynolds number is dependent on the relative motion in the direction of oscillation, particle size and kinematic viscosity. It is given by the expression:

$$Re = \frac{2a(u - v)}{\nu_f} \tag{3.8}$$

Empirical correction factors, $\phi(Re)$, have been found to account for higher Reynolds numbers. These are different for different conditions. The ones presented her are valid for no-slip conditions. The correction factors, $\phi(Re)$, are [15]:

$$\phi(Re) = 1 + (3/16)Re, \quad 0 < Re \leq 0.01 \tag{3.9}$$

$$\phi(Re) = 1 + 0.1315Re^{0.82-0.05w}, \quad 0.01 < Re \leq 20 \tag{3.10}$$

$$\phi(Re) = 1 + 0.1935Re^{0.6305}, \quad 20 < Re \leq 260 \tag{3.11}$$

$$\phi(Re) = 1.8335(Re)10^{-1.1242w+0.1558w^2}, \quad 260 < Re \leq 1500 \tag{3.12}$$

Where:

$$w = log_{10}Re \tag{3.13}$$

Giving an expression for drag force, valid for no-slip conditions and Reynolds numbers up to at least 1500 [15].

$$F_{drag} = 6\pi\mu_f a(u - v)\phi(Re) \tag{3.14}$$

History

The history force, or Basset force, is the term that takes into account previous movement of the particle. The particle movement generate vortices in the boundary layer, due to relative motion between the particle and the surrounding fluid. These vortices require some time to diffuse, and will affect the particles movement when moving. They are caused by the relative acceleration between particle and fluid, so in an oscillating system it is a force to consider. Basset's expression for the history force is [15]:

$$F_{history} = 6a^2\sqrt{\pi\eta_f\rho_f}\int_{-\infty}^{t}\left(\frac{du}{ds}-\frac{dv}{ds}\right)\frac{1}{\sqrt{t-s}}ds \tag{3.15}$$

Several other expressions have been developed.

The integration form of the equation can be simplified for different conditions [15], and the applicable equation for a rigid sphere particle, in no-slip conditions, is given as:

$$F_{history} = 6\pi\eta_f a\left[\frac{u-v}{\delta}+\frac{\delta\tau_v}{2}\frac{d(u-v)}{dt}\right] \tag{3.16}$$

This contain two new dimensionless parameters:

$$\tau_\nu = \frac{a^2}{\nu_f} \tag{3.17}$$

$$\delta = \sqrt{\frac{2\nu_f}{a^2\omega}} \tag{3.18}$$

τ_ν is a viscous diffusion time scale, and δ is the inverse Stokes number, the ratio between the oscillation time scale and the viscous diffusion time scale.

These are the equations used for modelling. For convenience, Equation (3.4) is repeated:

$$F_{total} = F_{drag} + F_{history} + F_{addedmass} + F_{buoyancy}$$

Where the terms used when modelling are:

$$\begin{aligned}
F_{drag} &= 6\pi\mu_f a(u-v)\phi(Re)\\
F_{history} &= 6\pi\eta_f a\left[\frac{u-v}{\delta}+\frac{\delta\tau_v}{2}\frac{d(u-v)}{dt}\right]\\
F_{addedmass} &= \frac{2}{3}\pi\rho_f a^3\left(\frac{du}{dt}-\frac{dv}{dt}\right)\\
F_{buoyancy} &= \frac{4}{3}\pi\rho_f a^3\frac{du}{dt}
\end{aligned}$$

3.3 Assumptions and methodology

The previously explained equations are used. As these equations are found in Weinstein [15], most of the assumptions are also found here. The models for viscous and inviscid motion are made for a single particle surrounded by fluid. The particle and fluid's axial flow through the pipe is considered unimportant, because the entire inertial reference frame is translating. This is also backed up by Weinstein's experimental results [15].

Most of the modelling in this thesis follows the work conducted by Weinstein [15], with respect to equations and assumptions. However, it deviates when it comes to concentrations. Weinstein's work concentrates around modelling particle movement, and model validation with experiment, investigating the movement of one single particle in fluid. The experiment Weinstein is conducting is directly comparable to the results from the model. This thesis investigate the effect of higher and varying concentrations. The effect of different inputs to the model will be compared to the measurements of different inputs to the flow rig. The model and experiments will not be compared numerically, but results from the model will be used to explain the measured response in the experiments.

Wall effects are assumed to be negligible, bubbles tend to stay in the middle of the pipe when flowing so most bubbles will be located far away from the walls. However, for bubbles closer than two radii from the wall, the drag forces are affected and this could be a source of error [15]. In this thesis the bubbles are considered small compared to the pipe diameter, and despite large concentrations of bubbles this effect is neglected. Droplets with higher density than the continuous phase will flow close to the walls, the *Handbook of multiphase flow metering* [5] states that the flow regime in a liquid/liquid mixture often can be seen as a dispersed flow. All though this assumption is concentration dependent, wall effects are assumed to be negligible also for the liquid/liquid modelling.

The motion of particles can be affected by surrounding particles. This could be by collisions between particles or particles creating wakes or disturbing the flow field so that other particles are affected. Weinstein [15] assumes so low concentrations that particle interactions are limited. The particle concentrations studied in this thesis are so large that this assumption can't be made. A particle could follow in another particles wake. If it catches up with the first particle, the pair will begin tumbling and could cause coalescence and turbulence in the continuous phase. This could lead to areas with high particle volume fractions, and other areas with almost no particle void fractions. A model that takes these interactions into account has not been developed [19]. Due to the lack of a better model, the one valid for low void fractions is used. Both Weinstein [15] and Ishii *et. al.* [17] explains that interactions and proximity to other particles can be seen as an increase in effective viscosity felt by the particle. All though a rough assumption, these equations are assumed valid for higher concentrations when introducing effective viscosity to compensate. Brennen [19] states that relative motion between phases decreases with increasing concentration, this is in agreement with the theory of increasing viscosity, Ishii *et. al.* [17]. In the the area where the model is assumed to be least valid (high particle concentrations), it is likely to believe that the drag force is increased by the increased concentrations.

Unfortunately the size of bubbles and droplets can't be observed or measured in the

flow rig. Morales *et al.* [20] studied droplet size and distribution from a centrifugal pump. They used different concentrations of oil in water, at different flow rates and varying pump speed. Experimental results show that close to the centrifugal pump droplet size is mostly dependent on pump speed. Flow rate and concentration have less impact. Based on this work, a mean droplet size is assumed. This size will be based on pump speed alone, neglecting the effects of flow rate, viscosity and concentration. Assuming the Coriolis flowmeter is located close enough to the pump for the pump effects to dominate the development of flow rate dependent flow regimes. Morales *et al.* do not investigate water in oil, their discoveries are used to estimate the size of water droplets as well, despite the fact that this might be wrong.

The final assumption might be somewhat rough. In real life, the particle will move through a pipe line. The oscillation amplitude is not uniform inside the Coriolis flowmeter. The amplitude felt by the particle will start at zero, and gradually increase as the particle moves towards the center point of the bend, then decrease again while moving towards the end of the measuring tube. When solving the equations, a constant amplitude is assumed. The magnitude of the results in therefore not directly comparable with the observed response, but the results may still be used to investigate the response when different parameters are altered.

MATLAB is used to obtain the results of particle motion. All input parameters are either assumed or found from measurements. The code for solving these equations are based on the software code written by Weinstein, and explained in Weinstein [15]. The equations are solved for particle velocity, *v(t)*, with ODE45, MATLAB's built-in differential-equation solver.

The software code is built to solve for different WLR. In the Coriolis flowmeter the frequency would change with changing density. The software code operates with a constant oscillation frequency when solving the equations, and does not change this when going though the WLR range. Based on experience, a change in continuous phase is expected at about $WLR = 45\%$, this value is used when solving the equations.

The software code uses MATLAB's built in functionality to estimate a transfer function between the input signal and particle response. From this transfer function phase shift and amplitude ratio are obtained. Calculating power dissipation is based on these values.

3.4 Calculating WLR

In CMR's flow rig, the WLR calculations are based on density measurements. Reference density, ρ_{ref} of diesel and water is measured, reference temperature , T_{ref} is measured

at the same time as reference density. The values are stored in the control software, and used for calculations of actual density and WLR. No phase-slip is assumed, i.e. $v_{diesel} = v_{water}$.

To find the density of the components, actual temperature, T is measured, and the following equation is used. β is a temperature dependent expansion factor.

$$\rho_{actual} = \frac{\rho_{ref}}{1 + \beta(T - T_{ref})} \tag{3.19}$$

When actual densities for water and diesel are calculated, WLR can be found. Actual liquid density is measured, and since no phase-slip is assumed, WLR can be calulated based on actual liquid density and actual density of the components:

$$WLR = 100\frac{\rho_{actual,liquid} - \rho_{actual,diesel}}{\rho_{actual,water} - \rho_{actual,diesel}} \tag{3.20}$$

The result of this calculation will be in percent fraction, the uncertainty of this calculation is estimated to be 1.1% of full scale, this estimate does not take decoupling effects into account. To find WLR as a fraction, divide by 100.

3.5 Calculating GVF

The ideal gas law, Equation (2.1) is used to find the volume of the gas, in the actual conditions. This is valid only for theoretical gases, so the calculations will have some error. This could be compensated for by using the correction factor for compressibility. However, this correction factor is close to 1 in the actual conditions, so the calculations are assumed valid. The Bronkhorst massflow controller will give mass flow in normal liters per minute. The normal conditions is defined as $0°C$ and at 1 atm. pressure. Assuming conservation of mass, n should be constant, R is also constant, giving:

$$\frac{P_1V_1}{T_1} = \frac{P_2V_2}{T_2} \tag{3.21}$$

$$V_2 = \frac{P_1V_1T_2}{T_1P_2} \tag{3.22}$$

Index 1 is for the gas flow measurement, from the Bronkhorst controller, index 2 is for the fluid flow, where pressure, temperature and flow is measured by the reference instruments in the flow rig. V_2 is the desired quantity to find, this is the volume of the gas when present in the fluid flow. Unit conversions are also necessary, to calculate from $\frac{l_n}{min}$ to $\frac{m^3}{h}$, atm. to Pa and $°C$ to K.

When the volume of the gas is found, Equation (2.31) can be used to calculate GVF.

No phase-slip is assumed. This is usually not the case for gas bubbles in liquid, but it is assumed that the mixing from the pump cause so small bubbles that phase-slip is minimal.

3.6 Estimating effective viscosity

In Section 2.8.4 effective viscosity is explained, and Equation (2.33) is given:

$$\frac{\mu_m}{\mu_c} = \left(1 - \frac{\alpha_d}{\alpha_{dm}}\right)^{-2.5\alpha_{dm}\frac{\mu_d+0.4\mu_c}{\mu_d+\mu_c}}$$

This equation is used to estimate the effective viscosity of a water/diesel mixture. A liquid/liquid mixture is a fluid particle system, so $a_{dm} = 1$. Our experiments show a switch in continuous phase at about $WLR = 45\%$, so for these estimations the mixture is assumed to switch from diesel-continuous to water-continuous at $WLR = 45\%$. Dynamic viscosity of water is $\eta_{water} \approx 1\ mPa\ s$. Kinematic viscosity at 40°C and density for the used diesel are found from the data sheet, Appendix C. Finding the kinematic viscosity for 20 °C is not a straight forward operation, this depends on diesel quality. Studies of temperature dependency of diesel have been made, and based on Oluwafunmilayo *et al.* [21] a qualified assumption of dynamic viscosity of diesel at 20°C is $\eta_{diesel} \approx 4\ mPa\ s$. Using these values, effective viscosity of the diesel/water mixture at 20°C has been calculated, and is shown in Figure 3.1

Assuming that Equation (2.33) is valid to estimate viscosity of a liquid/liquid/gas mixture, and using the viscosity estimation for diesel/water mixure as viscosity of the continuous phase. Calculating effective viscosity when $GVF = 1\ \%$ of nitrogen is present, show no significant change from the viscosity of a diesel/water mixture. No significant change in viscosity can be found for 1% nitrogen in pure water or pure diesel.

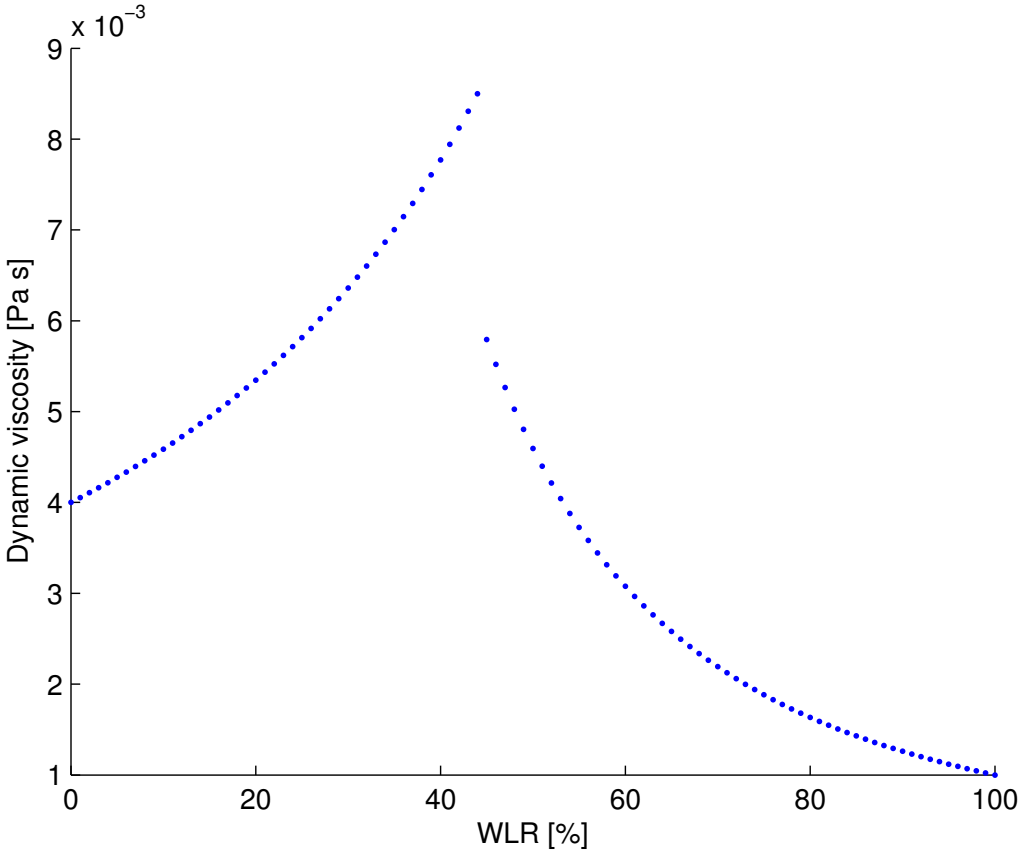

Figure 3.1: Estimated effective viscosity for different WLR of a diesel/water mixture, at 20°C . Viscosity of diesel, $\eta_{diesel} = 4\ mPa\ s$ and for water, $\eta_{water} = 1\ mPa\ s$. Change of continuous phase at WLR = 45%

3.7 Estimating decoupling ratio - Invicid model

Equation (3.2) gives an expression for the acceleration of a sphere particle in an inviscid system:

$$\frac{du_p}{dt} = \frac{du_f}{dt}\left(\frac{3\rho_f}{2\rho_p + \rho_f}\right)$$

Putting this in to an oscillating system, where:

$$Displacement = A_f\ sin(\omega t) \tag{3.23}$$

$$Velocity = u = \omega A_f\ cos(\omega t) \tag{3.24}$$

$$Acceleration = \frac{du}{dt} = -\omega^2 A_f\ sin(\omega t) \tag{3.25}$$

we get:

$$Acceleration = \frac{du_p}{dt} = \frac{-3\omega^2 A_f}{1 + 2(\frac{\rho_p}{\rho_f})} sin(\omega t) \tag{3.26}$$

$$Velocity = u_p = \frac{3\omega A_f}{1 + 2(\frac{\rho_p}{\rho_f})} cos(\omega t) \tag{3.27}$$

$$Displacement = \frac{3A_f}{1 + 2(\frac{\rho_p}{\rho_f})} sin(\omega t) \tag{3.28}$$

Fluid oscillation is equal to the Coriolis oscillation and fluid amplitude equal Coriolis amplitude. In this case $f = 400\ Hz$ and $A_c = 12.5\ \mu m$. Values for displacement and thus decoupling ratio can be found, Figure 3.2 show this for different scenario. In this case the water density, $\rho_{water} = 1000\ kg/m^3$, diesel density, $\rho_{diesel} = 830\ kg/m^3$, and nitrogen density, $\rho_{gas} = 1\ kg/m^3$. In the case of nitrogen bubble in liquid, water is used as continuous phase, using diesel instead would not alter the result noticeably.

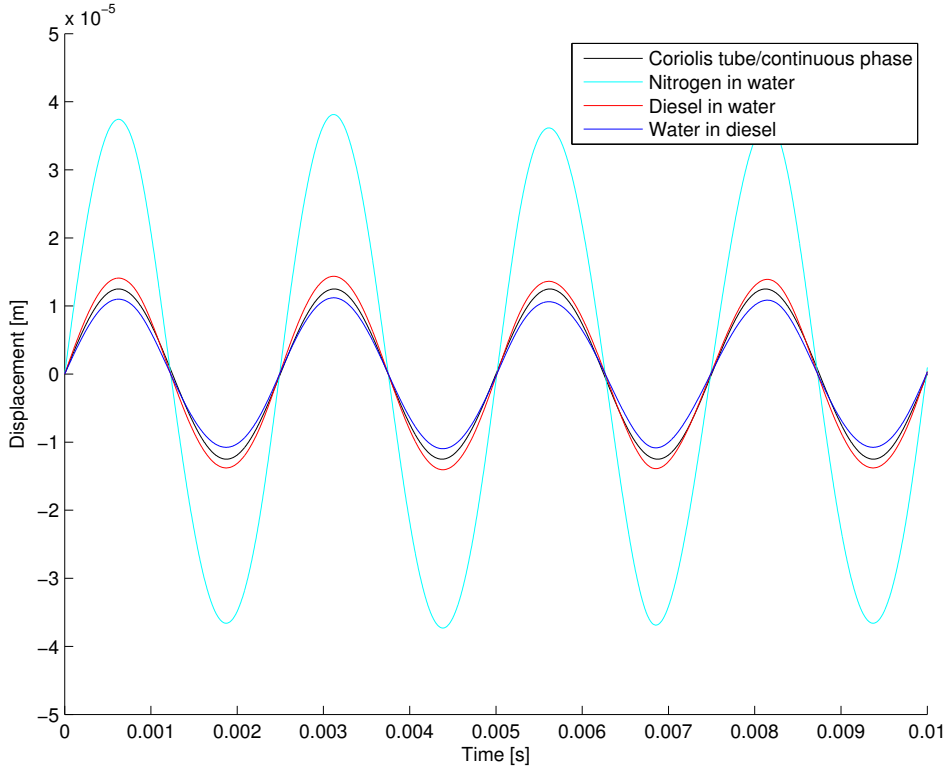

Figure 3.2: Results for particle displacement, using the invicid model. Showing displacement as a function of time, where frequency = 400 Hz, water density, $\rho_{water} = 1000\ kg/m^3$, diesel density, $\rho_{diesel} = 830\ kg/m^3$, and nitrogen density, $\rho_{gas} = 1\ kg/m^3$

Figure 3.2 show that nitrogen in water has an amplitude ratio of 3:1. Diesel in water has a ratio just above unity (≈ 1.13), and water in diesel has a ratio just below unity (≈ 0.88). This is expected as diesel and gas is less dense than water.

3.8 Estimating decoupling ratio - Viscous model

For the following calculations, some *reference conditions* are introduced.

Table 3.1: Reference conditions used when solving the viscous equations

Oscillating frequency	f	400 Hz
Tube/Fluid displacement amplitude	A_f	12.5 μm
Viscosity, water	μ_{water}	1 $mPa\ s$
Viscosity, diesel	μ_{diesel}	4 $mPa\ s$
Density, water	ρ_{water}	1000 kg/m^3
Density, diesel	ρ_{diesel}	830 kg/m^3
Density, gas	ρ_{gas}	1 kg/m^3

The result when solving for velocity, *v(t)* for a typical oil-in-water situation is shown in Figure 3.3. This is the result for a single droplet of diesel (red) in water (blue), concentration effects are considered, and $WLR = 60\%$ is used to compensate for high fractions of dispersed diesel. A small difference in ratio and phase can be observed. Due to difference in density, diesel will have a higher amplitude than the surrounding water. Viscous forces cause the phase shift.

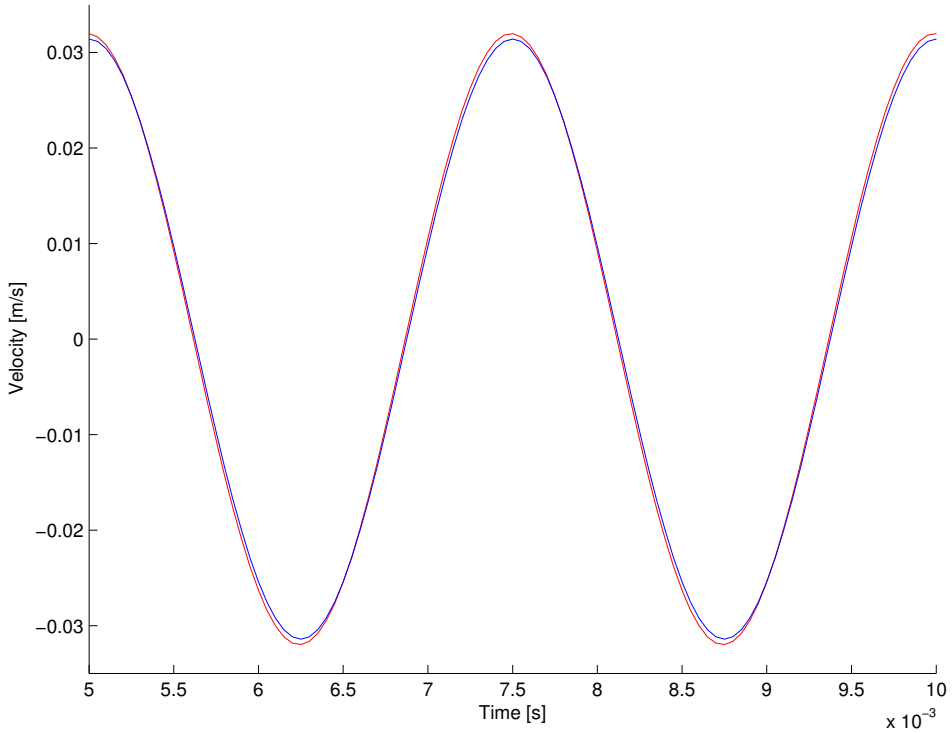

Figure 3.3: Results when solving the viscous model for velocity. Diesel droplet (red) in water (blue). Reference conditions, Table 3.1 are used, and WLR = 60%.

Figure 3.4 show a single gas bubble (red) in water (blue), using the relevant conditions

from Table 3.1. No concentration effects are present, as $WLR = 100\%$. Viscosity of the continuous phase is set to *1 mPas* and the gas bubbles density, $\rho_{gas} = 1kg/m^3$.

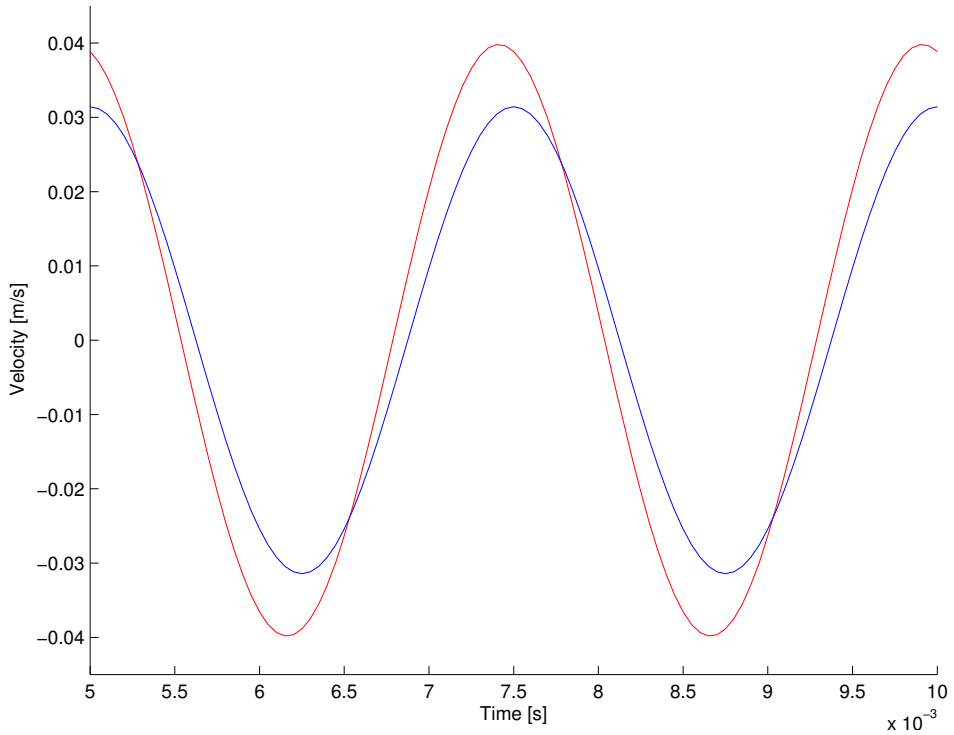

Figure 3.4: Results when solving the viscous model for velocity. Nitrogen bubble (red) in water (blue). Reference conditions, Table 3.1 are used, and WLR = 100%, no concentration effects are considered.

To analyse the effect of mixed liquids, the MATLAB software code is set to solve for all WLR. For each step phase shift and amplitude ratio are found. Figure 3.5 shows these results. In the area where water droplets are dispersed in diesel, the amplitude ratio is less than 1. This is expected as water has higher density than diesel. When the continuous phase shifts to water, a jump in amplitude ratio can be seen. Droplets with lower density than the continuous phase will result in an amplitude ratio higher than 1. The same applies for phase shift, which will be negative with dense droplets and positive with less dense droplets, relative to the surrounding fluid.

Based on phase shift and amplitude ratio, it is possible to calculate work and power dissipation. From Weinstein [15] an equation for work per cycle is given:

$$\frac{Work}{Cycle} = \pi \left(\frac{4}{3} \pi a^3 \rho_p \right) \omega^2 A_p A_f \left| \sin(\varphi) \right| \tag{3.29}$$

Where $\frac{4}{3}\pi a^3 \rho_p$ is the mass of the particle, assuming a sphere particle. $\omega^2 A_p$ is the particles acceleration amplitude, A_f is the fluid displacement amplitude and $|\sin(\varphi)|$ accounts for the phase shift. The absolute value makes the equation also valid for dense

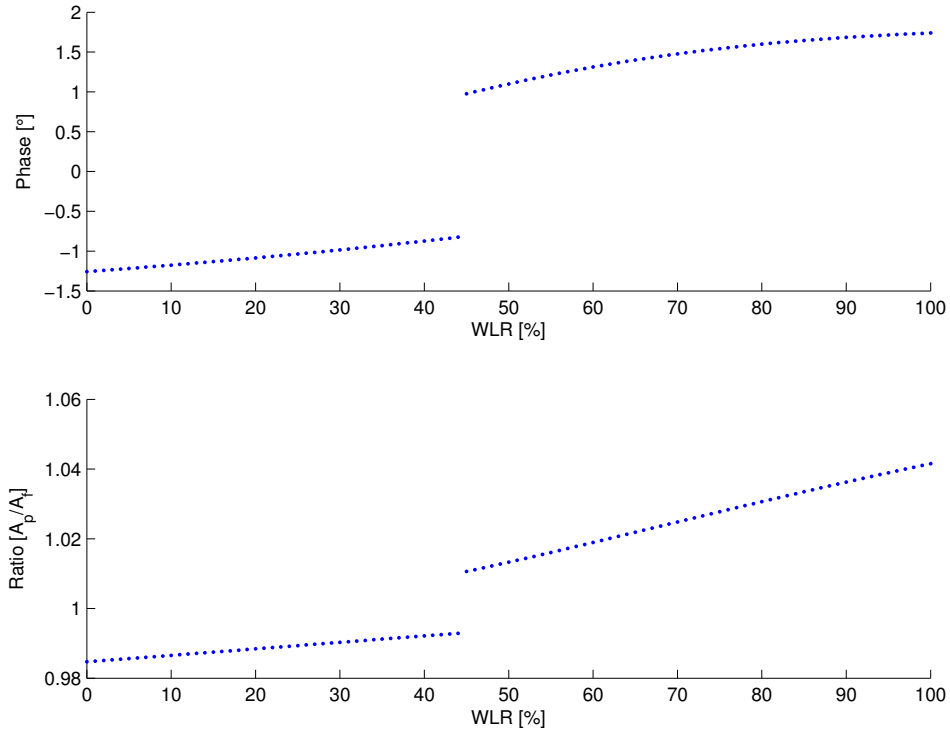

Figure 3.5: Phase difference and amplitude ratio between particle and continuous phase, when solving for reference conditions, Table 3.1. Results shown for all WLR, with continuous phase change at WLR = 45%.

particle which would lead to negative phase shift. Power is work over time, with the equation for work per cycle, we can easily find power per cycle by multiplying with frequency, and substituting $\omega = 2\pi f$:

$$\frac{Power}{Cycle} = \frac{1}{2}\left(\frac{4}{3}\pi a^3 \rho_p\right)\omega^3 A_p A_f \left|\sin(\varphi)\right| \tag{3.30}$$

To be able to compare different conditions, power per cycle per volume is found by dividing with the volume of the particle, still assuming a sphere particle:

$$\frac{Power}{Volume} = \frac{1}{2}\rho_p \omega^3 A_p A_f \left|\sin(\varphi)\right| \tag{3.31}$$

Power calculations for all WLR, using reference conditions from Table 3.1, are shown i Figure 3.6. When comparing to the effective-viscosity calculations, shown in Figure 3.1, it is clear that viscosity plays role in power dissipation.

All the previous calculations are done for a single droplet, located among other droplets. By accepting that the void fraction of the dispersed phase can be used to express a sum of the power from all droplets, total power dissipation per cycle can be assumed. For diesel continuous conditions, the dispersed void fraction is $\alpha_d = \frac{WLR}{100}$ and

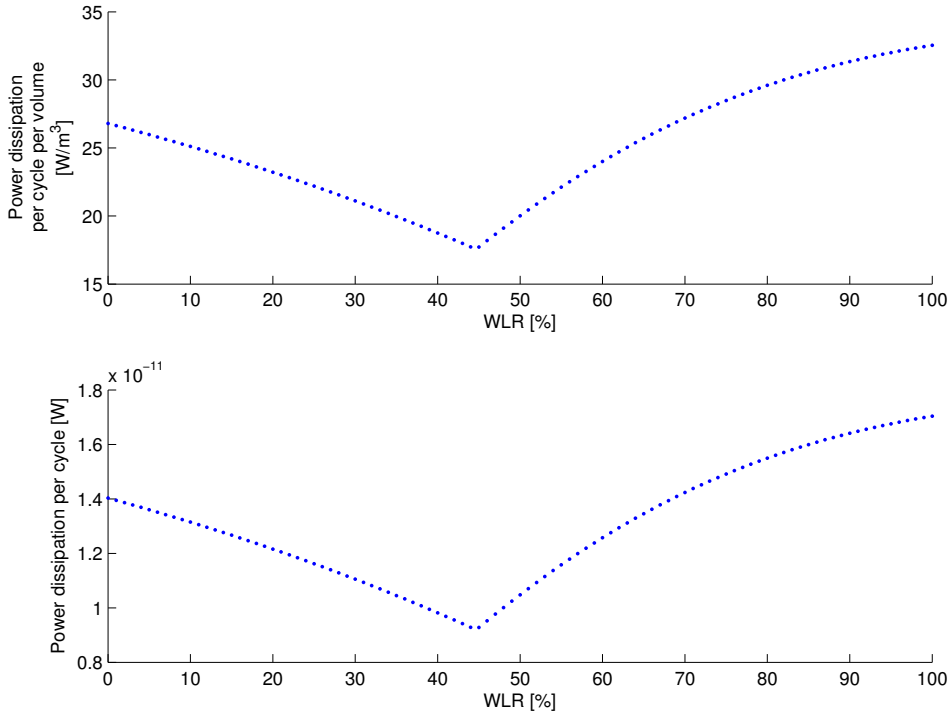

Figure 3.6: Power dissipation per cycle and power dissipation per volume, for each particle, when solving for reference conditions, Table 3.1. Results shown for all WLR, with continuous phase change at WLR = 45%.

for water continuous the same void fraction is $\alpha_d = \frac{100-WLR}{100}$.

$$\frac{Total\ power}{Cycle} = \alpha_d \frac{Power}{Cycle} \tag{3.32}$$

Giving the results found in Figure 3.7. Note that the values of this figure is not valid for anything but comparison to other conditions. When comparing with actual measurements, the shape of the curve is important.

In Appendix D the results when solving for different conditions are shown. The conditions used are presented in Table 3.2. These results are used to investigate the change in power dissipation when conditions changes.

Table 3.2: Conditions used to investigate change in power dissipation when conditions changes

Name	**Effect**	**Affected variable**	**Value**
High pump speed	Smaller droplets	Particle size, a	40 μm
Low pump speed	Larger droplets	Particle size, a	60 μm
High temperature	Lower viscosity	Diesel viscosity, μ_{diesel}	3 $mPa\ s$

These results show that higher pump speed, thus smaller droplets, gives smaller amplitude ratio and phase shift. Which again gives less power dissipation. The opposite

will occur for lower pump speeds. It is natural to assume more power dissipation per droplet as droplets increase in size, but the calculations also show that increasing droplet size will increase power dissipation per volume.

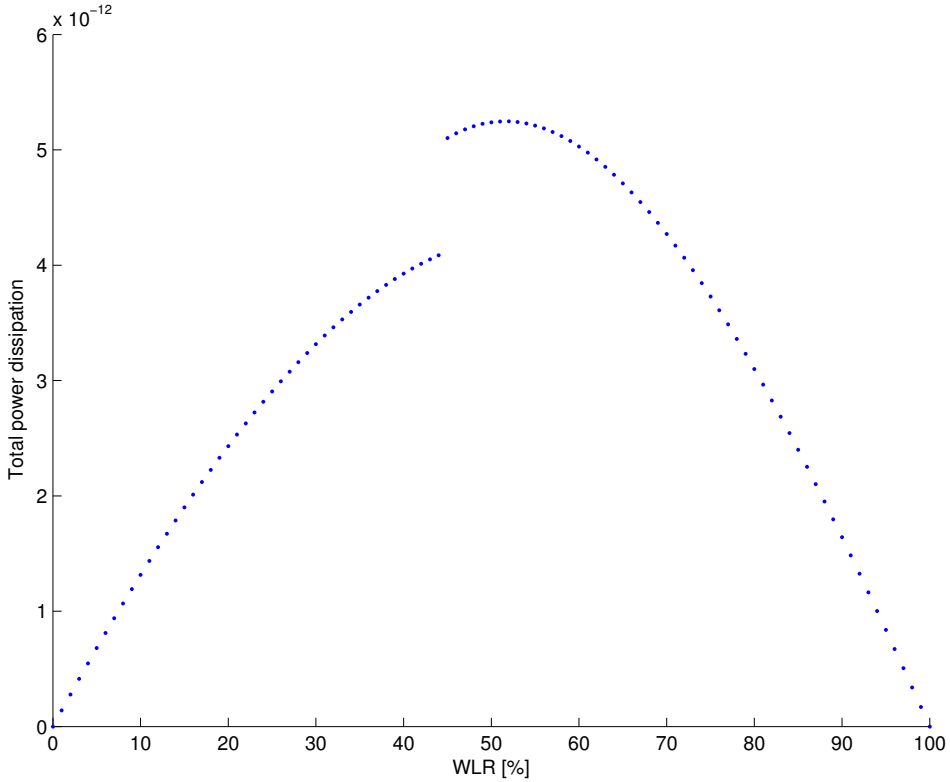

Figure 3.7: An expression for total power dissipation per cycle when solving for reference conditions, Table 3.1. Results shown for all WLR, with continuous phase change at WLR = 45%. Values for power dissipation are not valid for numerical comparison.

Chapter 4

Experimental set-up and methods

This chapter gives a presentation of the mulitphase flowloop and the gas flow controller used in the experiments. How everything is connected to make the experiment set-up, and details about the set-up will be given. The methods used for measurements will also be explained. The experimental results will follow in Chapter 5.

CMR is an independent research institute with long-time experience in multiphase flow modelling and measurements. A new flow loop was built in 2008 and opened in January 2009. The flow rig in use at CMR's location is used both for research, testing and qualification of new flow measurement technologies. The flow rig is used by CMR, but also by external companies [22]. The flow rig has Coriolis flowmeters installed for reference measurements, i.e. two Endress+Hauser ProMass 80F. The Promass 80F is a commonly used, multi-purpose Coriolis flowmeter.

In Chapter 2 it was explained how Coriolis meters calculate density based on the natural oscillating frequency of its measurement tube, and mass flow rate based on torque induced by the Coriolis force. Both density and mass flow rate measurements are affected by flow conditions. The reference instruments will be used to investigate these effects, when the flow consist of liquid mixtures, and entrained gas.

The experiments in this thesis are all conducted using CMR's multiphase flowloop, presented in Section 4.1. The general experimental set-up is therefore the same for all experiments. In some of the experiments gas is injected into the liquid flow, done using a Bronkhorst massflow controller. The details about the controller will be described in Section 4.2. The entire experimental set-up will be described in Section 4.3, this includes where and how the Bronkhorst controller is connected.

The general equipment list fot the measurement set-up is as follows:

- CMR Multiphase flow loop.
- LabVIEW software development tool for data acquisition from the flow loop.

- Bronkhorst F-201CV mass flow controller for gases, including an interface to a personal computer.
- Bronkhorst FlowDDE and FlowView, software for controlling the mass flow controller.
- Pressurized Nitrogen (N_2). Flow controlled by the Bronkhorst controller.

4.1 CMR multiphase flow loop

CMR's multiphase flow loop consists of a separator tank, facilities to generate nitrogen and two flow lines, 3" and 6". The flow loop is closed and pressurized, it contains diesel, salted water (NaCl) and nitrogen. Nitrogen is produced from air, by a compressor driven system. The separator contains approximately 10 m^3 diesel and 10 m^3 water. A simplified diagram of the multiphase flow loop is shown in Figure 4.1

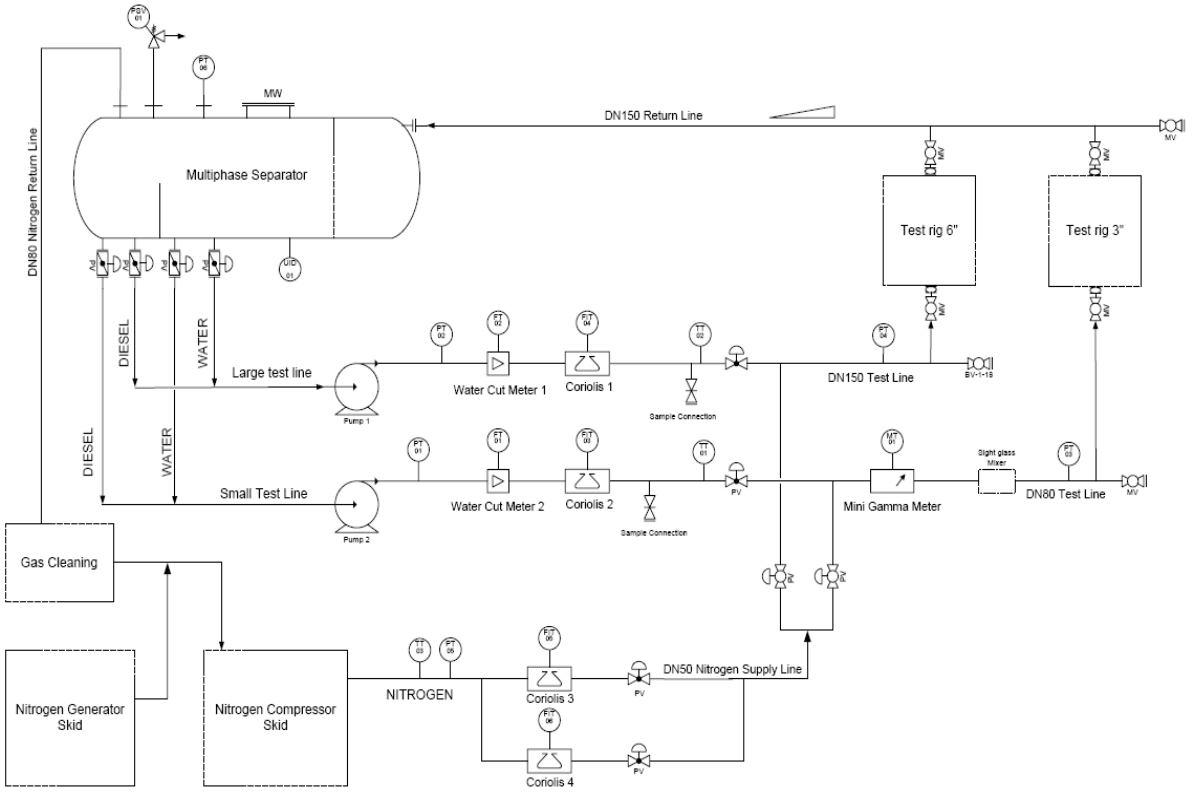

Figure 4.1: Simplified PI&D of the CMR multiphase flow loop. [22]

The separator tank has outlets for diesel, water and nitrogen. Nitrogen will return to the nitrogen generation facilities for recirculation. Both diesel and water have two sets of outlets, one set for the 3" line and one for the 6" line. The liquid outlets have

butterfly valves installed to adjust WLR. Coriolis flowmeters (Coriolis 1 and 2) are used as reference instruments, and butterfly valves are adjusted to get the desired WLR in the mix. The mixture of diesel and water will run through a circulation pump, this pump will provide mixing as well as pumping the liquid through the system. Together with the globe valve downstream Coriolis 1 and 2, the liquid flowrate can be controlled. The control system relies on reference measurements from Coriolis 1 and 2 when controlling flow rate and WLR. The pressure (PT-01 and PT-02) is measured upstream ot the Coriolis flow meter, and liquid temperature (TT-01 and TT-02) is measured downstream. More information about the mentioned instruments can be seen in Table 4.1.

Table 4.1: Reference instruments used in the CMR Multiphase flow loop, with ranges and uncertainties. Each instruments PI&D label, and flow line is also presented. [22]

Tag	Instrument	Range	Uncertainty (95%)	Flow line
Coriolis 2	E+H Promass 80F	3-100 $\frac{m^3}{h}$	$< 0.5\%$	3”
Coriolis 1	E+H Promass 80F	7-250 $\frac{m^3}{h}$	$< 0.5\%$	6”
PT-01	E+H Cerabar M PMC41	0-10 bar	0.2% (abs)	3”
PT-02	E+H Cerabar M PMC41	0-10 bar	0.2% (abs)	6”
TT-01	E+H Omnigrad M TR10	0-50 °C	0.15°C	3”
TT-02	E+H Omnigrad M TR10	0-50 °C	0.15°C	6”

Downstream the globe valve, nitrogen can be injected into the liquid. Nitrogen flow is also measured by Coriolis flowmeters. One is calibrated for high gas flowrates, and one for low gas flowrates. This part of the flow rig is not used in these experiments, as the nitrogen is injected after the liquid reference flowmeters.

After nitrogen injection the flow lines continue to the test area. In this area other instruments can be connected into the flow lines. When CMR and external companies do research, testing and qualification, the instruments are connected here. After the test area, the flow lines return to the separator tank for separation and recycling of the mixture.

For communication between the instruments and the control room, the Profibus fieldbus standard is used. CMR has developed control software for the flow loop using LabVIEW. Appendix A contains complete datasheet for the CMR Multiphase flow loop [22].

CMR has also calculated flow measurement uncertainties, presented in Table 4.2, based on the uncertainties in Table 4.1. These are calculated according to the ISO ”Guide to the expression of uncertainty in measurements” (1995). More parameters can be found in Appendix A.

Table 4.2: Uncertainties (95% conf. interval) in flow parameters in the CMR Multiphase flow loop [22].

Flow parameter	Uncertainty	Unit
Liquid flow	<1.2	% rel
WLR	1.1	% abs

4.2 Bronkhorst F-201CV

Bronkhorst F-201CV is a thermal flowmeter, measuring mass flow. It has a built in control valve, and can also control mass flow. Bronkhorst explains the working principle of the thermal mass flow meter in the datasheet for the instrument [23]. Gas flows into the instrument, where some of the gas flow gets separated into a measurement tube. The gas in the measurement tube is heated by heating elements, and the temperature inside the tube is measured by two resistance thermometer elements (T1 and T2). If the gas had been standing still within the tube, the temperature would be equal at both sensing elements. When gas flows though, the inlet temperature sensor is cooled and the outlet temperature sensor is heated. This temperature difference is measured.

$$\Delta T = T2 - T1 \tag{4.1}$$

Knowing the heat capacity at constant pressure, C_p for the gas, and a proportional factor, k, one can calculate mass flow rate, $\dot{M}$, which is proportional to the mass flow rate through the small measurement tube.

$$\Delta T = kC_p\dot{M} \tag{4.2}$$

Bronkhorst claims that they are able to perfectly split the flow, and lead it into the measurement tube, so that the sensor output is proportional to the total mass flow rate. F-201CV also has a fast, proportional electromagnetic control valve to control the flow though the instrument based on its internal measurements [23]. Table 4.3 show some technical data for the instrument.

Accuracy (incl. linearity)	± 0.5% of read value (Rd) ± 0.1 % of full scale (FS)
Turndown	1:50
Repeatability	<± 0.2 % Rd
Settling time (controller)	<2 seconds
Control stability	≤ ± 0.1% FS
Warm-up time	30 min. for optimum accuracy 2 min. for accuracy ± 2% FS

Table 4.3: Technical specifications for Bronkhorst F-201CV [23].

The F-201CV in use is equipped with the RS232 interface for communication with PC. It needs a DC power supply between 15 and 24 V_{dc} ± 10%.

4.3 Experimental set-up

In these experiments the Coriolis meters for liquid flow reference measurements are studied, Coriolis 1 and 2 in Figure 4.1. The flow loop's own nitrogen system can not be used to study the effect of entrained gas, due to the point of injection. To inject gas into the desired point of the flow loop, upstream the Coriolis meters, a tank of pressurized nitrogen is used. The nitrogen flow rate is measured and controlled by the Bronkhorst F-201CV. The controller and the nitrogen tank is placed next to the separator tank, and connected to a personal computer located in the same room. The computer is remotely controlled, using the Ethernet protocol, from the flow loop control room. Bronkhorst's own software FlowDDE and FlowView are used for flow control. To ensure best possible mixing of nitrogen into the liquid flow, the gas tube inlet is placed right before the appropriate centrifugal pump, marked Pump 1 and Pump 2 in Figure 4.1.

Endress+Hauser have provided access to hidden parameters in the Promass 80F. For the experiment it is set up to send the parameters listed below. The flow loop is used by other experiments, so the choice of parameters is somewhat limited due to the existing setup.

- **Excitation Current [A].** This is the current used to excite the Coriolis tube and thereby induce oscillations. Expected to be in the range 2-100 mA.
- **Volumetric Flow Rate** $[\frac{m^3}{h}]$**.** A derived size, based on mass flow rate. Range between 3-100 or 7-250 $\frac{m^3}{h}$, depending on flow line in use.
- **Density** $[\frac{kg}{m^3}]$**.** Derived size, based on frequency.
- **Frequency [Hz].** The natural frequency of the Coriolis tube, with contents.

Excitation Current (EC) is a measure of damping, as damping in the E+H Coriolis flometer is defined as:

$$D = \frac{I}{A} \tag{4.3}$$

Where D is damping, I is excitation current and A is the actual amplitude of oscillation. The instrument has limits on how much EC it can provide. Exceeding these limits will cause the amplitude to drop from its constant value. This limit is never exceeded in these experiments, so EC is considered to be proportional to the damping of the tubes.

In the flow rig two parameters can be altered to control the liquid flow rate, Valve Power rate (VP) and Pump Power rate (PP). Both parameters are rates, expressed in percent. The VP controls the opening of the valve downstream of the Coriolis flowmeter. In these experiments, this is usually controlled by a PID controller, to keep flow rate at a set speed. PP is the input variable to the frequency converter controlling the pump motor. The asynchronous motor has a rated rotational speed of 1465 rpm. The frequency converter is set up to give maximal output (100%) when receiving maximal input (100%), but 50% output when input is 0%. In other terms, if the pump power input is 100%, the motor will rotate at 1465 rpm. If the input is 0%, the motor will rotate at $\approx$ 732 rpm. 90% is a often used setting, this corresponds to $\approx$ 1392 rpm. The pump power rate is usually set to a fixed value in these experiments, and as mentioned before, the flow rate is controlled with the valve using a PID controller.

4.4 Methods

Two different methods for taking measurements are used in the experiments, one for taking *point measurements* and one for continuous measurements while going through a *WLR sweep*. The point measurements are for given steps in system input, e.g. different steps of pump power or different amounts of injected gas. The WLR sweep is a measurement for all different steps of WLR, while the other inputs are kept constant.

4.4.1 Point measurement

When taking a point measurement, all control variables are set, and kept constant, and the system is given time to stabilize. Sampling rate for the system i 1 $\frac{sample}{second}$. Each measurement consists of 60 samples, and is taken over a time span of 60 seconds. Both mean value, $\bar{y}$ and standard deviation, s is calculated for N samples. The following equations are used:

$$\bar{y} = \frac{1}{N}\sum_{i=1}^{N} y_i \tag{4.4}$$

$$s = \frac{1}{N-1}\sum_{i=1}^{N}(y_i - \bar{y})^2 \tag{4.5}$$

4.4.2 WLR sweep

The liquid flow is controlled by adjusting Valve Power rate (VP) downstream of the Coriolis flowmeter, and adjusting Pump Power rate (PP) of the centrifugal pump upstream the Coriolis flowmeter. In the WLR-sweep measurement method, the PP is set, and kept constant. Liquid flow is controlled by a PID controller working on the downstream valve.

This method was developed to study the effects on the whole WLR range. WLR is adjusted using two valves on the outlets of the separator tank. These valves are PID controlled.

Initial conditions are set, e.g. $WLR = 0\%$, and the system is given time to stabilize. When the system is stable, data acquisition is started. The acquisition is set to last for 10 minutes, with a sampling rate of 1 $\frac{sample}{second}$. The operator has to gradually change the set-point in the PID controller, to slowly move through the WLR range. A typical sweep through the WLR-range, over time, is shown in Figure 4.2.

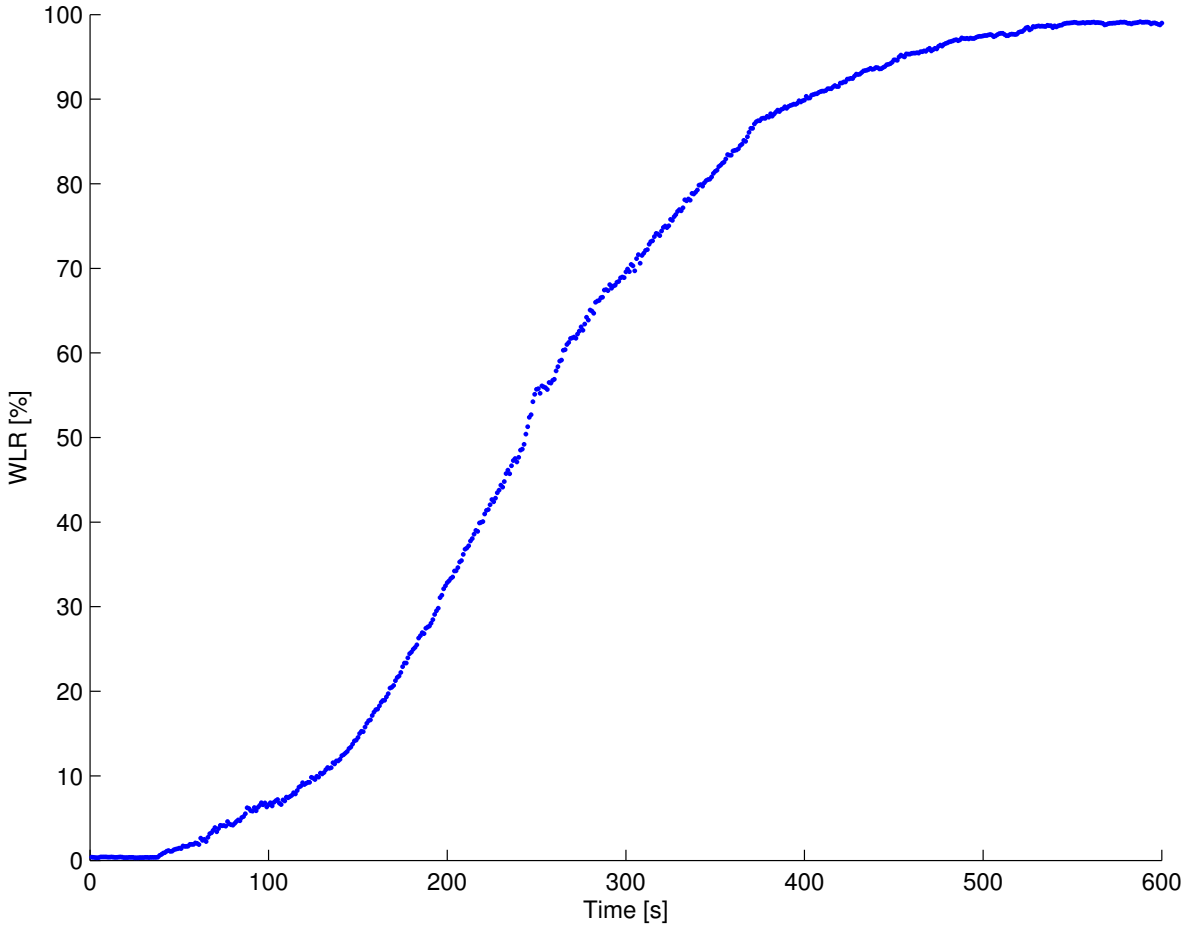

Figure 4.2: Typical sweep through WLR range over time, using the WLR sweep method.

It is clear that this method is not flawless. The rate of change in WLR is typically slow in the end regions, and varies faster where the continuous phase changes. This leads to an uneven distribution of samples. However, the measurements are taken over a long period of time, so a fairly good WLR resolution is achieved, even when WLR changes fast. Since the flow rig is used by several experiments, no large modifications to the software can be made.

When flow rates are very high, flows of pure water or diesel can not be achieved. Some entrainment of liquid from the separator tank will occur, i.e. some water will be entrained into a diesel flow.

Chapter 5

Experiments

The conducted experiments will be described in this chapter. The experimental set-up has already been described in Chapter 4, as well as methods for taking measurements. An overview of the experiments follows:

- **Experiment #1: The no-gas experiment.** This experiment was conducted without injection of gas. This experiment investigates how excitation current is affected by different WLR at various pump speed, when the liquid flow rate is kept constant. An effect of changed temperature can also be observed.

  The experiment aims to investigate if a liquid/liquid mix can be detected, according to Objective 1.

- **Experiment #2: The gas injection experiment.** The follow up experiment to *The no-gas experiment*. In this experiment, gas is injected to see the contribution from gas in the liquid flow, at different WLR and at various pump power settings.

  This experiment wants to investigate if gas can be detected in a liquid/liquid/(gas) mixture, according to Objective 2.

- **Experiment #3: The rig stress test.** This experiment is conducted to see if any entrained gas from the separator tank can be detected. Small amounts of gas is injected, to investigate the response in excitation current. This is followed by running the flow rig at high flow rates, without injecting gas. The presence of entrained gas is investigated by comparing measurements, to see if the response in excitation current indicate gas.

  This experiment investigates how small quantities of gas it is possible to detect, and what flow rates can be achieved without detecting entrained gas, according to Objectives 3 and 4.

5.1 Experiment 1: The no-gas experiment

The motivation for this experiment is to investigate how the excitation current is affected by change in WLR in a liquid/liquid mixture. Objective 1 in this thesis includes detecting if a liquid/liquid mixture is present, this will be investigated in this experiment. The results will be compared with the mathematical model of the Coriolis flow meter, from Chapter 3. It is also important to investigate how liquid flow rate and mixing affect excitation current, at different WLR.

5.1.1 Measurement set up

Limitations in flow loop capacity forced this experiment to be divided, and conducted over several days. This is clearly not ideal, and could affect the results. The temperature in the rig changes from day to day, during the day, and during the experiments. The measurements for $Q_l = 50\ \frac{m^3}{h}$ are split into two, conducted on different days with different temperatures. This could lead to results not being directly comparable. Measurements for $Q_l = 30\ \frac{m^3}{h}$ and $Q_l = 70\ \frac{m^3}{h}$ were conducted on the same day, a different day than both the $Q_l = 50\ \frac{m^3}{h}$ measurements.

The experiment set-up is as follows:

- Conducted with the general experiment set-up, explained in Chapter 4.
- Measurements were done in the 3" section of the loop.
- No gas injected into the liquid flow.

The 3" section of the loop is used for best possible comparison with Experiment 2.

5.1.2 Procedure

The measurements in this experiments are all taken with the WLR-sweep method, explained in Section 4.4. Desired parameters are set, e.g. Liquid flow rate, $Q_l = 50\frac{m^3}{h}$, Pump power $PP = 90\%$ and initial WLR = 100%. Measurements are taken while running through the entire WLR-range.

Based on knowledge about the flow rig and its limitations, test parameters were set. Three different liquid flow rates were investigated, $Q_l = 50,\ 70$ and $30\ \frac{m^3}{h}$. All at various PP. All measurements were taken with intial $WLR = 100\%$ and decreasing WLR towards $WLR = 0\%$. In some cases $WLR = 0\%$ could not be achieved within the measurement frame of ten minutes. In the end regions (WLR close to 0% or 100%),

the rate of change can be so small that even small WLR steps can take several minutes. Some of the measurements were also taken with initial value $WLR = 0\%$ increasing WLR towards $WLR = 100\%$. This was done to investigate the hysteresis between increasing and decreasing WLR. The hysteresis was checked once for each step in Q_l.

The results of this experiment are compared to the mathematical model i Chapter 3, and in particular Figure 3.7, the total power dissipation as a function of WLR.

Part 1: $Q_l = 50\frac{m^3}{h}$

Due to capacity limitations in the flow loop, this part of the experiment was conducted at two different days. On day 1, the hysteresis at $PP = 50\%$ was measured, and a measurement with $PP = 90\%$, for decreasing WLR. Table 5.1 show the settings of this part of the experiment.

Table 5.1: Experiment 1, part 1: Settings for measurements taken at $Q_l = 50\frac{m^3}{h}$, Day 1

Q_l $[\frac{m^3}{h}]$	PP [%]	Direction	WLR [%]
50	50	Down	100-0
50	50	Up	0-100
50	90	Down	100-0

A hysteresis test was not repeated on day 2 of this experiment. Measurements with different settings of PP were conducted, following the settings described in Table 5.2.

Table 5.2: Experiment 1, part 1: Settings for measurements taken at $Q_l = 50\frac{m^3}{h}$, Day 2

Q_l $[\frac{m^3}{h}]$	PP [%]	Direction	WLR [%]
50	40	Down	100-0
50	60	Down	100-0
50	70	Down	100-0
50	80	Down	100-0

Part 2: $Q_l = 70\frac{m^3}{h}$

With $Q_l = 70\ \frac{m^3}{h}$ the following measurements were conducted. The lowest pump power rate that can achieve this liquid flow rate is $PP = 70\%$, so the experiment limits itself by this. The settings used in part 2 of this experiment is presented in Table 5.3.

Table 5.3: Experiment 1, part 2: Settings for measurements taken at $Q_l = 70\frac{m^3}{h}$

Q_l $[\frac{m^3}{h}]$	PP [%]	Direction	WLR [%]
70	70	Down	100-0
70	80	Down	100-0
70	90	Down	100-0
70	90	Up	0-100

Part 3: $Q_l = 30\frac{m^3}{h}$

For best possible comparability between part of the experiment, similar conditions are necessary. The settings used for $Q_l = 70\ \frac{m^3}{h}$, were also used for $Q_l = 30\ \frac{m^3}{h}$, except for the hysteresis measurement. The settings used in part 3 of this experiment is presented in Table 5.4.

Table 5.4: Experiment 1, part 3: Settings for measurements taken at $Q_l = 30\frac{m^3}{h}$

Q_l $[\frac{m^3}{h}]$	PP [%]	Direction	WLR [%]
30	70	Up	0-100
30	70	Down	100-0
30	80	Down	100-0
30	90	Down	100-0

5.1.3 Results and discussion

Part 1: $Q_l = 50\frac{m^3}{h}$

Figure 5.1 shows the Excitation Current (EC) vs. WLR for Pump Power rate (PP) 50% (blue) and 90% (red). At constant liquid flow rate, a PP of 50% gives a higher EC at most WLR. At $WLR = 100\%$ the EC is the same for both $PP = 50\%$ and $PP = 90\%$. $WLR = 0\%$ was not reached for $PP = 50\%$, it is however likely that the curve would reach the same endpoint as the $PP = 100\%$ curve. The graphs have two local maxima, one for the diesel continuous part of the WLR range, and one for the water continuous part. The maximum for water continuous flow is higher than the one for diesel continuous flow. The top of $PP = 90\%$'s maxima are slightly shifted with respect to each other, compared to the top of $PP = 50\%$'s maxima. In both curves, there is a local minimum located at about $WLR = 40\%$

Since this part of the experiment was conducted on two different days, data from day two is presented separately. Figure 5.2 shows the EC vs. the WLR for pump power rates 40, 60, 70 and 80%. These measurements were taken with a higher temperature in the flow loop than the measurements from day one. Higher PP gives lower EC. As

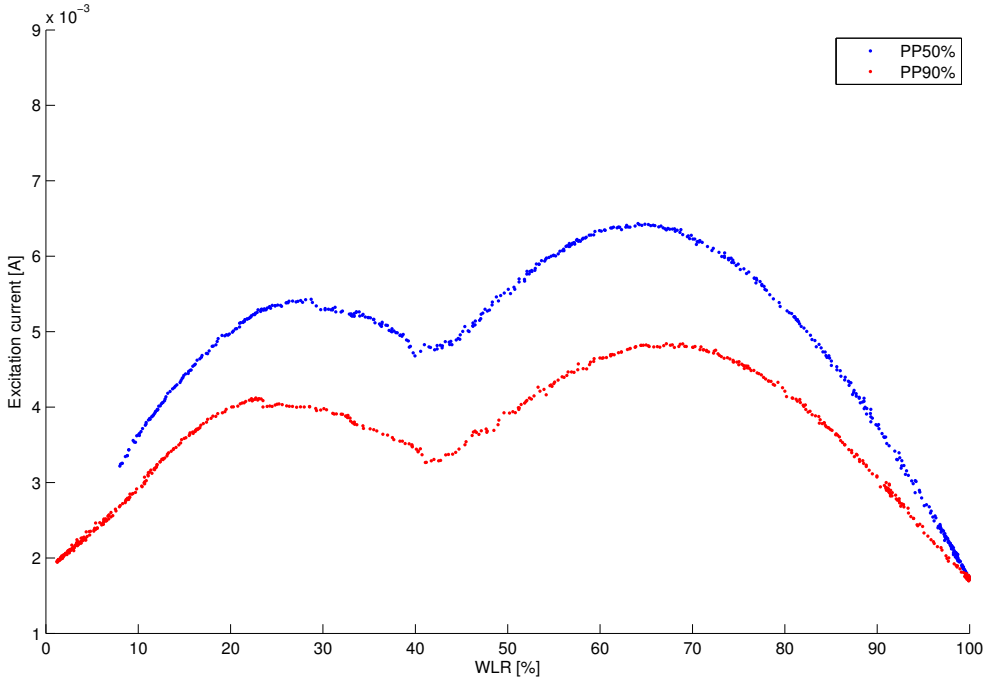

Figure 5.1: Experiment 1, part 1, day 1. Excitation current vs. WLR at pump power rates 50% (blue) and 90% (red), and $Q_l = 50\frac{m^3}{h}$.

for Figure 5.1, higher PP gives two maxima located closer together than for lower PP. A local minimum is present at about $WLR = 40\%$, as in Figure 5.1.

The shape of the curves in this experiment only partly match the shape of Figure 3.7, but there is also some resemblance. The model does not predict a large drop in EC around the point of continuous-phase change. What really happens in the tube at this point is unknown, due to lack of observations. The model does not consider any changes in droplet size due to concentration effects or viscosity. If large concentrations of dispersed phase cause increased uncertainties in the model, this would have the largest impact in the area around continuous-phase change. However, the model predicts a change in EC in the area around continuous-phase change, and also that the same void fraction of diesel in water and water in diesel will result in different excitation currents.

It is clear that PP plays a role in the amplitude of the EC vs. WLR curve. Higher PP, and therefore higher pump speed will give lower EC. This is in agreement with Morales *et al.* [20], who conclude that higher pump speed will give smaller droplets. Morales *et al.* also expect a more uniform distribution of particle sizes with higher pump speed. From Chapter 3 (and Appendix D) we expect lower EC from smaller droplets, caused by less power dissipation per volume than for larger bubbles. A more uniform droplet size distribution can not be recognized in these measurements.

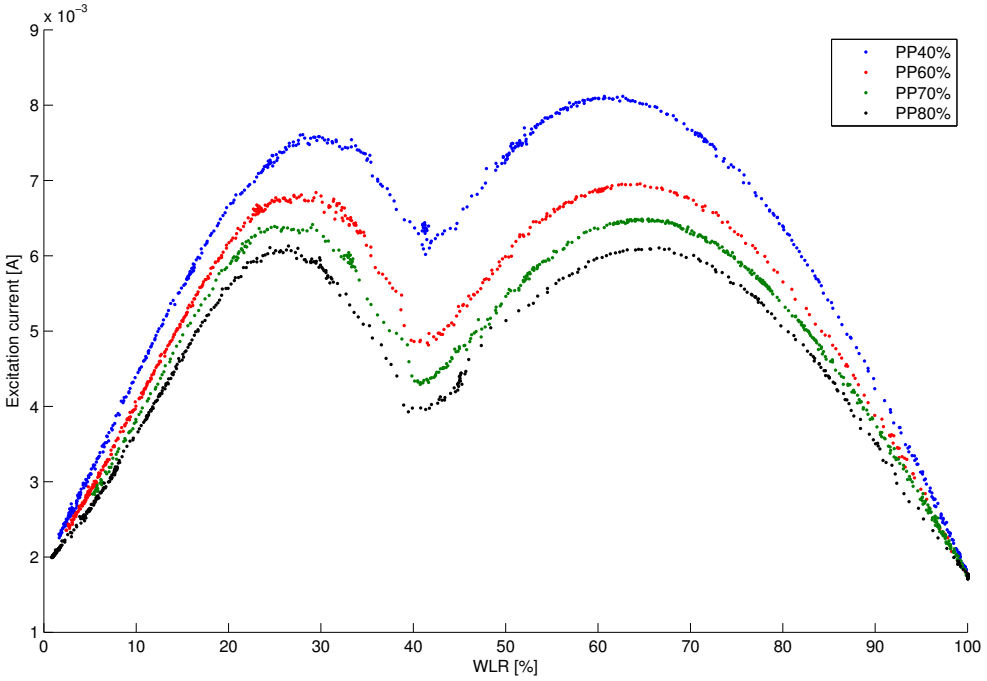

Figure 5.2: Experiment 1, part 1, day 2: Excitation current vs. WLR at pump power rates: 40 (blue), 60 (red), 70 (green) and 80% (black), and $Q_l = 50\frac{m^3}{h}$.

The temperature has an effect on viscosity. How much effect depends on what substance it is affecting, i.e. the temperature dependence of diesel is higher than that of water. Since a part of this experiment had to be done over two days, effects of temperature difference could be observed. The temperature in the flow rig was about 20°C on day 1, and 30°C on day 2. The EC response to diesel-continuous mixture becomes more like the response from a water-continuous mixture when the temperature increases. The model in Chapter 3 predicts a similar change. The entire EC vs. WLR curve (except from its end points) is also lifted, in accordance to the model.

For the measurements at $Q_l = 50\ \frac{m^3}{h}$, measurements for hysteresis were done at a PP = 50%. Measurements were taken when increasing and decreasing WLR through the WLR range. Figure 5.3 shows that for decreasing WLR, the local minimum is slightly lower than for increasing WLR, and at a somewhat lower WLR. If this is random fluktuations or actual differences is hard to say, due to lack of observation of conditions inside the tube.

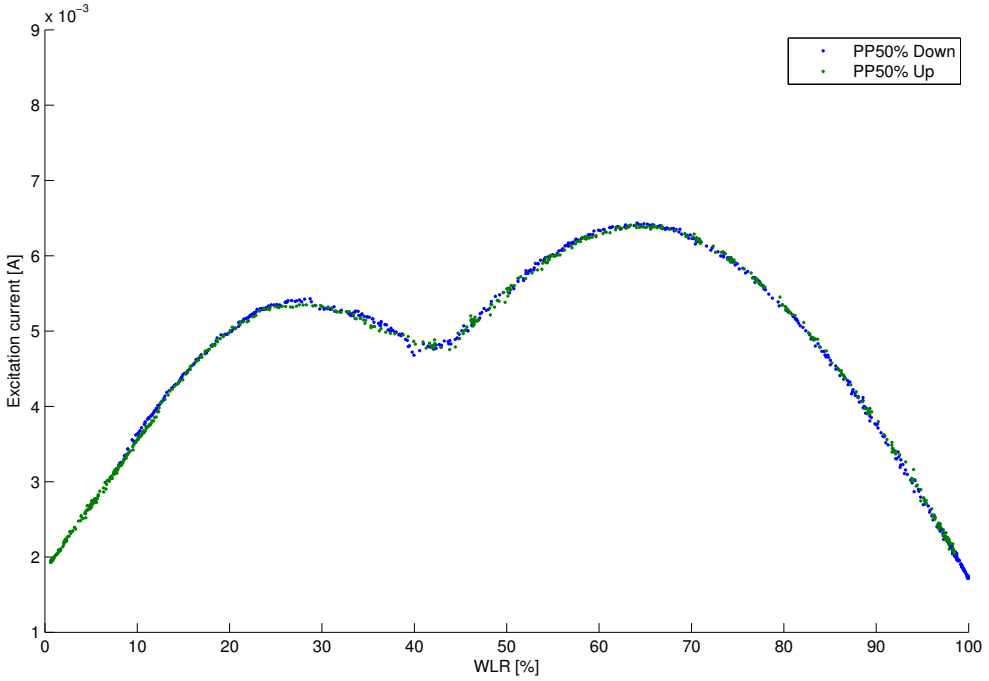

Figure 5.3: Experiment 1, part 1: Hysteresis plot of excitation current vs. WLR at pump power rate 50% and $Q_l = 50\frac{m^3}{h}$. Increasing WLR is marked with green, and decreasing WLR with blue.

Part 2: $Q_l = 70\frac{m^3}{h}$

Figure 5.4 shows a difference in Excitation Current (EC) between measurements taken with different Pump Power rate (PP). As for the measurements with $Q_l = 50\ \frac{m^3}{h}$, higher PP will give lower EC. The minimum is located just above $WLR = 40\%$ for all pump power rates. Hysteresis measurements were taken at pump power rate 90%, shown in Figure 5.5. There is no difference in measurements for increasing (green) and decreasing (blue) WLR.

These results show the same as the results from Part 1, day 1, with respect to the magnitude of EC. Note that these measurements are taken in different days so the numbers are not directly comparable. There was not much difference in flow rig temperature for these measurements. The hysteresis plot is also similar to the hysteresis plot from Part 1.

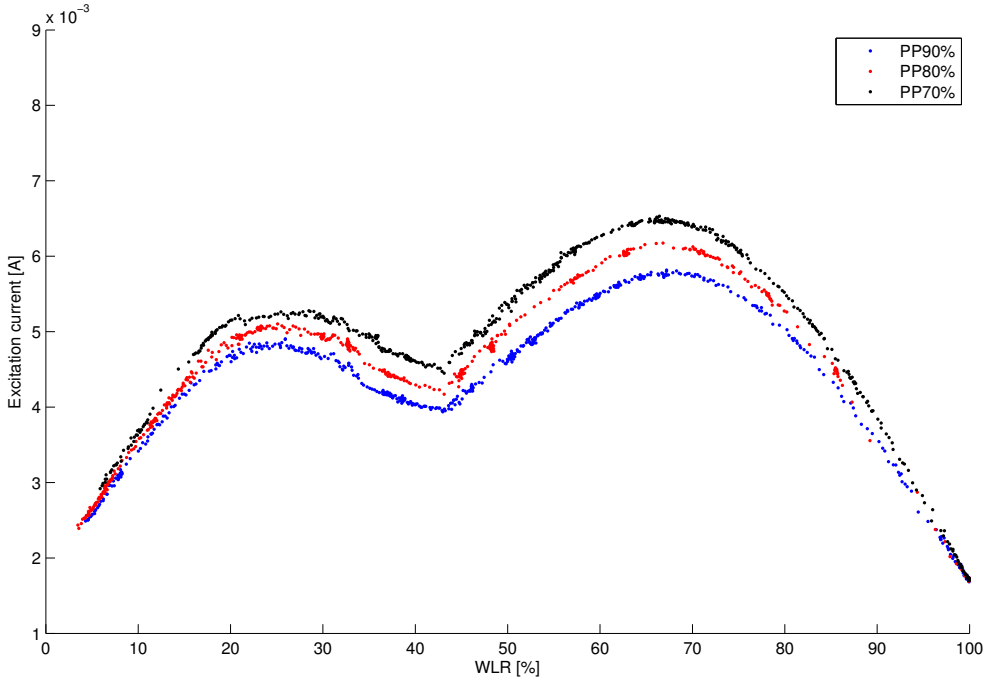

Figure 5.4: Experiment 1, part 2: Excitation current vs. WLR at pump power rates: 70 (black), 80 (red) and 90% (blue), and $Q_l = 70\frac{m^3}{h}$.

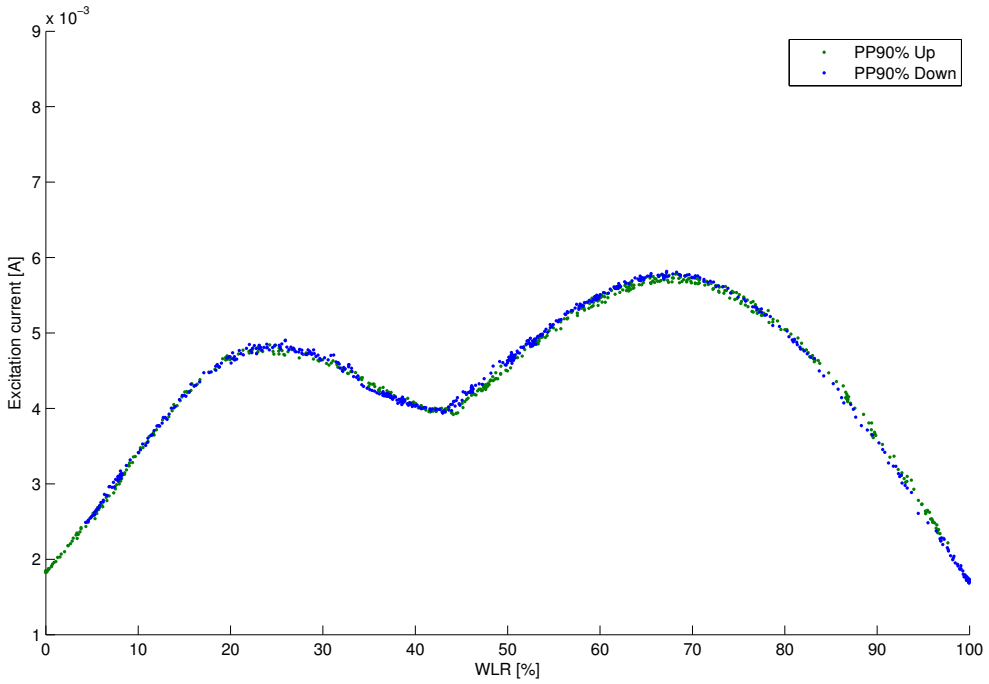

Figure 5.5: Experiment 1, part 2: Hysteresis plot of excitation current vs. WLR at pump power rate 90%, and $Q_l = 70\frac{m^3}{h}$. Increasing WLR is marked with green, and decreasing WLR with blue.

Part 3: $Q_l = 30\frac{m^3}{h}$

Figure 5.6 shows EC against WLR for the $Q_l = 30\ \frac{m^3}{h}$ part of the experiment. For the water-continuous maximum, the difference in EC between different PP is smaller than for the $Q_l = 50\frac{m^3}{h}$ and $Q_l = 70\frac{m^3}{h}$ parts of the experiment. The diesel-continuous maximum ($WLR \approx 25\%$) is close to, or has an even higher EC than the water-continuous maximum ($WLR \approx 65\%$). This resembles the effect one could expect from high temperatures. The temperature in the flow rig is the same in this part of the experiment, as for Part 2, so this explanation is not likely. The minimum is shifted to a lower WLR, and has a steep transition towards the diesel-continuous maximum. Each point in the plot represents a sample taken with 1 second intervals between them, so the transition period between the diesel-continuous maximum and the minimum must be just a few seconds.

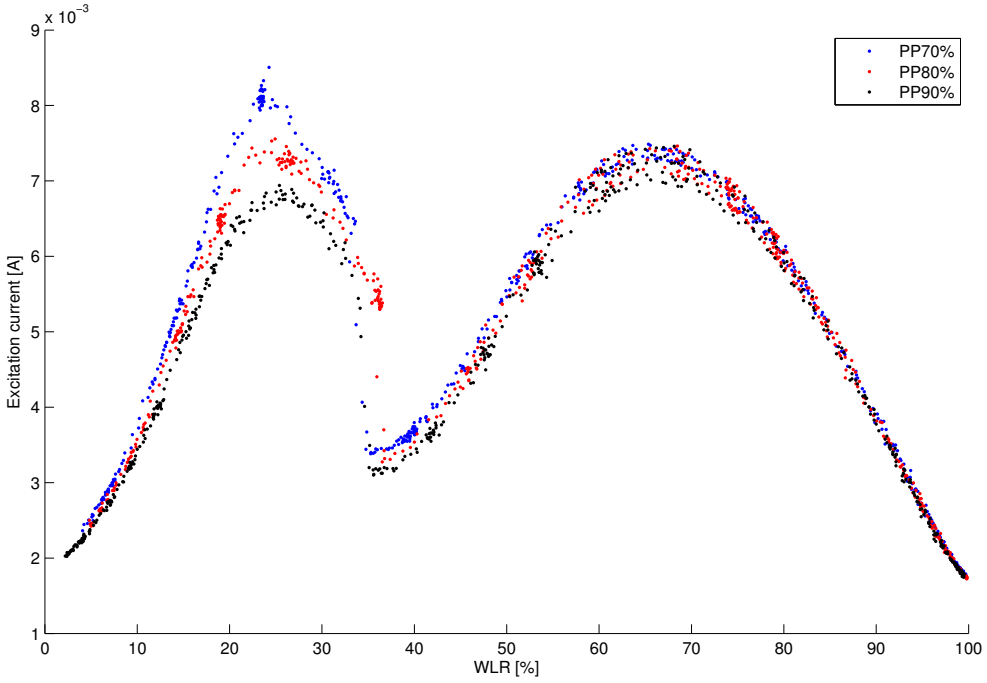

Figure 5.6: Experiment 1, part 3: Excitation current vs. WLR at pump power rates: 70 (blue), 80 (red) and 90% (black), and $Q_l = 30\frac{m^3}{h}$.

It is observed that for $Q_l = 30\ \frac{m^3}{h}$, the EC response is higher for diesel than for water. This is unexpected, and something the model does not predict. The low flow rate will give the liquid more time to alter or develop the flow regime. This could lead to large droplets of water, which would demand large EC. This is supported by the fact that better mixing seem to not only lower the EC vs. WLR curve, but also keep the samples in an orderly manner. This could be explained by a more uniform mixture when mixing is better. Why this only happens on the diesel continuous part of the WLR range is

unclear.

The hysteresis was measured at PP 70%. Figure 5.7 shows that the directions give similar outcome in the regions from WLR = 0% to about 30% and from about WLR = 55% to 100%. For increasing WLR we have a steep transient area between WLR = 50% and 55%, with the minimum located just above 50%. For decreasing WLR, the steep transient area is located between WLR = 35% and 30%. The minimum for decreasing WLR is located at about WLR = 35%. The maximum for diesel-continuous flow is higher than the maximum for water-continuous flow.

The hysteresis is different for the different conditions investigated. Comparing the hysteresis measurements from Parts 1, 2 and 3 shows that hysteresis is not constant. It is not an unknown phenomenon that the point where continuous phase changes is different dependent on which direction WLR is changed. In this experiment it seems like the hysteresis is more dependent on liquid flow rate than pump speed. This could be due to the fact that lower flow rate will give the liquid more time to develop a flow regime according to conditions, and mixing from the pump is less important.

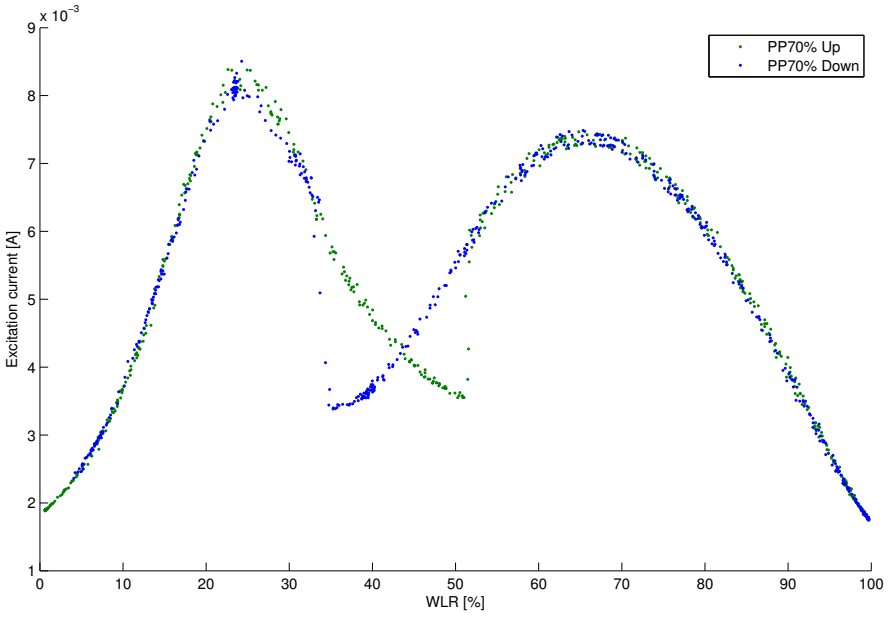

Figure 5.7: Experiment 1, part 3: Hysteresis plot of excitation current vs. WLR at pump power rate 70%, and and $Q_l = 30\frac{m^3}{h}$. Increasing WLR is marked with green, and decreasing WLR with blue.

One important observation is that the EC is more or less the same for clean liquids, even though they have different densities and viscosities. A pure liquid will give a single, low response in EC. This experiment shows that a liquid/liquid mix can be suspected based on the magnitude of the EC. Due to hysteresis and non-linearity, this can not be a measure of WLR alone.

5.2 Experiment 2: The gas-injection experiment

Experiment 2 is meant to build on the observations in Experiment 1. The procedure is mainly the same, but gas is injected into the liquid flow, right before the centrifugal pump. The motivation behind this experiment is to investigate if gas in the liquid flow can be detected, and how different rates of gas injections in the liquid flow affect Coriolis measurements, according to Objective 2.

5.2.1 Measurement set up

The experiment has the following set-up:

- Conducted with the general experiment set-up, explained in Chapter 4.
- Measurements were done in the 3" section of the loop.
- Gas injected into the liquid flow, controlled by the Bronkhorst mass flow controller.

The 3" line of the flow rig is used, since this gives the highest GVF.

5.2.2 Procedure

The measurements in this experiment are all taken using the WLR-sweep method, as explained in Section 4.4.

Part 1: A hysteresis measurement was taken, and used as a measurement of behaviour of the flow rig. This was compared to the one in part 1 of Experiment 1, to see if the flow rig had significantly different response, with the same settings. The hysteresis measurement was taken with liquid flow rate, $Q_l = 50\ \frac{m^3}{h}$, pump power rate, PP = 90% and no gas injection, the same as in Experiment 1.

Part 2: It is of interest to see how different GVF will influence on the EC. The liquid flow rate was kept constant at $Q_l = 50\ \frac{m^3}{h}$, pump power rate constant at PP = 90% and gas was injected in the steps shown in Table 5.5. Experiment 1 and best practises promote as high mixing as possible. Normally the flow rig is operated at 90% pump power rate, so this value was chosen. Liquid flow rate has less influence on the response, so a choice were made, $Q_l = 50\ \frac{m^3}{h}$, this is a typical rate used in the 3" flow line.

Table 5.5: Experiment 2, part 2: Steps of GVF used for measurements

GVF [%]					
0.0	0.1	0.2	0.3	0.4	0.5

Part 3: The effect of PP on the EC with injected gas was studied. The "worst case"-scenario of $GVF = 0.5\%$ was chosen. The liquid flow rate was kept constant at $Q_l = 50\ \frac{m^3}{h}$, and the PP changed in the steps as shown in Table 5.6

Table 5.6: Experiment 2, part 3: Steps of pump power rates used for measurements

PP [%]		
90	80	70

5.2.3 Results and discussion

Part 1: The hysteresis measurement, shown in Figure 5.8, is different from the hysteresis measurement from Experiment 1, Figure 5.3. The point that is assumed to be an indication of change in continuous phase is not located at the same WLR for increasing and decreasing WLR. Outside the area where phase change occurs, the samples follow each other, and the samples form tight, defined "lines".

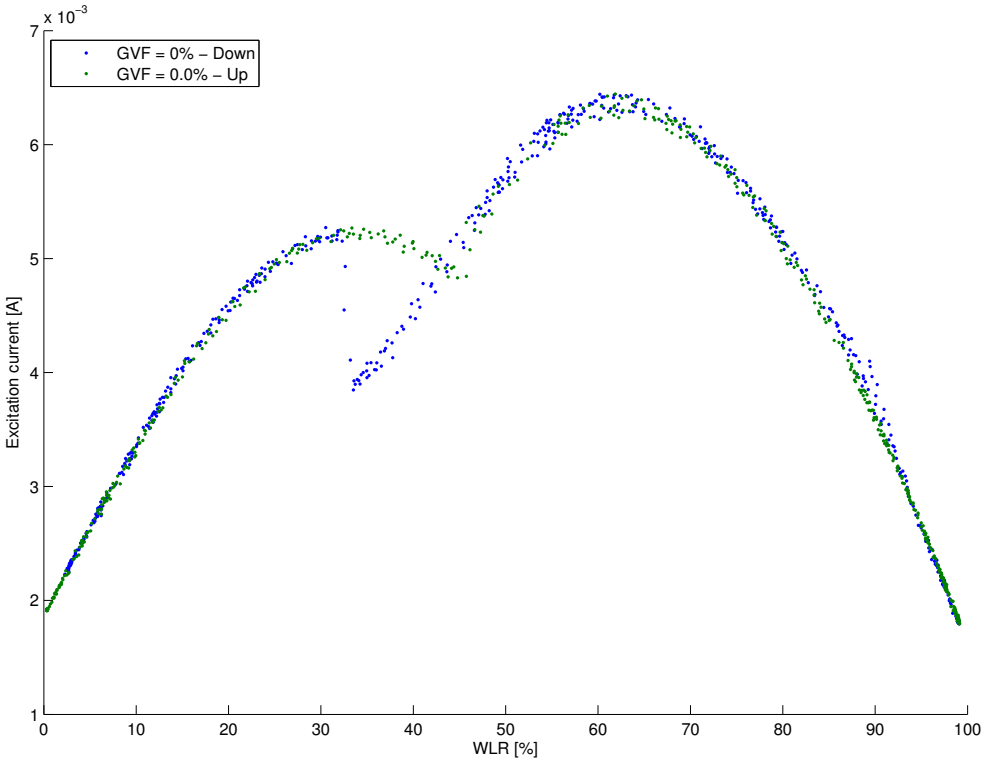

Figure 5.8: Experiment 2, part 1: Hysteresis plot. Excitation current vs. WLR at pump power rate 90%. $Q_l = 50\ \frac{m^3}{h}$. Increasing WLR is marked with green, and decreasing WLR with blue.

As this experiment is meant to follow Experiment 1, it is natural to compare the two. The hysteresis plot shows a different response than the plot from Experiment 1, even if

the controllable inputs were the same. It is evident that other factors than mixing and flow rate play a role in where and how phase change occur. Temperature differences between the measurements could a be part of an explanation.

Part 2: Gas was injected at different GVF into the liquid flow, as shown in Figure 5.9. In the diesel-continuous part of the WLR-range these amounts of gas do not seem to have any significant effect. With no gas present (green) a defined line is created in the water-continuous part of the WLR-range, as seen in the hysteresis plot. Injecting gas seems to create some disturbance. If one is willing to accept the presence of an imaginary line, created by the samples. Injected gas seems to make the samples deviate from this line, and more gas will spread the samples more. The response in EC is also increasing with increasing GVF.

Figure 5.9 shows that the curve created by the samples is similar with different amounts of gas, but with a large response to gas injection. In the diesel-continuous part of the WLR range, the gas has little or no effect. This could be due to the viscosity of diesel holding the gas bubbles in place. For the point of continuous-phase shift, where the effect of viscosity should be highest, this is not the case. Effective viscosity seem not to have the same effect on gas bubbles as it has on the two liquids in the mixture.

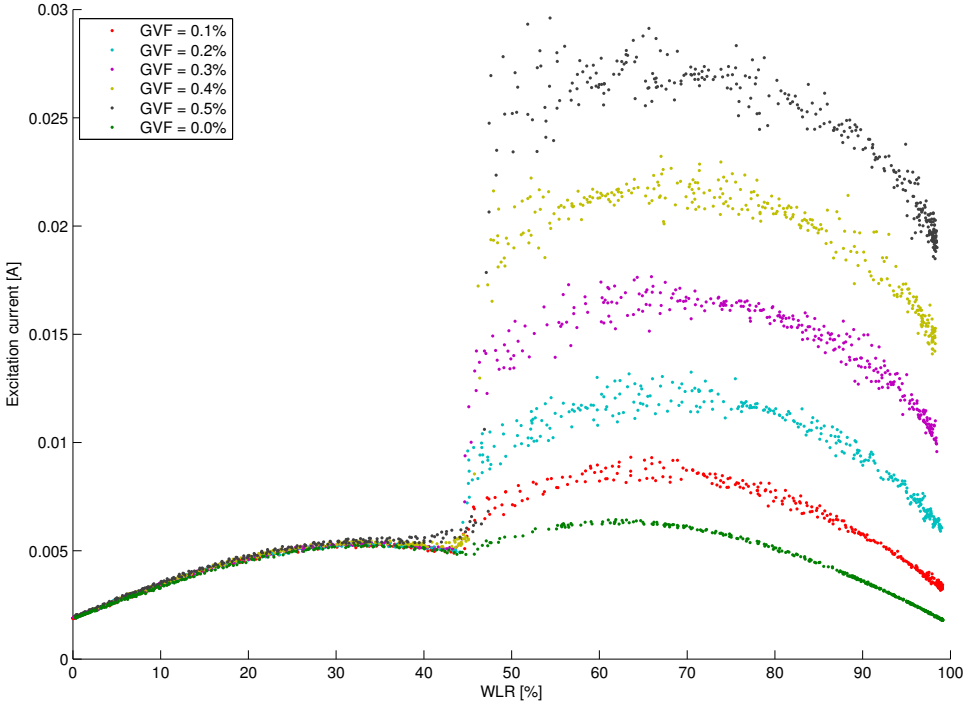

Figure 5.9: Experiment 2, part 2: Excitation current vs. WLR. PP = 90. GVF injected in 0.1% steps, and $Q_l = 50\ \frac{m^3}{h}$. 0.0% is green, 0.1% - red, 0.2% - turquoise, 0.3% - magenta, 0.4% - yellow and 0.5% - black

Part 3: The response in EC for different levels of PP, is shown in Figure 5.10. This is conducted with $Q_l = 50\ \frac{m^3}{h}$. and GVF = 0.5%. The results show that more mixing decreases the response marginally, and perhaps also keeps the samples more along the imaginary line. In the diesel-continuous part of the plot, some separation between the different measurements can be observed.

Better mixing gives less response in excitation current, and a somewhat smaller spread in the samples. This could be explained by smaller gas bubbles and smaller narrower distribution of bubble sizes, assuming the the theory of Morales *et al.* [20] also applies for gas bubbles. Due to large difference in density between gas and either of the present liquids, we expect large impact from decoupling effects. This can be seen in the high EC needed to keep the Coriolis tubes oscillating at constant amplitude.

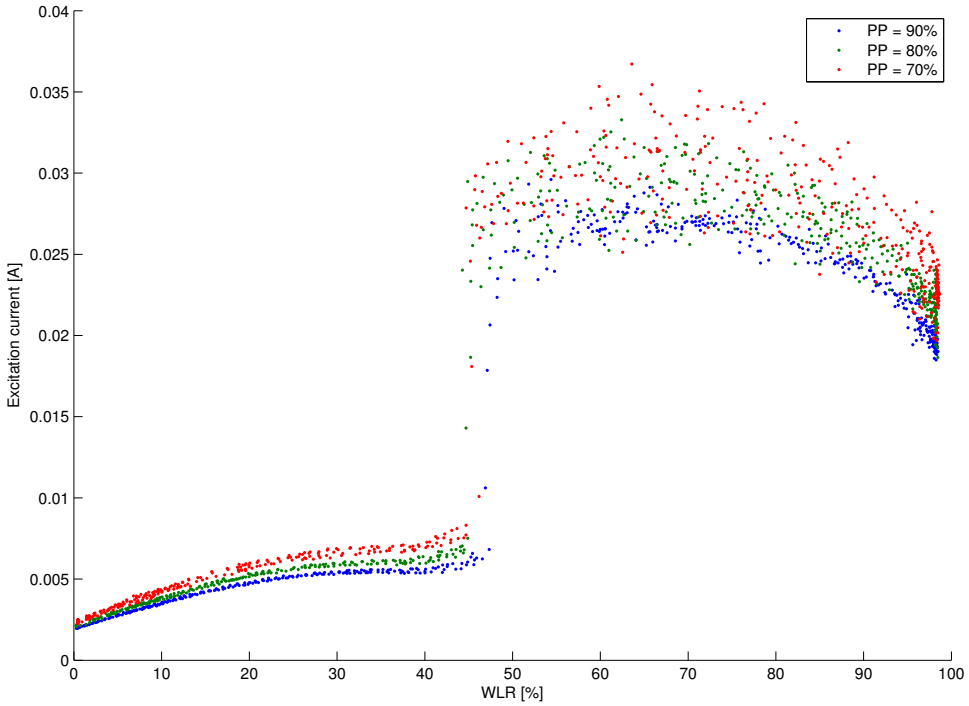

Figure 5.10: Experiment 2, part 3: Excitation current vs. WLR. GVF = 0.5%. PP = 70 (red), 80 (green) and 90% (blue), and $Q_l = 50\ \frac{m^3}{h}$

This experiment has shown that gas can have huge impact on EC in the Coriolis flowmeter. Various conditions can alter the response, and there is quite a spread between samples, so based on EC measurements alone, the amount of gas in the liquid flow can not be quantified.

5.3 Experiment 3: The CMR flow-rig stress test

An important part of the motivation of the thesis work is to use the reference Coriolis flowmeter to investigate if it is possible to detect and quantify entrained gas from the separator tank. Based on the results from previous experiments, and this experiment, this is investigated. It is of interest to see if any entrained gas can be detected, and what flow rates entrained gas occurs. With this experiment, Objectives 3 and 4 are investigated.

5.3.1 Measurement set up

The experiment follows this set up:

- Conducted with the general experiment set-up, explained in Chapter 4.
- Measurements were done in the 6" section of the loop.
- Gas injected into the liquid flow, controlled by the Bronkhorst mass flow controller.

This experiment is conducted in the 6" section of the flow rig. In this section, the highest liquid flow rate can be achieved. This means all liquid in the system is circulated through faster, giving less time for gas to separate in the separation tank. Thus, we are more likely to experience entrained gas.

5.3.2 Procedure

This experiment uses significantly higher liquid flow rates than those used in earlier experiments. The response from different WLR has been studied in the previous experiments, these have shown that the highest Excitation Current (EC) response, if gas is present, is around WLR = 65%. In this experiment WLR was kept at this level.

Part 1: The different flow rates, and Pump Power rate (PP) settings used in part 1, are shown in Table 5.7. For all steps gas was injected, with GVF steps 0.02 % from 0.0 to 1.0%. These measurements were taken using the *Point measurement*-method described in Section 4.4.

Table 5.7: Experiment 3, part 1: Measurement steps, pump power rates and liquid flow rates.

PP [%]	Q_l $[\frac{m^3}{h}]$
80	120
90	120
90	140
90	160
90	180

Part 2: Higher flow rates were tested, without gas. All of these measurements were done using WLR = 65% and PP = 90%, with no gas injected. The steps used in part 2 are presented in Table 5.8. 250 $\frac{m^3}{h}$ is the highest flow rate achievable in the CMR flow rig. The experiment starts out by taking big steps, but change to smaller steps in the area where entrained gas could be expected, if present. These measurements were taken using the *Point measurement*-method described in Section 4.4.

Table 5.8: Experiment 3, part 2: Measurement steps, different liquid flow rates

Q_l $[\frac{m^3}{h}]$							
160	170	180	190	200	205	210	215
220	225	230	235	240	245	250	

Part 3: To investigate the response of changing WLR at high liquid flow rates, a *WLR-sweep* measurement was conducted at $Q_l = 250$ $\frac{m^3}{h}$ and PP = 90%. WLR was changed from 0% to 100%, in the same way as in previous experiments. No gas was injected. The *WLR-sweep* method is described in Section 4.4.

Part 4: To investigate the effects of gas at $Q_l = 250$ $\frac{m^3}{h}$, *point measurements* were taken while injecting gas. WLR was set to 65%, PP to 90% and $Q_l = 250$ $\frac{m^3}{h}$. The steps of gas injection are presented in Table 5.9.

Table 5.9: Experiment 3, part 4: Measurement steps, different GVF

GVF [%]									
0.0	0.005	0.01	0.015	0.02	0.03	0.04	0.05	0.06	0.07

5.3.3 Results and discussion

In **Part 1** of this experiment, presented in Figure 5.11, the plot shows that increasing GVF will increase Excitation Current (EC). This happens for all the different settings tested. Two different Pump Power rate (PP) were used for $Q_v = 120\frac{m^3}{h}$, higher PP seems to decrease response in EC. Increasing liquid flow rate seems to increase the same response. With no gas injection the difference is quite small, but with higher GVF, the difference escalates. One standard deviation for each measurement is presented as error bars, increasing GVF gives higher standard deviation.

In previous experiments, as well as in this, we see an increase in EC when gas is present. This is expected and explained by decoupling effects due to large differences in density. The standard deviation is clearly affected by gas in the flow, and increasing with increasing GVF. This might be used as an indication of gas, together with high EC.

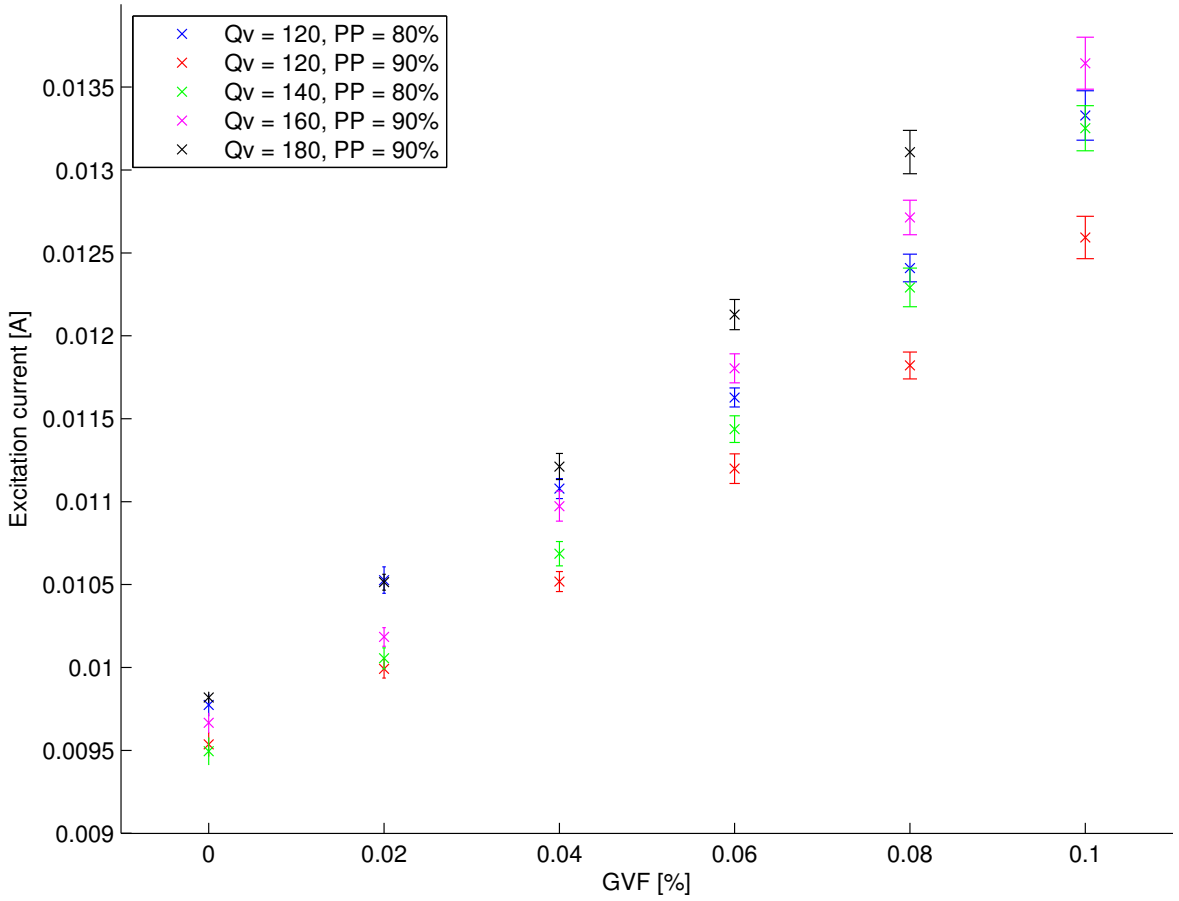

Figure 5.11: Experiment 3, part 1: Excitation current against GVF, at high liquid flow rates. One standard deviation is shown as error bars. Blue: $Q_l = 120\frac{m^3}{h}$ and $PP = 80\%$. Red: $Q_l = 120\frac{m^3}{h}$ and $PP = 90\%$. Lime: $Q_l = 140\frac{m^3}{h}$ and $PP = 90\%$. Magenta: $Q_l = 160\frac{m^3}{h}$ and $PP = 90\%$. Black: $Q_l = 180\frac{m^3}{h}$ and $PP = 90\%$.

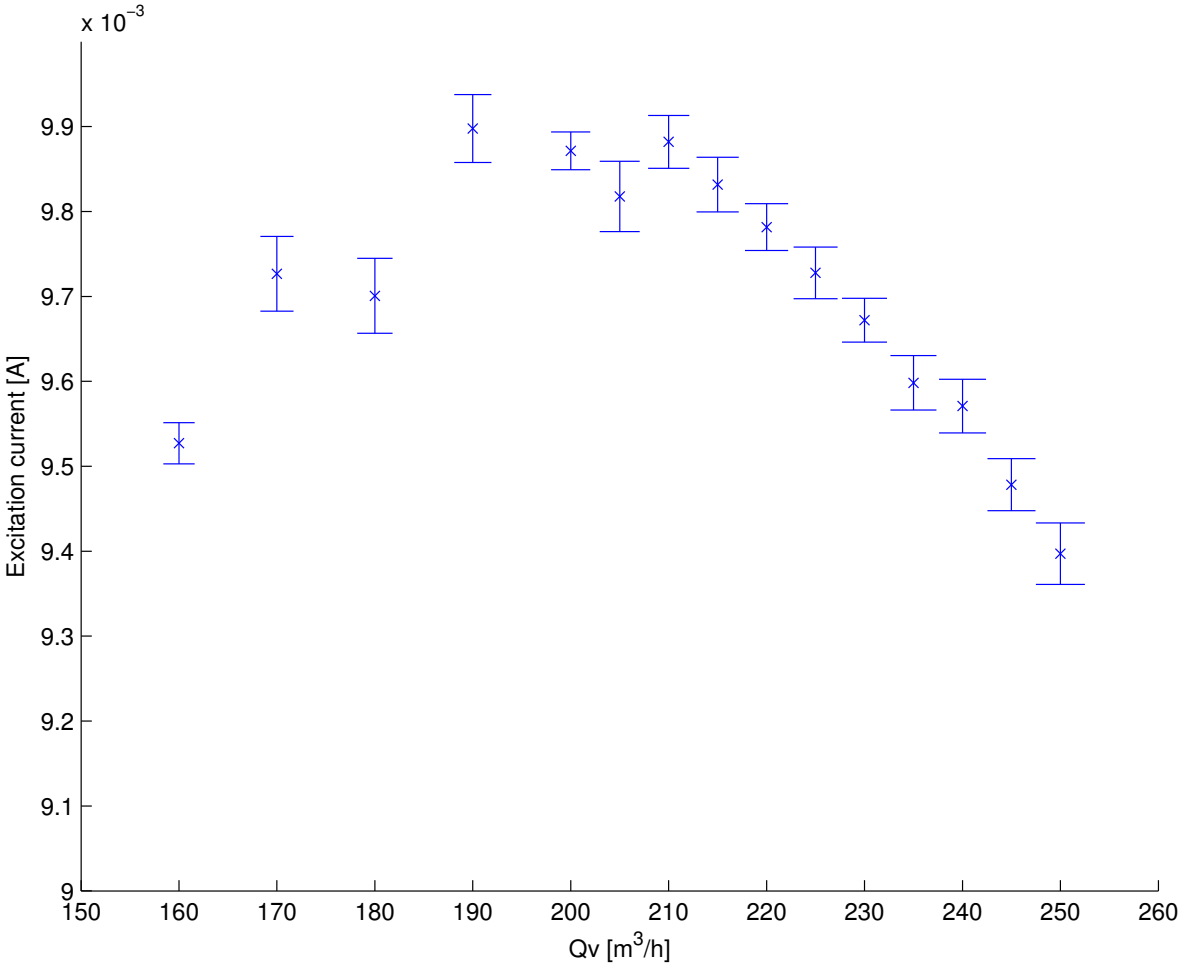

Figure 5.12: Experiment 3, part 2: Excitation current against high liquid flow rates, no injected gas. One standard deviation is shown as error bars.

In **Part 2**, presented in Figure 5.12, EC increases with increasing flow rate up to a point where increasing flow rate will cause a decrease in EC. The measurements done in part 1 were all in the area where higher flow rate causes higher EC. The standard deviations are quite similar in the entire range, and even though there is a change in EC, the change is quite small.

The observed increase in EC, associated with increasing flow rate, has shown not to be consistent. EC decrease when liquid flow rate increase beyond $\approx 200\ \frac{m^3}{h}$ in the studied case. Morales *et al.* [20] observe a slight increase in bubble size with increasing liquid flow rate. It is hard to determine if this is the effect observed in this experiment, due to lack of observations, but it could explain some increase in EC. However, it can not explain why the EC falls again when increasing liquid flow rate even more. The differences in EC caused by flow rate are quite small compared to the impact other effects have.

Figure 5.13 shows the data from **Part 3** of the experiment. The WLR-sweep mea-

surement was conducted with liquid flow rate $Q_V = 250\ \frac{h^3}{h}$ and PP = 90%. Comparing this to previous experiments, the well known shape of the curve is present. The line they form is quite defined across WLR range. The magnitude in EC is in the same area as seen in previous experiments, where no gas was injected. Due to high flow rates, WLR = 0% and WLR = 100% could not be achieved, due to entrainment of water and diesel, respectively.

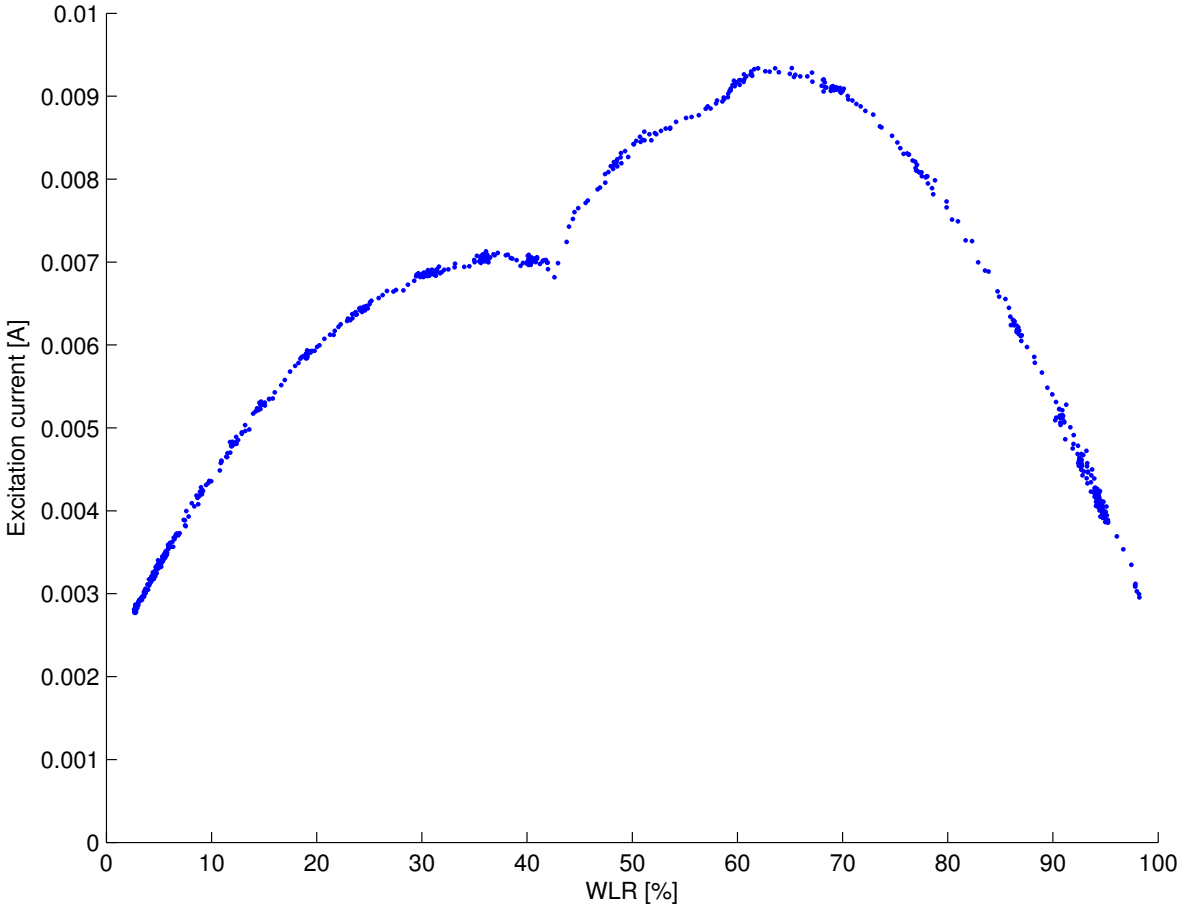

Figure 5.13: Experiment 3, part 3: Excitation current against WLR, at liquid flow rate $Q_V = 250\ \frac{h^3}{h}$ and PP = 90%.

Figure 5.14 shows **Part 4**, where gas is injected while running the rig at full speed. This was done to investigate how the response in EC is when known quantities of gas is present. An increasing response can be observed, when increased fractions of gas are injected. The standard deviation also increases with increasing GVF.

The standard deviation is clearly affected by gas in the flow, and increasing with increasing GVF. In the measurements taken with no gas injected, the standard deviation is lower than 45 μA, see both Figure 5.12 and the first measurement in Figure 5.14. The two next measurements in Figure 5.14 shows injected gas with GVF = 0.005% and 0.01%, standard deviations are below 45 μA. For gas injected with GVF = 0.015% and

0.02%, the standard deviations are in the same region. For all injected gas fractions higher than 0.02%, the standard deviation is larger than 100 μA. This might be used as an indication of gas present in the system, at least for higher gas fractions.

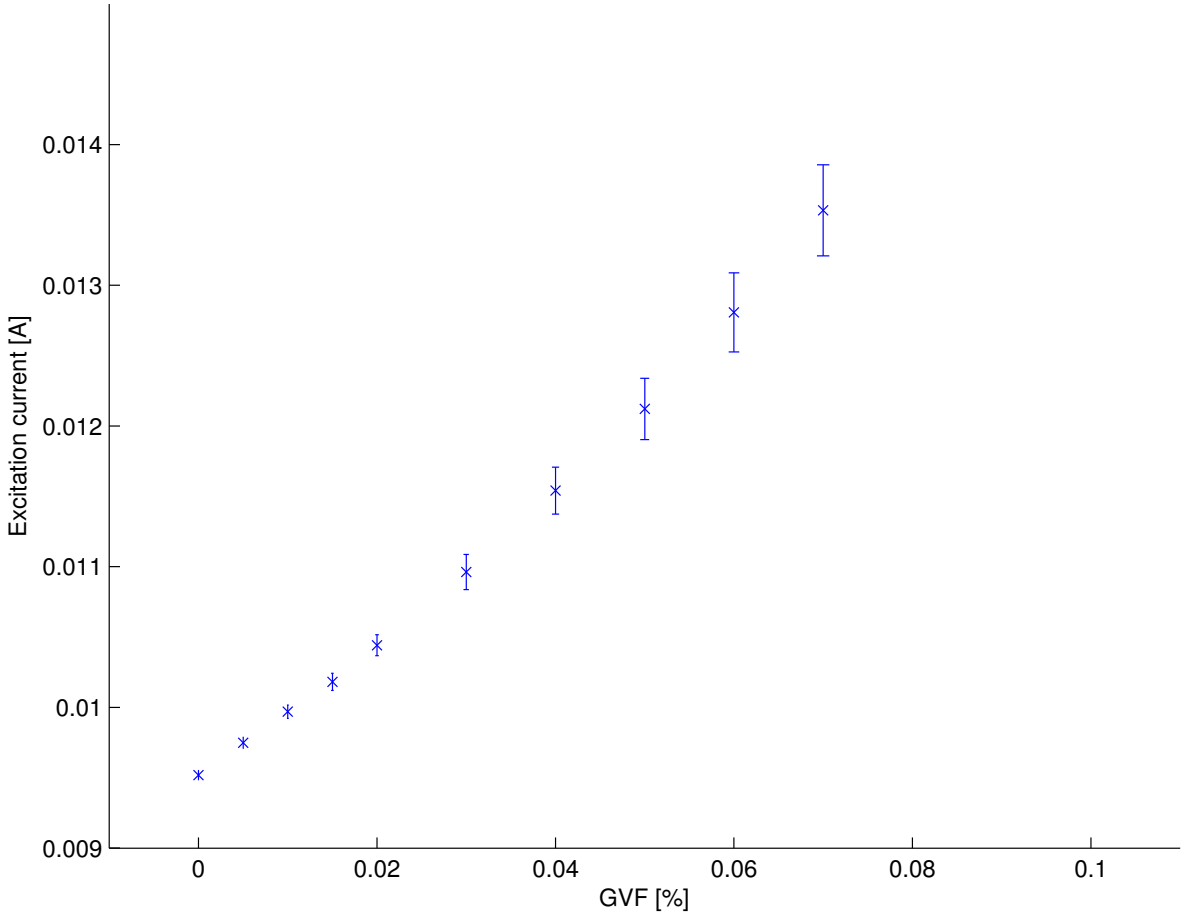

Figure 5.14: Experiment 3, part 4: Excitation current against GVF, at liquid flow rate $Q_V = 250\ \frac{h^3}{h}$ and PP = 90%. One standard deviation is shown as error bars.

In this experiment a tight distribution in the WLR-sweep measurement is observed. Previous experiments have shown wider distribution for GVF from 0.1% and more. There is no reason to expect these levels of gas in the flow. There is no sign of entrained gas in the mixture, at this flow rate, but GVF up to 0.02% can not be disproved with this experiment.

It seems like GVF over 0.02% can be detected. Because the magnitude of EC changes with conditions, it is not possible to quantify GVF based on these measurements alone. When liquid flow rate increases to very high levels, an EC is decreasing. From this it can be assumed that an increase in EC at these levels indicates entrained gas.

Chapter 6

Measurement uncertainty and error sources

Error sources and how they contribute to uncertainty will be discussed in this chapter. Uncertainty calculations, based on both results from the model in Chapter 3, and the experiments in Chapter 5 are also presented.

Weinstein [15] focuses on predicting density error, due to decoupling. The model presented and used for density error calculations agrees with previous models with the same purpose. The calculations for density error are based on amplitude ratio, and no phase angle is considered. A model for density error that takes phase difference into account has not been developed, nor has a model for mass flow errors. A starting-point for developing a model that considers phase difference is proposed in Weinstein [15], and it is assumed that this could be expanded to predict mass flow error.

Due to the lack of models to predict mass flow error, only density error is estimated in this thesis. No phase angle is used in the model, even if the mathematical model, descibed in Chapter 3, predicts some phase difference. Solving for the diesel/water mixture used in this thesis, using the *reference conditions* defined in Chapter 3, the magnitude of the phase angle is less than 2 degrees. This is considered so small that a good approximation for density error can be achieved.

6.1 Model uncertainties

In this thesis, many assumptions have been made. The largest contributors to model uncertainty is assumed to be the assumption that the equations are valid for high particle concentrations. The impact of this would be most significant in the area around continuous-phase change. This is also the area where the model and measurements

correspond least.

Particle size is an important contributor to power dissipation, and the particle sizes used in this thesis is chosen based on studies of diesel droplets in water. It is unlikely that the diesel quality is the same as used in CMR's flow rig, so different behavior is not unlikely. Further, the particle sizes from the study is used for water droplet in diesel, this is probably a rough assumption, and a large contributor to model uncertainty.

Viscosity of diesel for different temperatures is assumed based on a study of temperature dependency of different oils. Diesel is one of the oils studied, but the quality is not the same as the for the one used in CMR's flow rig. This could also contribute to the uncertainty of the model.

The model also assume constant oscillation amplitude, even if the particle would experience different oscillation amplitudes depending on its location in the tube. This is however assumed to be less important, as the results are not compared numerically, but changes in response are compared with the difference in measurements of different conditions.

6.2 Measurement uncertainties

This thesis studies the response of the Coriolis flowmeter used as a reference meter in CMR's flow rig. The flow rig is used by other experiments as well, so no major changes to the set up or software can be made. This means that some of the measurements taken in this thesis are taken with the same instrument being investigated. Both volume flow rate and WLR is controlled by PID controllers, and measurements of both are dependent on density. Volume flow rate is also dependent on measurements of mass flow rate. Both density and mass flow rate are affected by decoupling, so by injecting gas into the liquid flow, the PID controllers will get erroneous input values, and alter the conditions accordingly. The WLR calculation assume only diesel and water in the flow, and present gas will reduce mixture density, and thus decrease WLR estimations. This is a large contributor to the measurement uncertainties in this thesis, and is hard to correct for as the impact of these contributions are unknown. This will also affect GVF calculations, as these depend on fluid flow rate. Based on the model, density error contributions can be estimated.

6.3 Density error

The Coriolis flowmeter measures density of the mixture within the tubes. Consider the case where water, $\rho_{water} = 1000\frac{kg}{m^3}$ contains 5% air, $\rho_{air} \approx 1\frac{kg}{m^3}$. The measured density

is $\rho_{mix} \approx 950\frac{kg}{m^3}$. If your intentions are to measure the density of water, this could be interpreted as a density error of $\approx 5\%$. However, the density of the mixture is measured correctly.

From here on *actual* density is used for mixture density. What the observer expect to see, is not considered. It is the measurement of what's really in the tube that is important.

The actual density of a two phase (two component) mix, defined in terms of volume fraction of the dispersed phase, α is [15]:

$$\rho_{actual} = \rho_f(1-\alpha) + \rho_p\alpha \tag{6.1}$$

This is the actual density of the mixture. Decoupling cause measurement errors due to movement in CG. The measured density of a mixture experiencing decoupling will therefore be different. Weinstein [15] presents a term for the decoupled density. This is the density measured if decoupling is present. By studying the movement of CG caused by fluid displacement and particle displacement, the following term is derived:

$$\rho_{decoupled} = \rho_f(1-\alpha) - (\rho_f - \rho_p)\alpha\left(\frac{A_p}{A_f} - 1\right) \tag{6.2}$$

An expression for the non-contributing part of the density was found. This is dependent on amplitude ratio, $\frac{A_p}{A_f}$. This part is subtracted from the actual density to find the measured, decoupled density.

To find an expression for density error, decoupled density is subtracted from actual density:

$$\rho_{error} = \rho_{decoupled} - \rho_{actual} = -(\rho_f - \rho_p)\alpha\left(\frac{A_p}{A_f} - 1\right) \tag{6.3}$$

This can be expressed as a percent of the actual density:

$$\rho_{error,\%} = 100\left(\frac{\rho_{decoupled} - \rho_{actual}}{\rho_{actual}}\right) = 100\left(\frac{-(\rho_f - \rho_p)\alpha\left(\frac{A_p}{A_f} - 1\right)}{\rho_f(1-\alpha) + \rho_p\alpha}\right) \tag{6.4}$$

In the theoretical case of an infinitely viscous fluid, containing a gas bubble, the amplitude ratio is zero, thus the density error caused by decoupling is zero. In the invisid case, maximum amplitude ratio for a light particle is 3:1, and maximum density error is then two times the volume fraction of the gas.

In the case of a bubble in a liquid mixture, e.g. nitrogen in a diesel/water mixture, this model is not sufficient. Assuming the bubbles movement is held back by effective viscosity, and that the bubble will not move further than it would in a clean liquid. The

worst case scenario would be a nitrogen bubble in pure water, as this has the highest density difference and lowest viscosity.

6.4 Density error calculations

Using the reference condition defined in Section 3.8, estimations for density error can be found. Equation (6.4) is solved for all different WLR, the result is presented in Figure 6.1. As predicted, and explained, all errors are negative. Maximum negative density error for a diesel/water mixture, in the given conditions, is $\approx 0.14\%$.

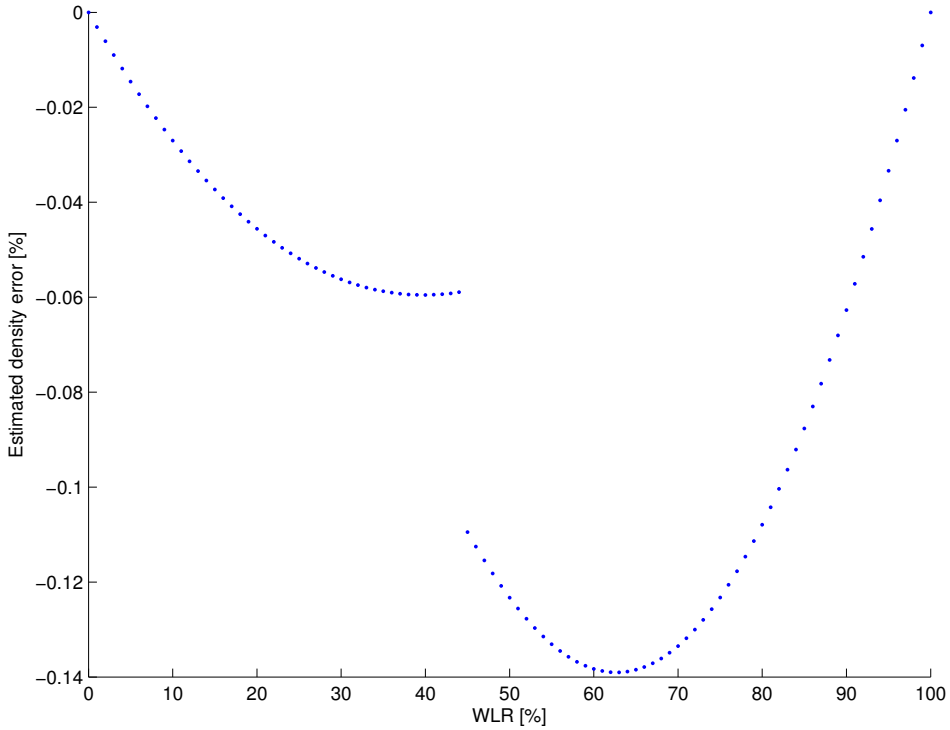

Figure 6.1: Estimated density error for different WLR, using reference conditions. Continuous-phase change at WLR = 45%.

The cases of high pump speed, low pump speed and high temperature are also investigated. Alle scenarios are the same as presented in Section 3.8. High pump speed, reduce maximum density error to less than 0.10%. Low pump speed will increase the maximum density error to $\approx 0.19\%$. High temperature will give a small increase, to $\approx 0.15\%$. Density error contributions are shown in Appendix E.

The results for a nitrogen bubble in water are shown i Figure 6.2. All the relevant settings from the *reference condtitions* in Section 3.8 are used, including bubble size. From this it is clear that the viscous case has a smaller density error than the theoretical invisid case.

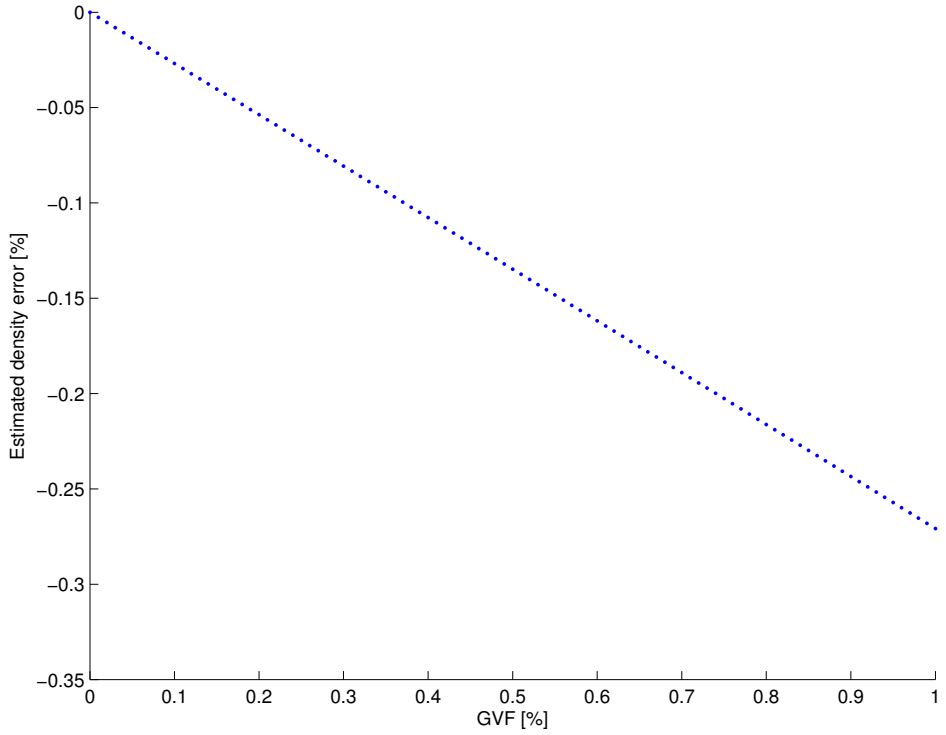

Figure 6.2: Estimated density error for different GVF, nitrogen bubble in water

6.5 Discussion

Unfortunately, the particle size can not be observed, and are therefore assumptions. The results are still clear that high Pump Power rate (PP) is desired, to minimize droplet size and thus decoupling ratio. Temperature can not be controlled in CMR's flow rig. The case of high temperature could be valid for hot days or in the end of days where the rig has been used at high flow rates for long periods of time. The change in density error is small, but the temperature in the flow rig should be kept as low as possible.

If the droplets were ten times larger than the ones used in Figure 6.1, the density error would be $\approx -1\%$ If feels safe to assume that the density error, caused by decoupling in a diesel/water mixture is less than -0.5%, for all WLR. Endress+Hauser is probably correcting for some of this, before measured values are presented. It is therefore unclear if it is necessary to include this in the uncertainty of WLR and volume flow rate.

In the case of entrained gas with GVF $= 0.02\%$, which is an assumed maximum of entrained gas, the density error is just $\approx 0.005\%$. The results when changing bubble size and viscosity suggests that it is fair to assume that density error will be less than -0.01% from entrained gas in the CMR flow rig. Bear in mind that compressibility effects have not been considered, and that this contribution would be in positive direction.

Chapter 7

Summary and conclusion

This thesis has studied some of the effects of two and multiphase flow in Coriolis flowmeters. The working principles of the Coriolis flowmeter has been explained, and how mixtures and flow conditions can affect it has been described. A mathematical model of particle movement inside an oscillating environment has been presented, and MATLAB has been used to solve the model equations for relevant conditions. Several experiments have been conducted, and compared with the theoretical result, and observations have been explained.

We are able to detect if the flow consist of more than one component, as wanted in **Objective 1**. This will show as an increase in excitation current. However, the magnitude of excitation current is not consistent from experiment to experiment, so the data from one experiment is not directly comparable to the data from another. Other factors, such as temperature, can significantly alter viscosity, and therefore excitation current. The temperature in the flow rig is not controlled. This means that one single measurement of excitation current is not sufficient to explain the content of the Coriolis flowmeter. This is shown in Experiment 1, where temperature plays an important role.

Uncertainty estimations show that for a diesel/water mixture, expected density error caused by decoupling is less than -0.5%. Density error is dependent on decoupling rate, as a rough measure EC indicate density measurement error. However, the density error calculations are based on amplitude ratio alone, EC is dependent on phase shift as well as amplitude ratio. More EC gives higher magnitude of density error. It is unknown if Endress+Hauser compensate for effects caused by inhomogeneities in a liquid/liquid mixture. Compressibility errors have not been investigated in this thesis. These are assumed to have small magnitude compared to the magnitude of decoupling errors, especially for liquid mixtures. Compressibility errors are positive, and will reduce the overall uncertainty when decoupling errors are present. Decoupling errors can not be compensated in full extent by compressibility errors.

Detecting large quantities of gas is easy, this was part of **Objective 2**. This will show as a large increase in excitation current. In some cases so large that only one single measurement can indicate presence of gas. Taking several samples will give large standard deviations if large quantities of gas is present. This might be used as an indication of present gas. Due to impact from uncontrollable inputs, such as temperature, the EC can not be used as a measurement of gas quantities.

Gas in the mixture gives a large contribution to uncertainty, due to viscosity the density error estimation is less than for a theoretical invisid maximum of 2 times the void fraction of present gas, i.e. 5% void fraction of gas could in theory give 10% density error.

Small quantities of gas have shown difficult to prove. This was a part of **Objective 3** to investigate. The response in excitation current does not need to be larger than responses from other effects, and when only small fractions of gas is present the standard deviation is in the same range as for no gas.

We do not know how large quantities of gas that can or will be entrained, so it is difficult to say if we are able to detect it, if it occurs. If a specific flow rate is studied thoroughly, it is assumed that GVF over 0.02% can be detected.

In **Objective 4** it is of interest to find what flow rates can be achieved in the flow rig, without gas entrainment from the separator tank. Running the rig at full power show no evidence of entrained gas, but entrained gas cannot be disproved. Based on the results from Experiment 3 it can be assumed that if any entrained gas is present, GVF is less than 0.02%, based on both magnitude of excitation current and standard deviation. Contribution to density error from entrained gas is assumed to be less than -0.01%. Based on calculations done for worst case scenarios.

To find methods for reducing the effects caused by inhomogeneities is part of **Objective 5**. These experiments, and literature on best practises have shown that to minimize effects of entrained gas and liquid/liquid mixture, it is important to run the pump as fast as possible. This is the main contributor to bubble or droplet size, as long as the flow rate is large enough for mixing to dominate over unforced flow regimes.

For CMR in particular, this means to use the 3" flow line, if possible. As it's hard to prove entrained gas in the 6" section, it will be surprising if entrained gas occurs in the 3" section of the flow rig. High viscosity fluids are recommended, but this is not a choice CMR can make, as the content of the rig is determined. CMR use *volume flow rate*, as Coriolis flowmeters measure *mass flow rate* and *density*, volume flow is a derived quantity, see Equtaion 2.13. In the case of entrained gas, mass flow rate will not be affected to any extent. Density will to some degree be affected by the gas, and thus will volume flow rate. To reduce the impact from any entrained gas, mass flow rate

should be the parameter of choice for measuring flow rate.

7.1 Outlook

Due to many assumptions it is natural to propose studies examining whether these are correct or not. This could be studies of actual bubble sizes in the flow, and the viscosity of the different components in the flow rig. Since the measurements from Coriolis meter examined is used for flow control and WLR, consequential errors occurs. For further studies in the CMR flow rig, a set of reference instruments should be installed on the outlet pipes from the separator tank. Instruments to examine the actual conditions of the flow should also be installed close to the Coriolis flowmeter.

Better models should be found, and used. Both for predicting particle movement in fluid, with large particle concentrations, and also a model for better estimates of density errors, which take phase shift into account. A model for mass flow errors could probably be developed from the model phase-shift density model.

Bibliography

[1] Omega. (1999). Transactions in measurement and control, [Online]. Available: http://www.omega.com/literature/transactions/volume4/ (visited on 08/01/2015).

[2] Wikipedia. (Jun. 3, 2015). Daniel bernoulli, [Online]. Available: https://en.wikipedia.org/w/index.php?title=Daniel_Bernoulli&oldid=665336343 (visited on 08/01/2015).

[3] ——, (Mar. 2, 2015). Pitot tube, [Online]. Available: https://en.wikipedia.org/w/index.php?title=Pitot_tube&oldid=649599011 (visited on 08/01/2015).

[4] J. P. Bentley, *Principles of measurement systems*, ed. 4. Pearson Education Limited, 2005.

[5] S. Corneliussen, J.-P. Couput, E. Dahl, E. Dykesteen, K.-E. Frøysa, E. Malde, H. Mostue, P. O. Moksnes, L. Scheers, and H. Tunheim, *Handbook of multiphase flow metering*, www.nfogm.no, 2005.

[6] Wikipedia. (May 22, 2015). Fluid, [Online]. Available: https://en.wikipedia.org/w/index.php?title=Fluid&oldid=663553121 (visited on 08/02/2015).

[7] J. Weinstein, "Multiphase flow in coriolis mass flow meters - error sources and best practices," *International North Sea Flow Measurement Workshop*, no. 28, 2010.

[8] Wikipedia. (Aug. 24, 2015). Coriolis effect, [Online]. Available: https://en.wikipedia.org/w/index.php?title=Coriolis_effect&oldid=677662762 (visited on 08/24/2015).

[9] O. Andersen, "Two component coriolis measurement of oil and water at low velocities," *North Sea Flow Measurement Workshop*, 2004.

[10] H. Zhu, M. Nuber, A. Rieder, and W. Drahm, "Entrained air, particles and wet gas - myths and truth in coriolis flow measurement," *NEL - The Americas Workshop*, no. 4, 2011.

[11] K. Eriksson, D. Estep, and C. Johnson, *Applied Mathematics: Body and Soul: Volume 3: Calculus in Several Dimensions*. Springer Science & Business Media, 2004.

[12] K. O. Plache, "Measuring mass flow using the coriolis principle," *Transducer technology*, 1980.

[13] J. R. Reizner, "Exposing coriolis mass flowmeters' dirty little secret," *Chemical Engineering Progress*, vol. 100, 3 2004.

[14] J. Hemp, H. Yeung, and L. Kassi, "Coriolis meters in two phase conditions," *IEE One Day Seminar on Advanced Coriolis Mass Flow Metering*, 2003.

[15] J. Weinstein, "The motion of bubbles and particles in oscillation liquids with applications to multiphase flow in coriolis meters," PhD thesis, University of Colorado, 2008.

[16] J. Hemp and J. Kutin, "Theory of errors in coriolis flowmeter readings due to compressibility of the fluid being metered," *Flow Measurement and Instrumentation*, no. 17, 2006.

[17] M. Ishii and N. Zuber, "Drag coefficient and relative velocity in bubbly, droplet or particulate flows," *AlChE Journal*, vol. 25, 5 1987.

[18] N. T. Basse, "A review of the theory of coriolis flowmeter measurement errors due to entrained particles," *Flow Measurement and Instrumentation*, no. 37, 2014.

[19] C. E. Brennen, *Fundamentals of Multiphase Flow*, ed. Paperback. Cambridge University Press, 2009.

[20] R. Morales, E. Pereyra, S. Wang, and O. Shoham, "Droplet formation through centrifugal pumps for oil-in-water dispersions," *SPE Journal*, Feb. 2013.

[21] O. A. Aworanti, S. E. Agarry, and A. O. Ajani, "A laboratory study of the effect of temperature on densities and viscosities of binary and ternary blends of soybean oil, soy biodiesel and petroleum diesel oil," *Advances in Chemical Engineering and Science*, vol. 2, pp. 444–452, 2012.

[22] CMR. (2014). Web page, [Online]. Available: `www.cmr.no` (visited on 02/10/2015).

[23] Bronkhorst. (). Datasheet f-201cv, [Online]. Available: `http://www.bronkhorst.com/files/downloads/datasheets/el-flow/f-201cv.pdf` (visited on 17/03/2015).

Appendix A

CMR Multiphase Flow Loop

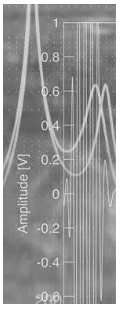

CMR Multiphase Flow Loop

FEATURES

- Location: Indoor
- Fluids: Nitrogen, gas oil (diesel) and salted (NaCl) water
- Pipe diameter: 6” and 3”
- Pressure range: 5-10 bara
- Temperature range: 15 - 35°C (no temperature control)
- Gas flow rate: 1100 Sm^3/h
- Liquid flow rate: 250 m^3/h
- Pipe material: 316 L (acid-proof)

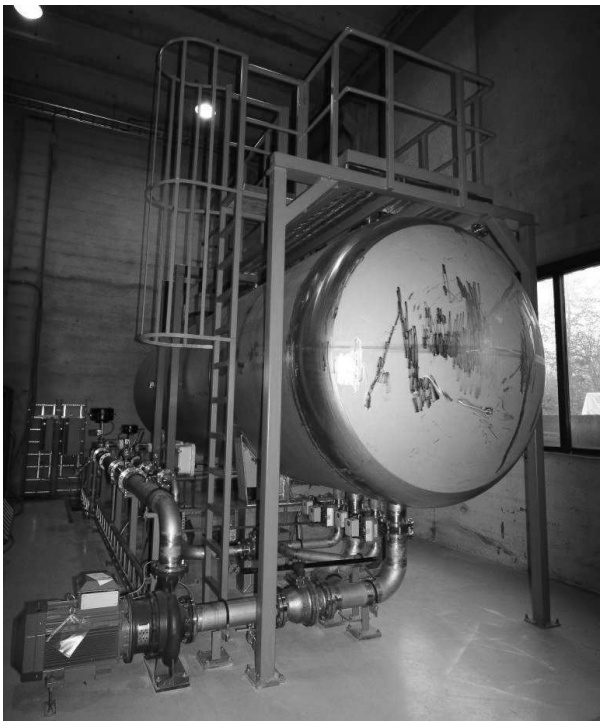

DESCRIPTION

Christian Michelsen Research AS has had a multiphase flow facility since early in the 1990’s, and has significant experience and expertise on flow monitoring. CMR Instrumentation built a new multiphase flow loop during 2008. The rig was financed by CMR with support from the Research Council of Norway and Roxar. It was operative from January 2009.

The new CMR Multiphase Flow Loop is an important tool for CMR when new multiphase metering technologies are being tested and verified during own R&D projects or R&D projects in cooperation with external customers.

The test facility consists of 6” and 3” flow loops, a 32 m^3 separator tank, centrifugal pumps and reference instrumentation for determination of phase fractions, flow rates, flow pressures and temperatures. The fluid media are salted tap water, diesel and pressurised gas. The gas consists of nitrogen in the 95-100% concentration range; the rest fraction in the gas phase is air. The nitrogen is produced from air by a nitrogen generating system driven by a compressor. Another compressor drives the gas circulation through the flow rig.

The flow loop and test area are in rig halls, with a 100 m^2 floor area available for test sections. The entrance door to the test hall is 5 m wide and 3.3 m high. A travelling crane with capacity of 5 tons and lift height of 6.1 m is available.

CMR AS
P.Box 6031
NO-5892 Bergen, Norway

Visiting address:
Fantoftvegen 38
Fantoft

Telephone: +47 55 57 40 40
Telefax: +47 55 57 40 41
www.cmr.no

Bank: 5201 05 11755
NO 965 243 798 VAT

OPERATION

The separator is a three-phase gravity separator and it typically contains approximately 10 m^3 of diesel and 10 m^3 of water. The liquid phases enter the loop through separate pipe legs with butterfly valves at each leg to adjust the Water-in-Liquid Ratio (WLR). Two sets of outlets exist; one for the 3" liquid pipe, the other for the 6" pipe. Downstream of a water-oil mixing junction (T-piece), the liquid enters the centrifugal pump. The pump is, together with a downstream Coriolis meter and the butterfly valves, part of an electronic control loop connected to automatic flow controllers. This control loop is used to set the liquid flow rate and the WLR to a chosen pre-defined set point.

The nitrogen gas from the compressor is stored in a separate tank at a pressure of 13-14 bara. Before injection in the liquid lines the gas is measured at a pressure of 10 bara by Coriolis meters. Two meters can be used, one for gas volumes up to 325 Sm^3/h, the other for gas volumes up to 1100 Sm^3/h. There is also a control loop for the gas valve, but the flow controller is normally run in manual mode in order to decrease the response time of the adjustment of the gas injected into the loop.

The gas returns to the compressor for recirculation after passing through the separator. No gas is released to the environment during testing. The pressure is only taken down during calibration of instruments, replacement of diesel or change of water conductivity. The reference instruments are calibrated once a year, typically in July.

MECHANICAL OUTLINE

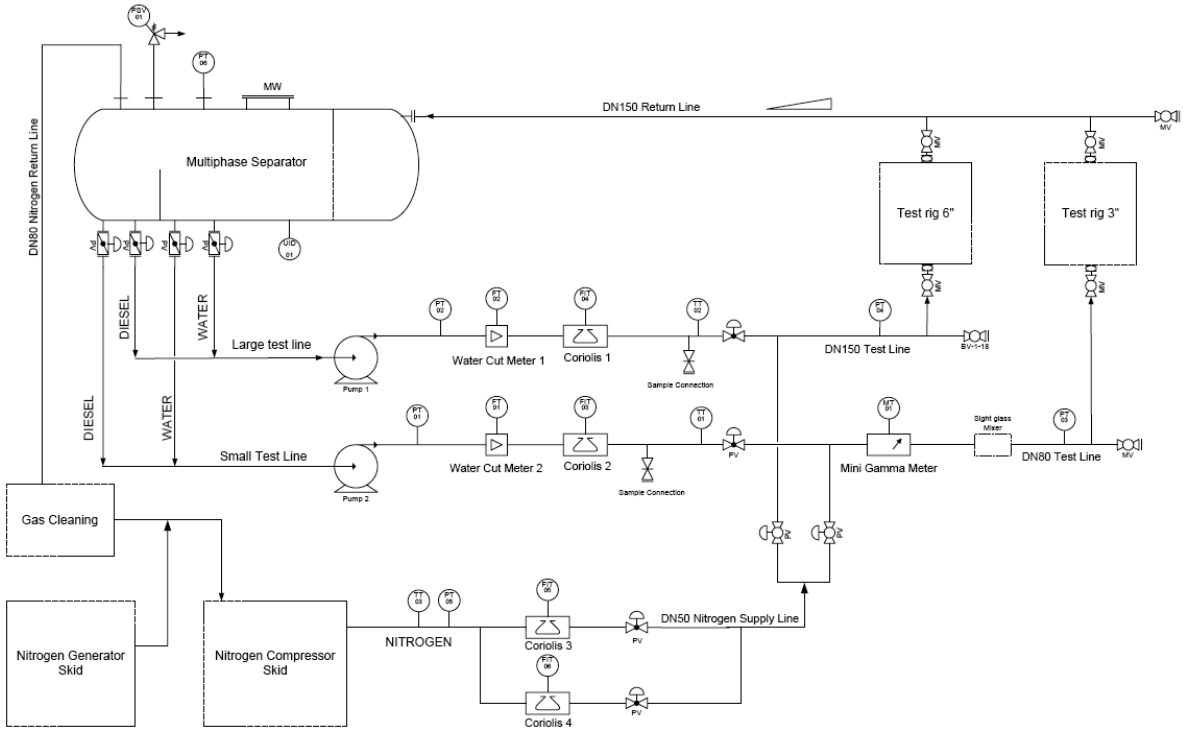

Figure 1: Simplified P&ID of the CMR Multiphase Flow Loop.

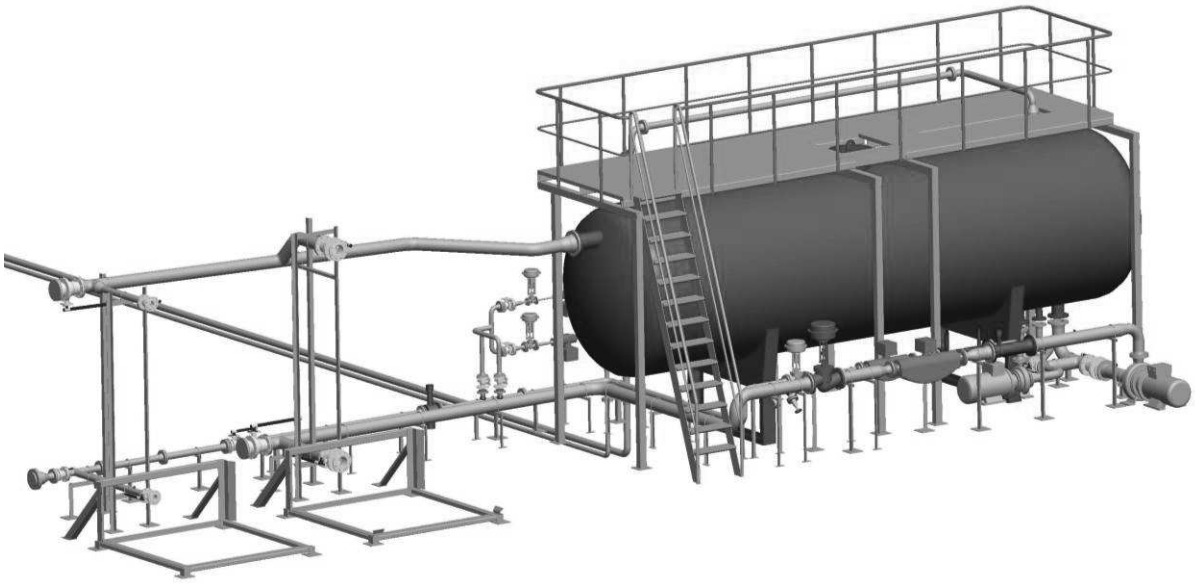

Figure 2: The CMR Multiphase Flow Loop. Test area to the left, separator and reference instruments to the right. The nitrogen generation facility is not included in the drawing. Drawing by Prototech, a subsidiary company in the CMR Group.

TECHNICAL SPECIFICATIONS

Key Specifications

- Location: Indoor
- Fluids: Nitrogen, gas oil (diesel) and salted (NaCl) tap water
- Pipe diameter: 6" and 3"
- Pressure range: 5-10 bara
- Temperature range: 15 - 35°C (no temperature control)
- Gas flow rate: 1100 Sm^3/h
- Liquid flow rate: 250 m^3/h
- Pipe material: 316 L (acid-proof steel)

Table 1: Reference instrumentation in the CMR Multiphase Flow Loop

Tag	Instrument	Range	Expected uncertainty (95% conf level)
FT-01-001	Coriolis meter, Liquid	3-100 m^3/h	< 0.5 %
FT-01-002	Coriolis meter, Liquid	7-250 m^3/h	< 0.5 %
FT-01-003	Coriolis meter, Gas	345-1400 kg/h	< 1 %
FT-01-004	Coriolis meter, Gas	30-390 kg/h	< 1 %
PT-01-001	Pressure transmitter	0-10 bar	0.2 % (abs)
PT-01-002	Pressure transmitter	0-10 bar	0.2 % (abs)
TT-01-001	Temperature transmitter	0-50 °C	0.15 °C
TT-01-002	Temperature transmitter	0-50 °C	0.15 °C
TT-01-003	Temperature transmitter	0-50 °C	0.15 °C
TT-01-004	Temperature transmitter	0-50 °C	0.15 °C

Table 2: Uncertainties (95 % conf level) in flow parameters in the CMR Multiphase Flow Loop

Flow Parameter	Uncertainty	Unit
Gas flow (Q_{gas}>24 Sm^3/h)	< 1.2	% rel
Liquid flow	< 0.5	% rel
Oil flow	< 1.2	% rel
Water flow	< 1.2	% rel
WLR	1.1	% abs
GVF	< 0.5	% abs

The flow parameter uncertainties given in Table 2 are calculated from the uncertainties in Table 1. The uncertainties of the reference instrumentation have been calculated according to the ISO "Guide to the expression of uncertainty in measurements" (1995). All reference instruments are calibrated at accredited laboratories and traceable to international standards. The reference instruments are subject to calibration once a year. Calibration certificates are available on request.

CMR Instrumentation has a HSE and QA system in accordance with ISO 9001 and is certified from June 2012.

Appendix B

Bronkhorst F-201CV Datasheet

Datasheet F-201CV

Mass Flow Controller for Gases

EL-FLOW *Select* Mass Flow Controller model F-201CV

> Introduction

Bronkhorst High-Tech model F-201CV Mass Flow Controllers (MFCs) are suited for precise control of virtually all conventional process gases. The MFC consists of a thermal mass flow sensor, a precise control valve and a microprocessor based PID controller with signal and fieldbus conversion. As a function of a setpoint value, the flow controller swiftly adjusts the desired flow rate. The mass flow, expressed in normal litres or millilitres per minute or per hour, is provided as analog signal or digitally via RS232 or fieldbus. The flow range, wetted materials and orifice size for the control valve are determined depending of the type of gas and the process conditions of the application.

Although all specifications in this datasheet are believed to be accurate, the right is reserved to make changes without notice or obligation.

> Technical specifications

Measurement / control system

Accuracy (incl. linearity)	: ± 0,5% Rd plus ± 0,1% FS
(Based on actual calibration)	
Turndown	: 1 : 50 (in digital mode up to 1:187,5)
Multiple fluid capability	: • storage of max. 8 calibration curves • optional Multi Gas / Multi Range functionality up to 10 bar
Repeatability	: < ± 0,2% Rd
Settling time (controller)	: 1…2 seconds; option: down to 500 msec
Control stability	: ≤ ± 0,1% FS (typical for 1 l_n/min N_2)
Max. Kv-value	: 6,6 x 10^{-2}
Temperature range	: -10…+70°C
Temperature sensitivity	: zero: < ± 0,05% FS/°C;
(nominal range)	span: < ± 0,05% Rd/°C
Leak integrity (outboard)	: < 2 x 10^{-9} mbar l/s He
Attitude sensitivity	: max. error at 90° off horizontal 0,2% FS at 1 bar, typical N_2
Warm-up time	: 30 min. for optimum accuracy 2 min. for accuracy ± 2% FS

Mechanical parts

Material (wetted parts)	: stainless steel 316L or comparable
Pressure rating	: 64 bar abs
Process connections	: compression type or face seal male
Seals	: standard : Viton; options: EPDM, Kalrez
Ingress protection (housing)	: IP40

Electrical properties

Power supply	: +15…24 Vdc ±10%		
Power consumption	: Supply	at voltage I/O	at current I/O
(based on N/C valve)	15 V	290 mA	320 mA
	24 V	200 mA	215 mA
Extra for fieldbus:	PROFIBUS DP: add 53 mA (15 V supply) or 30 mA (24 V supply)		
(if applicable)	EtherCAT®: add 66 mA (15 V supply) or 41 mA (24 V supply)		
	DeviceNet™: add 48 mA (24 V supply)		
Analog output	: 0…5 (10) Vdc, min. load impedance > 2 kΩ;		
	0 (4)…20 mA (sourcing), max. load impedance < 375 Ω		
Analog setpoint	: 0…5 (10) Vdc, min. load impedance > 100 kΩ;		
	0 (4)…20 mA, load impedance ~250 Ω		
Digital communication	: standard RS232; options: PROFIBUS DP, DeviceNet™, EtherCAT®, Modbus RTU/ASCII, FLOW-BUS		

> Ranges (based on Air)

Model	minimum	nominal	maximum
F-201CV-020	0,16…8 ml_n/min	0,16…20 ml_n/min	0,16…30 ml_n/min
F-201CV-050	0,4…20 ml_n/min	0,4…50 ml_n/min	0,4…75 ml_n/min
F-201CV-100	0,8…40 ml_n/min	0,8…100 ml_n/min	0,8…150 ml_n/min
F-201CV-200	1,6…80 ml_n/min	1,6…200 ml_n/min	1,6…300 ml_n/min
F-201CV-500	4…200 ml_n/min	4…500 ml_n/min	4…750 ml_n/min
F-201CV-1K0	8…400 ml_n/min	8…1000 ml_n/min	8…1500 ml_n/min
F-201CV-2K0	16…800 ml_n/min	16…2000 ml_n/min	16…3000 ml_n/min
F-201CV-5K0	0,04…2 l_n/min	0,04…5 l_n/min	0,04…7,5 l_n/min
F-201CV-10K	0,08…4 l_n/min	0,08…10 l_n/min	0,08…15 l_n/min
F-201CV-20K	0,16…8 l_n/min	0,16…20 l_n/min	0,16…25 l_n/min

Intermediate ranges are available

Bronkhorst®
HIGH-TECH

> Model number identification

F – N N NAA – NNN – A A A – NN – A

Base
2 Controller

Pressure rating
0 64 bar

Ranges
1CV 0…8 / 0…25000 ml_n/min

Nominal range
Factory selected

Communication (I/O)
A RS232 + analog (n/c control)
B RS232 + analog (n/o control)
D RS232 + DeviceNet (n/c)
E RS232 + DeviceNet (n/o)
M RS232 + Modbus (n/c)
N RS232 + Modbus (n/o)
P RS232 + PROFIBUS DP (n/c)
Q RS232 + PROFIBUS DP (n/o)
R RS232 + FLOW-BUS (n/c)
S RS232 + FLOW-BUS (n/o)

Analog output
A 0…5 Vdc
B 0…10 Vdc
F 0…20 mA sourcing
G 4…20 mA sourcing

Supply voltage
D + 15…24 Vdc

Connections (in/out)
1 1/8" OD compression type
2 ¼" OD compression type
3 6 mm OD compression type
8 ¼" Face seal male
9 other
0 none

Internal seals
V Viton (factory standard)
E EPDM
K Kalrez (FFKM)

> Thermal mass flow measuring principle

The heart of the thermal mass flow meter/controller is the sensor, that consists of a stainless steel capillary tube with resistance thermometer elements. A part of the gas flows through this bypass sensor, and is warmed up heating elements. Consequently the measured temperatures T_1 and T_2 drift apart. The temperature difference is directly proportional to mass flow through the sensor. In the main channel Bronkhorst High-Tech applies a patented laminar flow element consisting of a stack of stainless steel discs with precision-etched flow channels. Thanks to the perfect flow-split the sensor output is proportional to the total mass flow rate.

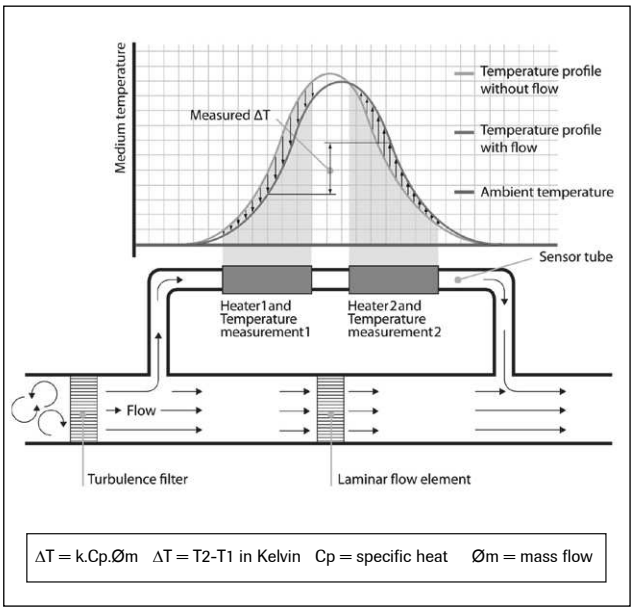

Functional scheme of the thermal mass flow sensor

> State of the art digital design

Todays EL-FLOW® series are equipped with a digital pc-board, offering high accuracy, excellent temperature stability and fast response (settling times t_{98} down to 500 msec). The basic digital pc-board contains all of the general functions needed for measurement and control. In addition to the standard RS232 output the instruments also offer analog I/O. Furthermore, an integrated interface board provides DeviceNet™, PROFIBUS DP, Modbus RTU/ASCII or FLOW-BUS protocols.

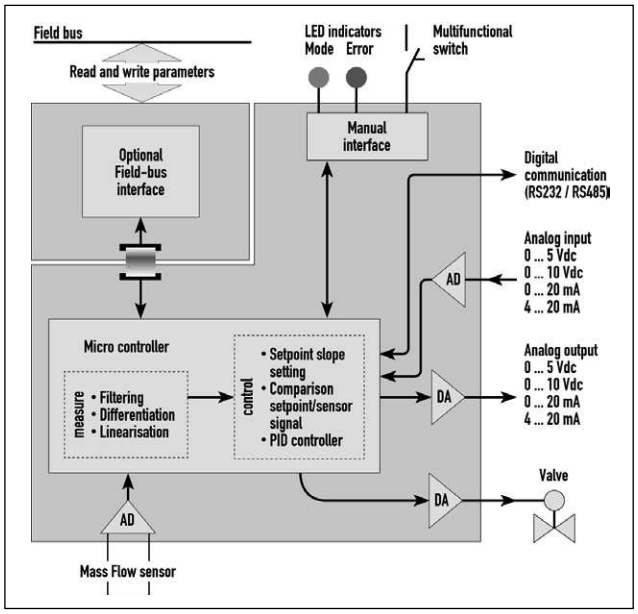

Functional scheme of the digital PC-board

> Hook-up diagram for analog or RS232 communication

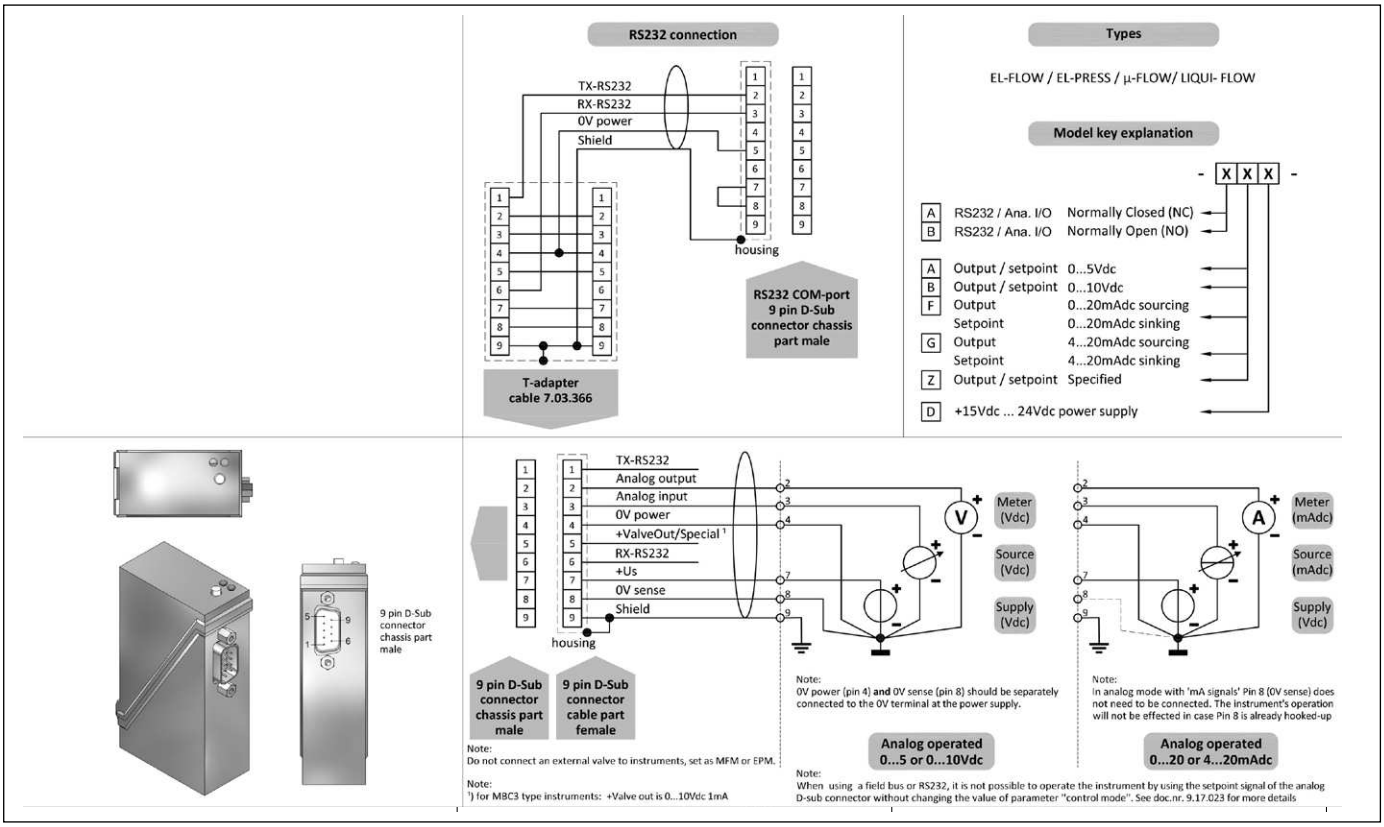

> Hook-up diagrams for fieldbus communication

For the available fieldbus options we refer to the various hook-up diagrams as indicated below. If you are viewing this datasheet in digital format, you may use the hyperlink to each of the drawings. Otherwise please visit the download section on www.bronkhorst.com or contact our local representatives.

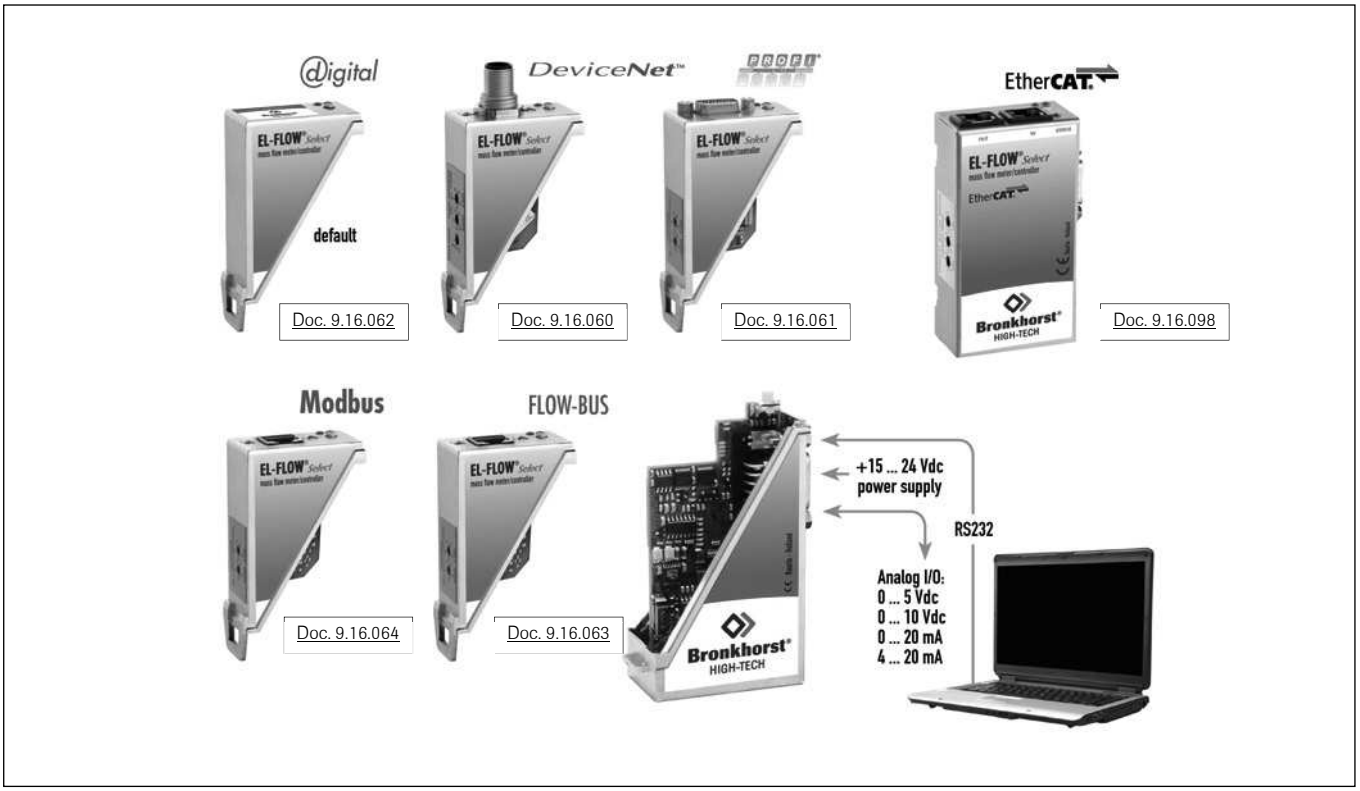

Doc. 9.16.062 | Doc. 9.16.060 | Doc. 9.16.061 | Doc. 9.16.098

Doc. 9.16.064 | Doc. 9.16.063

> Dimensions (mm) and weight (kg)

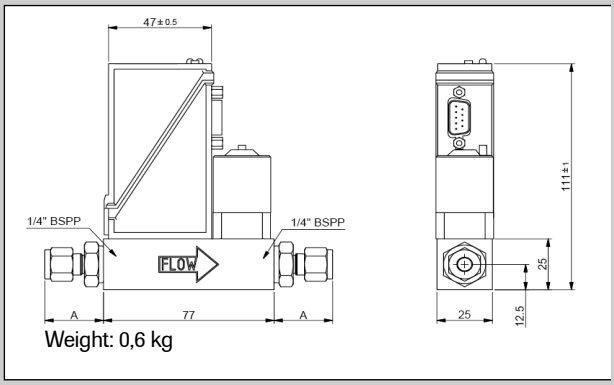

Weight: 0,6 kg

Dimension table adapters (RS-type)

Compression type	1/4"BSPP Size A
adapter 3 mm OD	26.1
adapter 6 mm OD	28.4
adapter 8 mm OD	29.4
adapter 10 mm OD	30.2
adapter 12 mm OD	32.5
adapter 1/8" OD	26.1
adapter 1/4" OD	28.4
adapter 3/8" OD	29.9
adapter 1/2" OD	32.7

Face-seal male	Size A
adapter 1/4" inlet	23.2

Compression type

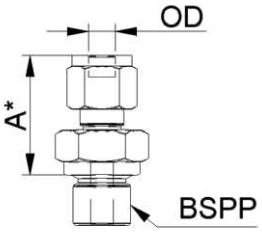

*) Dimension A is typical finger-tight.

> Options and accessories

- Multi-Gas / Multi-Range option, with free configuration software. - Free software support for operation, monitoring, optimizing or to interface between digital instruments and windows software.	
- IN-LINE filters for protection against particulates	
- BRIGHT compact local Readout/Control modules - E-8000 Power Supply/Readout systems	
- Interconnecting cables for power and analog/digital communication - PiPS Plug-in Power Supply	

> Alternatives

- IQ^{+}FLOW, world's smallest Mass Flow Controller	
- MFC with integrated 24V shut-off valve	
- LOW-ΔP-FLOW series MFC for low pressure drop applications or corrosive gas service	
- Metal sealed MFC for Semiconductor or other high purity applications - Mass Flow Controller for standardised modular platform systems (top-mount version)	
- Pre-assembled multi-channel solutions: series FLOW-SMS	

Bronkhorst®
HIGH-TECH

Nijverheidsstraat 1a, NL-7261 AK Ruurlo The Netherlands
T +31 (0)573 45 88 00 **F** +31 (0)573 45 88 08 **I** www.bronkhorst.com **E** info@bronkhorst.com

E.DS.F-201CV.0115.N

Appendix C

Diesel Quality Certificate

CERTIFICATE OF QUALITY

ExxonMobil
Refining & Supply

Sample Name : 140730054
Product : AUTO DIESEL BASE SU:NO
Product Description : ADO .001%S -12CFPP 0%A DIESEL :NO
Product Specification: ADO_0011_BASE

Sample Date : 30/07/2014
Document No: COA14211008

Sample Point: TK802

Test	Method	Units	Result
In case of arbitration, the meth. in CENEN590 are to be used	-	-	-
DENSITY AT 15 DEG. C VAC.	EN ISO 12185	KG/M3	840.6
DENSITY AT 15 DEG. C AIR	EN ISO 12185	KG/M3	839.5
SULPHUR CONTENT	EN ISO 20846	MG/KG	6.7
APPEARANCE AT MAX 20 DEG C	ASTM D 4176	TEXT	PASS
WATER CONTENT BY KARL FISHER	ISO 12937	MG/KG	52
CLOUD POINT	EN 23015	DEGC	-10
COLD FILTER PLUGGING POINT	EN 116	DEGC	-28
FLASH POINT	EN ISO 2719	DEGC	60
TEMP AT 10% RECOVERED	EN ISO 3405	DEGC	202
TEMP AT 50% RECOVERED	EN ISO 3405	DEGC	259
TEMP AT 90% RECOVERED	EN ISO 3405	DEGC	325
TEMP AT 95 % RECOVERED	EN ISO 3405	DEGC	342
% RECOVERED AT 250 DEG. C	EN ISO 3405	VPCT	43
% RECOVERED AT 350 DEG. C	EN ISO 3405	VPCT	96
CALCULATED CETAN INDEX	EN ISO 4264	NUMBER	48.1
DERIVED CETAN NUMBER	EN 15195	NUMBER	51.2
IGNITION DELAY	EN 15195	MS	3.99
VISCOSITY AT 40 DEG. C	EN ISO 3104	MM2/S	2.48
TOTAL ACID NUMBER	ASTM D 974	MGKOH/G	<0.02
TOTAL AROMATICS CONTENT	EN 12916	WPCT	26
DI,TRI & ABOVE POLYAROMATICS	EN 12916	WPCT	4.7
CONTAMINATION	EN12662	MG/KG	1
CORROSION CU 3H/50 DEG. C	EN ISO 2160	CLASS	1
E S S O G U A R A N T E E:Not tested on every batch.	-	-	
Oxidation Stability (Accelerated)	EN ISO 12205	G/M3	<25
Ash content	EN ISO 6245	WPCT	<0.01
Carbon Residue on 10% BTMS	EN ISO 10370	WPCT	<0.30
High Frequency Reciprocating Rig	ISO 12156	MICRON	<460
Fatty Acid Methylester	EN 14078	VPCT	<0.2
ADDITIVES ADDED DURING LOADING	-	-	
CETANIMPROVER	-	VPPM	550
LUBRICITYIMPROVER	-	VPPM	200
FLOWIMPROVER	-	VPPM	0
STATIC DISSIPATOR 450	-	VPPM	1

Some tests may have been performed by 3rd party laboratory. More information given upon request.

Above test results performed by lab:

Kari A Christensen

30/07/2014

Additives injected according to the CoA.

Ship : BIRGIT KNUTSEN

Dispatcher / Date : 30/7-14

Esso Norge AS
Laboratory Slagen
PB 2001
3103 Tønsberg
Norway

SLAGEN REFINERY

Tlf: 33377529
Fax: 33377528

Appendix D

Viscous motion, results

Reference conditions

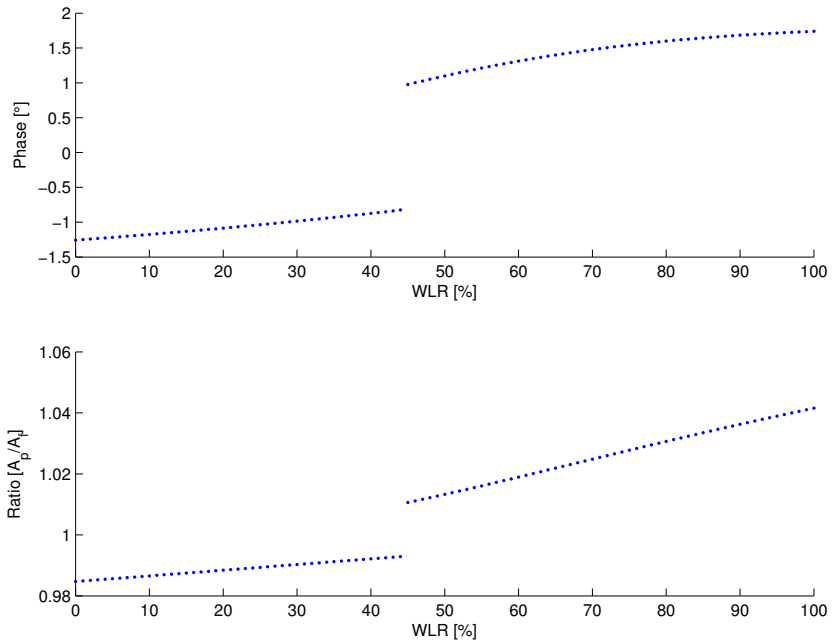

Figure D.1: Phase difference and amplitude ratio between particle and continuous phase, when solving for reference conditions, Table 3.1. Results shown for all WLR, with continuous phase change at WLR = 45%.

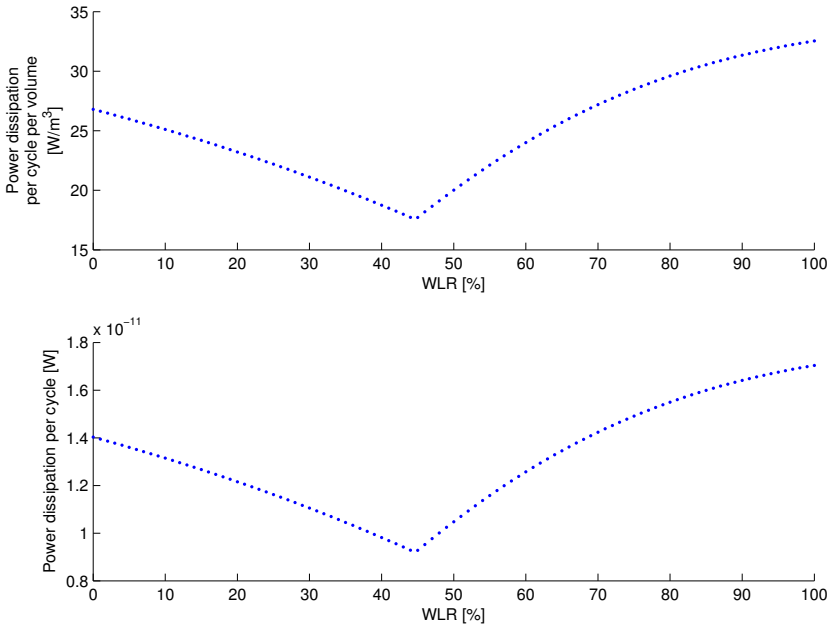

Figure D.2: Power dissipation per cycle and power dissipation per volume, for each particle, when solving for reference conditions, Table 3.1. Results shown for all WLR, with continuous phase change at WLR = 45%.

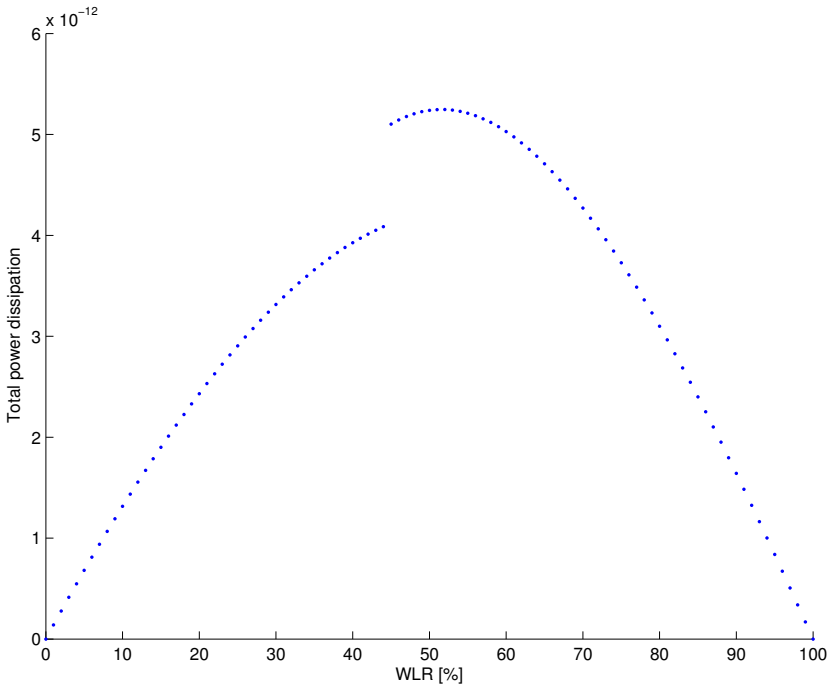

Figure D.3: An expression for total power dissipation per cycle when solving for reference conditions, Table 3.1. Results shown for all WLR, with continuous phase change at WLR = 45%. Values for power dissipation are not valid for numerical comparison.

High pump speed

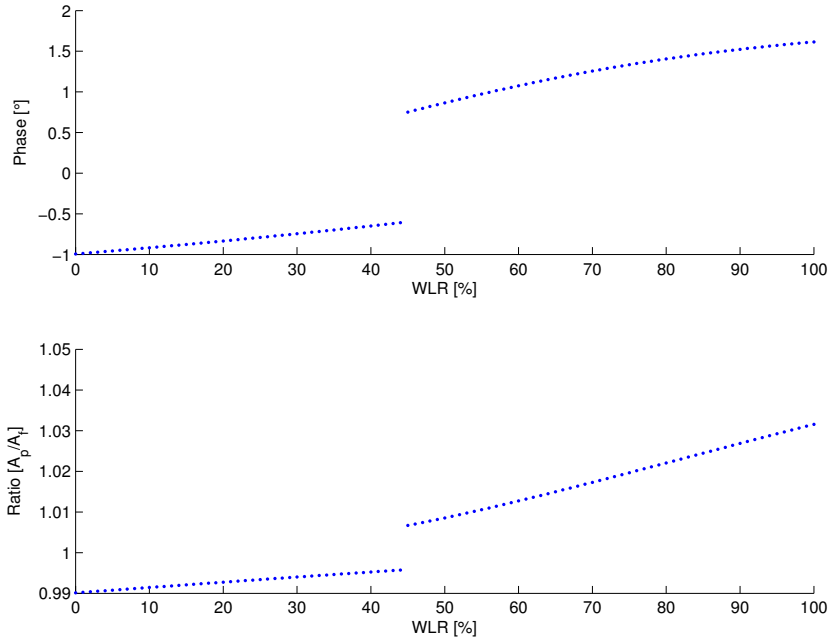

Figure D.4: Phase difference and amplitude ratio between particle and continuous phase, when solving for high pump speed conditions, Table 3.2. Results shown for all WLR, with continuous phase change at WLR = 45%.

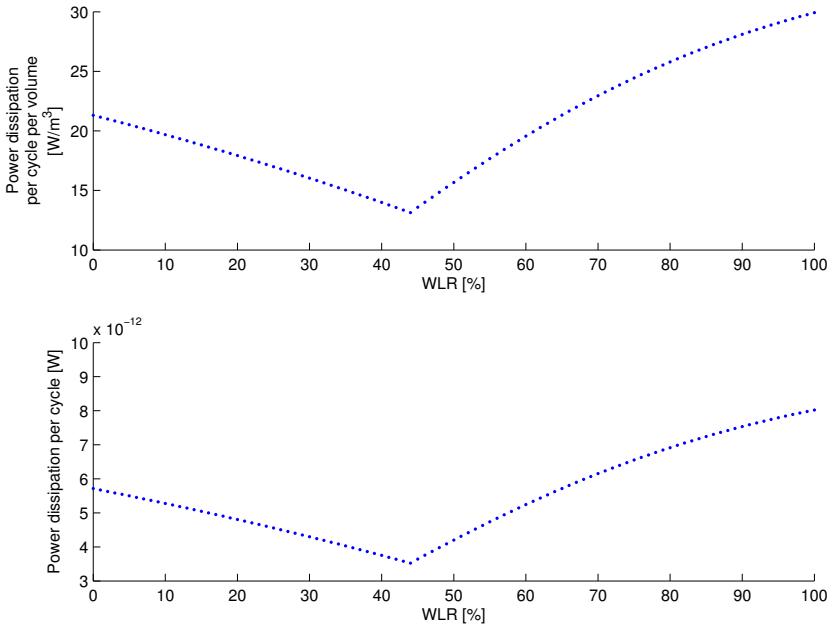

Figure D.5: Power dissipation per cycle and power dissipation per volume, for each particle, when solving for high pump speed conditions, Table 3.2. Results shown for all WLR, with continuous phase change at WLR = 45%.

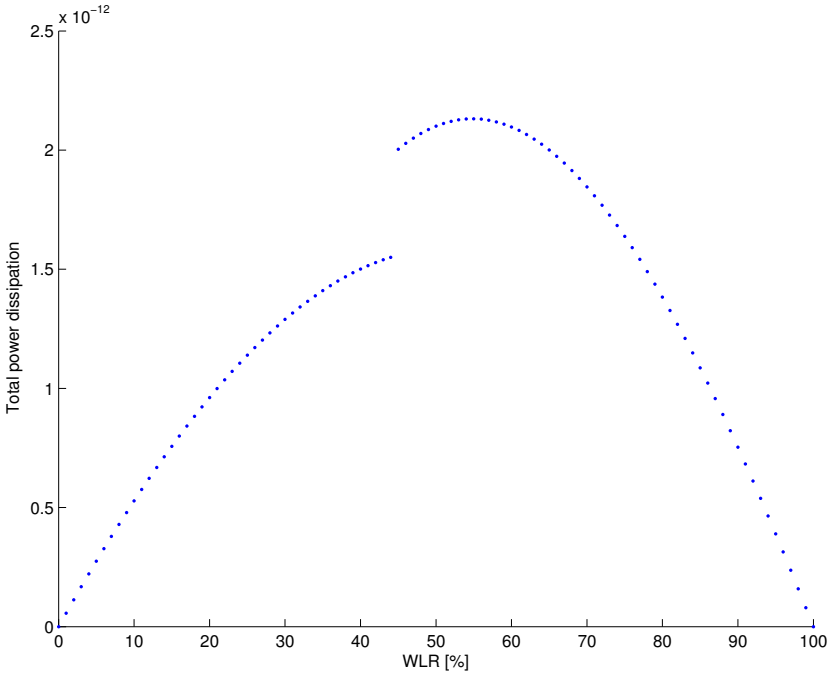

Figure D.6: An expression for total power dissipation per cycle when solving for high pump speed conditions, Table 3.2. Results shown for all WLR, with continuous phase change at WLR = 45%. Values for power dissipation are not valid for numerical comparison.

Low pump speed

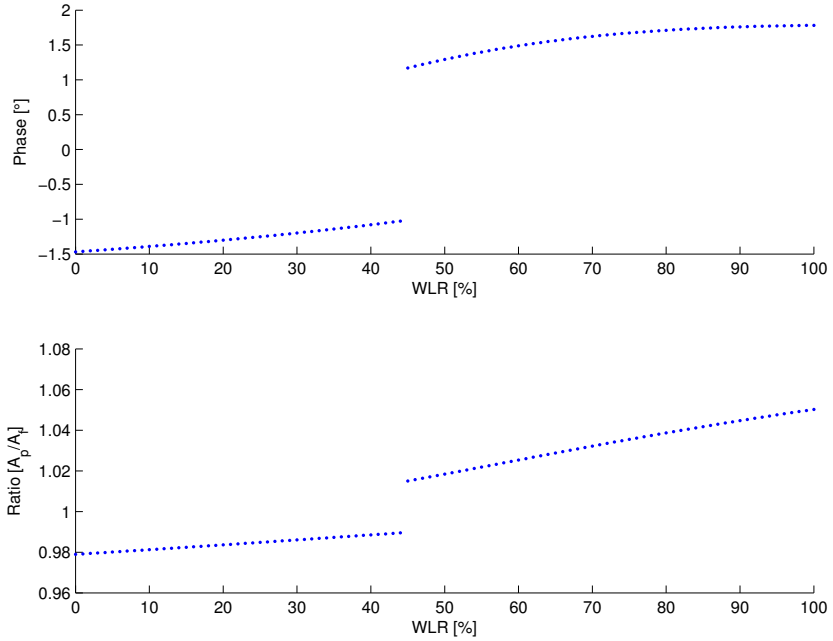

Figure D.7: Phase difference and amplitude ratio between particle and continuous phase, when solving for low pump speed conditions, Table 3.2. Results shown for all WLR, with continuous phase change at WLR = 45%.

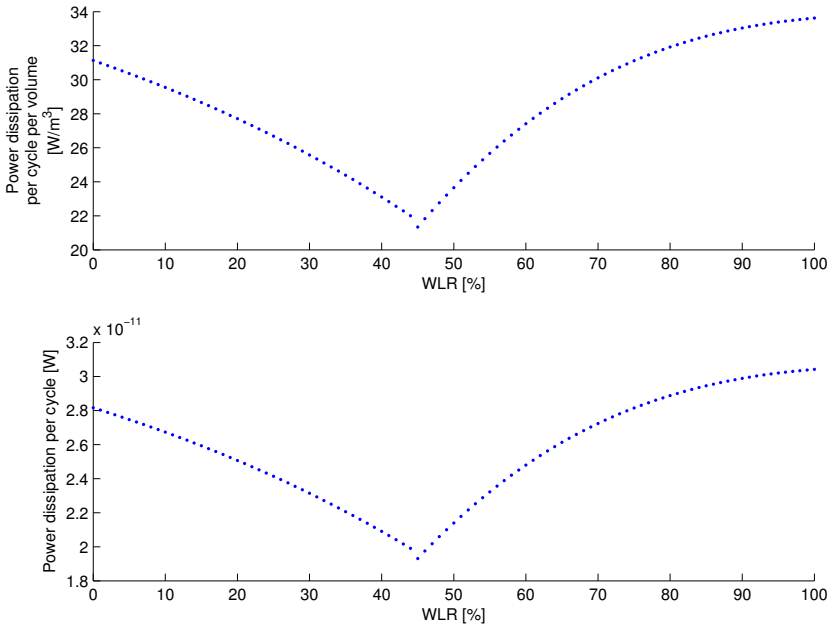

Figure D.8: Power dissipation per cycle and power dissipation per volume, for each particle, when solving for low pump speed conditions, Table 3.2. Results shown for all WLR, with continuous phase change at WLR = 45%.

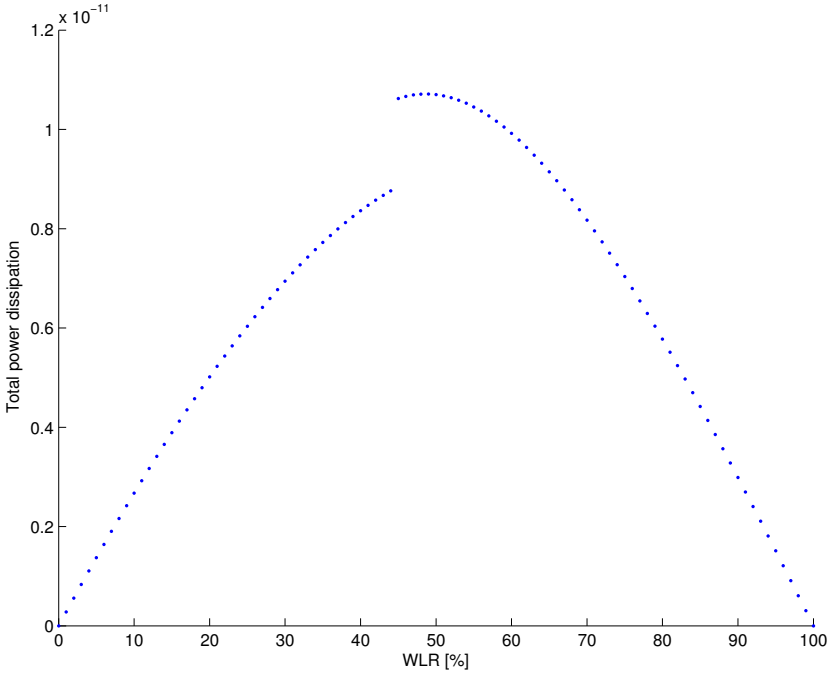

Figure D.9: An expression for total power dissipation per cycle when solving for low pump speed conditions, Table 3.2. Results shown for all WLR, with continuous phase change at WLR = 45%. Values for power dissipation are not valid for numerical comparison.

High temperature

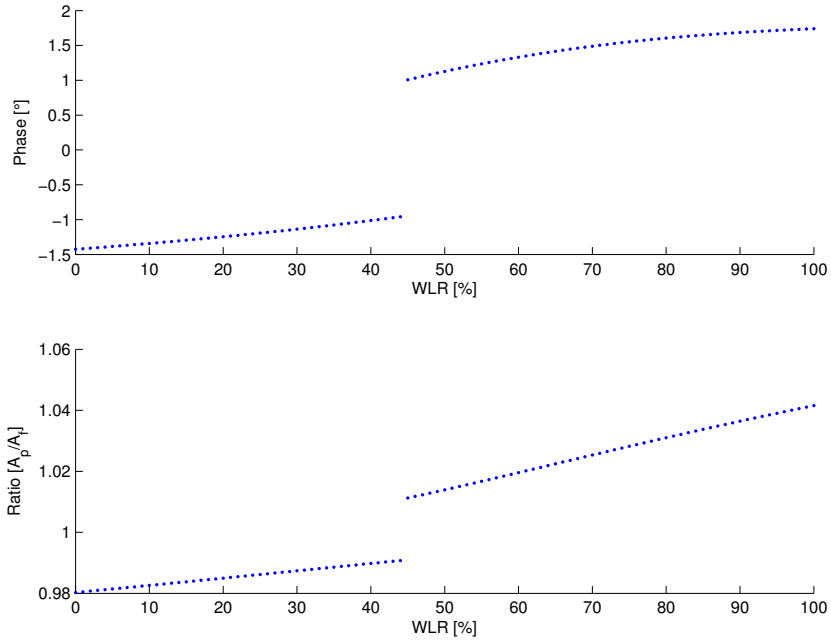

Figure D.10: Phase difference and amplitude ratio between particle and continuous phase, when solving for high temperature conditions, Table 3.2. Results shown for all WLR, with continuous phase change at WLR = 45%.

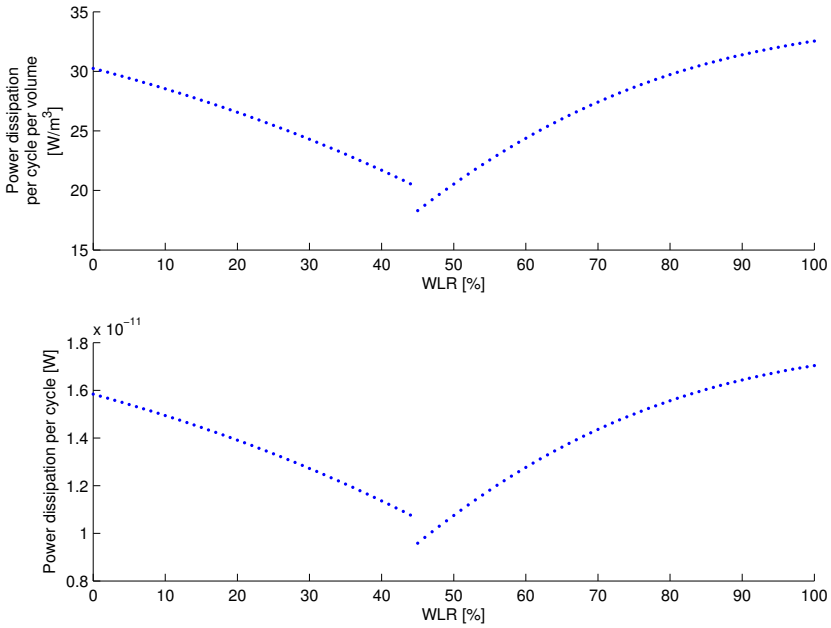

Figure D.11: Power dissipation per cycle and power dissipation per volume, for each particle, when solving for high temperature conditions, Table 3.2. Results shown for all WLR, with continuous phase change at WLR = 45%.

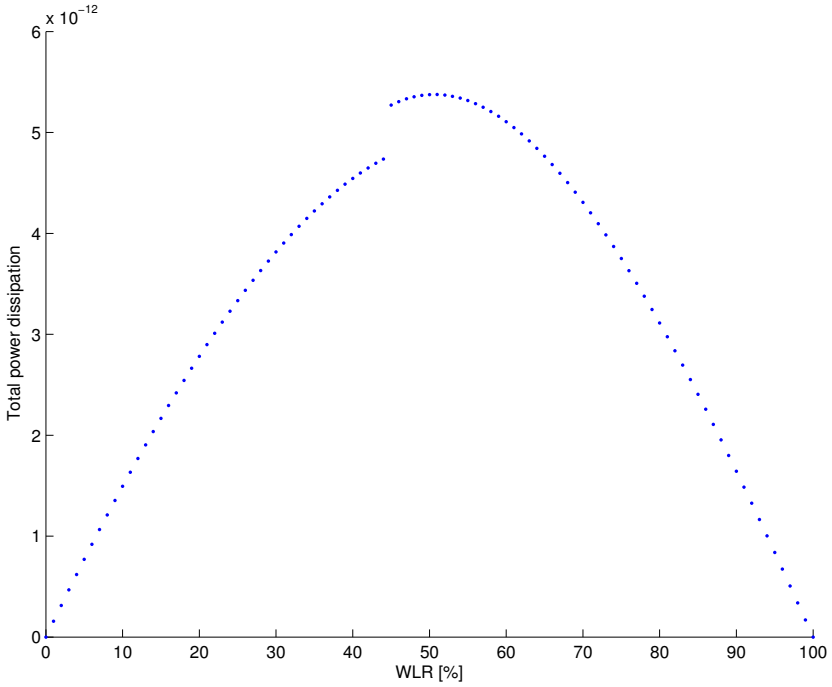

Figure D.12: An expression for total power dissipation per cycle when solving for high temperature conditions, Table 3.2. Results shown for all WLR, with continuous phase change at WLR = 45%. Values for power dissipation are not valid for numerical comparison.

Appendix E

Density error estimations

Reference conditions

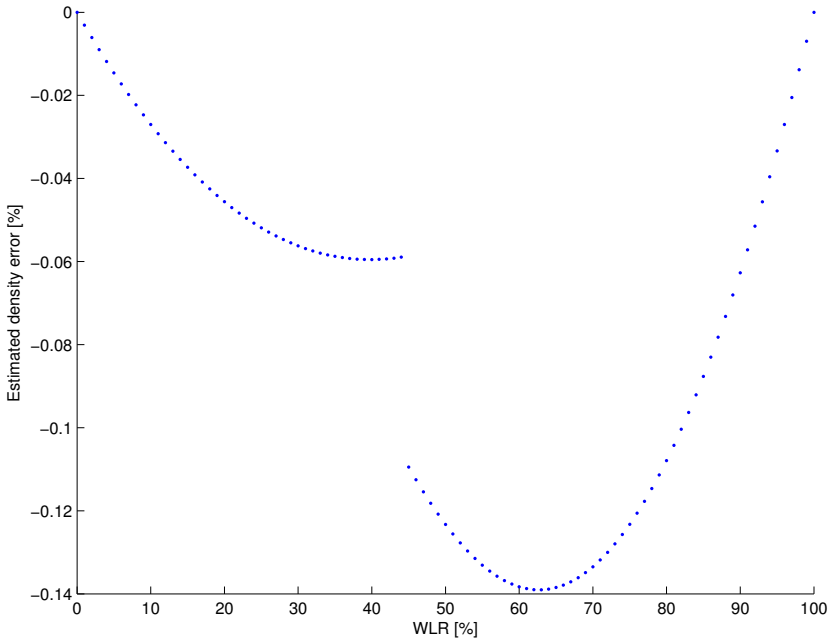

Figure E.1: Estimated density error for different WLR, using reference conditions. Continuous-phase change at WLR = 45%.

High pump speed

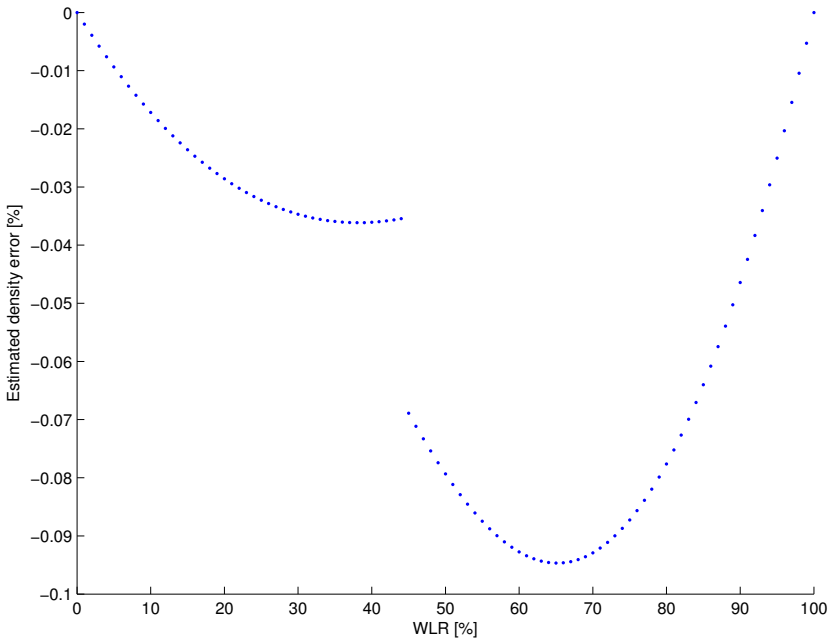

Figure E.2: Estimated density error for different WLR, using high pump speed conditions. Continuous-phase change at WLR = 45%.

Low pump speed

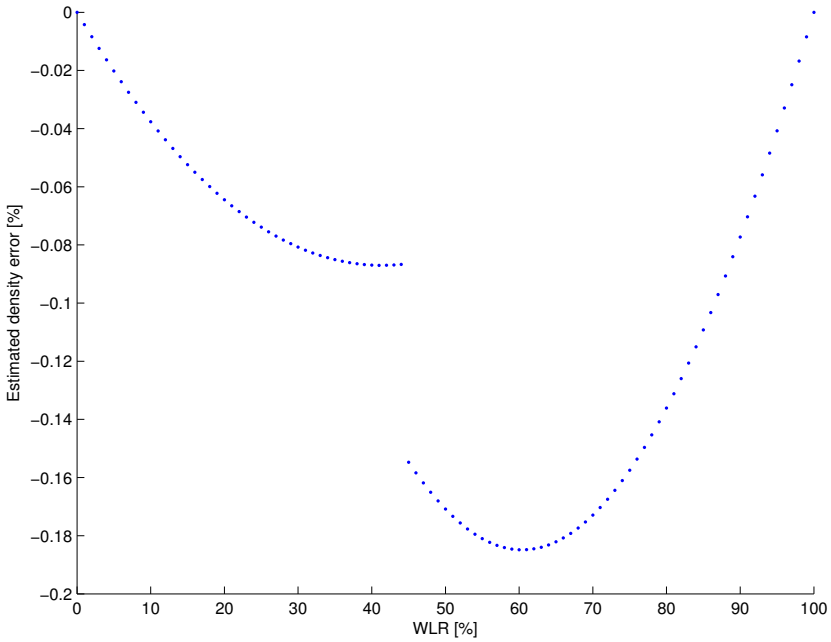

Figure E.3: Estimated density error for different WLR, using low pump speed conditions. Continuous-phase change at WLR = 45%.

High temperature

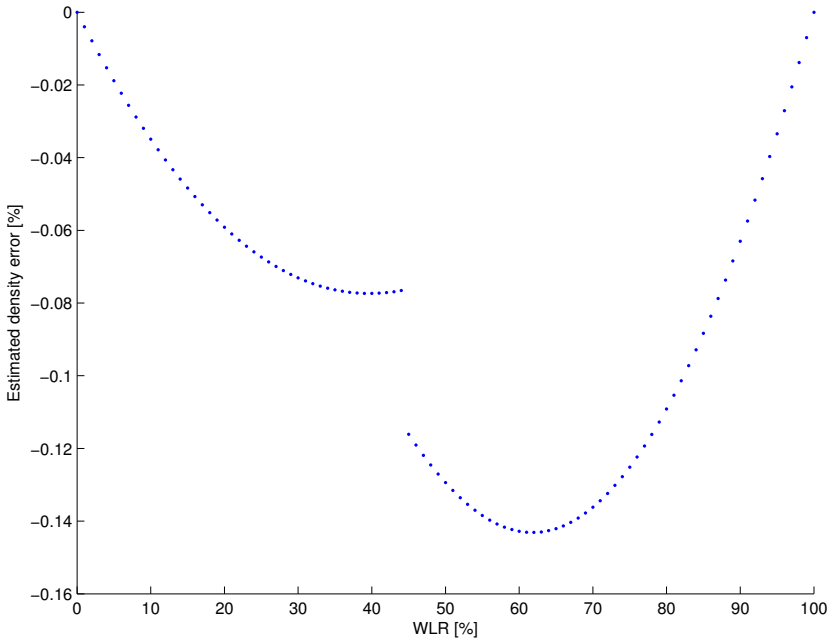

Figure E.4: Estimated density error for different WLR, using high temperature conditions. Continuous-phase change at WLR = 45%.